

Delta Oscillations: Prevalence, Propagation, and Relation to Motor Dysfunction in Mouse Models of Parkinson's Disease

Timothy Carvin Whalen

February 2021

Neuroscience Institute
Dietrich College of Humanities and Social Sciences
Carnegie Mellon University
Pittsburgh, PA 15213

Thesis Committee:

Robert S. Turner, Ph.D., Department of Neurobiology, University of Pittsburgh, Chair
Aryn H. Gittis, Ph.D., Neuroscience Institute, Carnegie Mellon University
Jonathan E. Rubin, Ph.D., Department of Mathematics, University of Pittsburgh
William R. Stauffer, Ph.D., Department of Neurobiology, University of Pittsburgh
Charles J. Wilson, Ph.D., Department of Biology, University of Texas at San Antonio

Submitted in partial fulfillment of the requirements
for the degree of Doctor of Philosophy

Copyright © 2021, Timothy C. Whalen

This research was supported by NSF awards DMS 1516288 and 1724240, NIH awards F31NS101821, R01NS117058, R01NS101016, R01NS104835, and R21NS095103, and the Michael J. Fox Foundation for Parkinson's Research

Delta Oscillations: Prevalence, Propagation, and Relation to Motor Dysfunction in Mouse Models of Parkinson's Disease

Timothy C. Whalen

Carnegie Mellon University, 2021

Pathological neural oscillations, particularly in the beta and delta bands, are hallmarks of dysfunction in the basal ganglia (BG) of patients with Parkinson's disease (PD). While Parkinsonian beta oscillations have received more attention than delta oscillations in the scientific literature, it remains unclear how these oscillations emerge, propagate through the brain, and relate to motor symptoms in PD. Animal models of PD have been a valuable tool for studying these oscillations, but the oscillatory landscape of awake, behaving mice, a common animal model for the study of PD, has not been investigated.

Here, we record from the substantia nigra pars reticulata (SNr), the primary output nucleus of the mouse BG, and other BG nuclei in the dopamine depleted (DD) mouse model of PD. Using a novel signal processing method to distinguish oscillations from neural noise, we establish that delta, but not beta, oscillations are present in single neural units throughout the BG in dopamine depletion, and that these oscillations arise due to insufficient activation of D2 receptors. We also establish that the prevalence of delta oscillations in SNr neurons correlates with the overall level of motor dysfunction and dopamine loss and dynamically correlates with bouts of akinesia. These oscillations in SNr neurons lead DD-induced delta oscillations in motor cortex (M1), suggesting a subcortical basis for their generation, and their relationship to M1's oscillations define a novel dichotomy of SNr into active-predicting (AP) and inactive-predicting (IP) subpopulations of neurons.

Next, we take a computational modeling approach to further investigate how these oscillations propagate in the brain and how the AP and IP subpopulations of SNr neurons arise. Using a realistic conductance-based model of SNr neurons, we test if delta oscillations in GPe

neurons which project to our model SNr neurons are sufficient to replicate the SNr oscillations we observe *in vivo*. We demonstrate that a simple connection architecture, in which GPe and other SNr neurons compete for a limited number of synapses on each SNr neuron, is sufficient to generate AP and IP populations in SNr whose firing properties match experimental data. This model demonstrates how delta oscillations can effectively propagate through the basal ganglia despite neural noise.

Finally, we review how these results fit within and inform our understanding of neural oscillations and Parkinsonian motor dysfunction. We discuss and attempt to reconcile the disparities between observations in different animal models and human PD and explore potential mechanisms by which delta oscillations could cause Parkinsonian dysfunction. We close with a discussion of the future directions we envision for these topics and how they may inform new potential targets and treatments for PD.

PREFACE

I have an incredible number of incredible people to thank for their help making this dissertation a reality. First, to my advisors. Aryn Gittis and Jon Rubin, who have been the most gracious and supportive mentors I could have asked for. You always fostered and supported my autonomy and curiosity but provided wisdom and guidance to keep that independent streak from running off the rails. I'm extremely grateful to have been able to learn from and work alongside two people whom I greatly admire, and you have shaped the scientist I am today. I would also like to thank the other members of my thesis committee. Rob Turner and Bill Stauffer, you provided valuable feedback in and out of our meetings and your expertise shaped my research for the better; Charlie Wilson, thank you for your effort and time serving as my external – the fundamental and rigorous research you've pursued throughout your career has and continues to be an inspiration for my work, and it was an honor to meet you and earn your approval on this thesis.

To my present and former colleagues in the Gittis Lab, you gave me more support than you know. Three former labmates saved my life countless times –Amanda Willard, Kevin Mastro, and Rachel Bouchard, you taught me everything I know about running a successful experiment. I came into this lab with so little experimental knowledge, but your guidance, feedback, and immense patience brought me to where I am today. Victoria Corbit and Kevin Zitelli, thank you for being my first real scientific collaborators – I consistently try to emulate the tenacity and hard work you always showed in our work together. Teresa Spix, your positive, open and generous attitude toward everything you do completely defined the culture of the Gittis lab – thank you for always striving to make the lab a safe, welcoming, and positive space. Brian Isett and Kat Nguyen, I become a better thinker each time I speak with you – thank you for our scientific discussions and challenging me to think in new ways. Ian Rosner, Mary Cundiff and Liz Wendel – we may not have had the chance to collaborate directly, but your ingenuity and sheer kindness made every day in lab better. To our other current and former lab techs Jenna Schwenk, Christen Snyder and Layne Picard – you keep this whole operation running and made so much of this work possible. And to the newest members of the lab, Asier Aristieta, Shruti Nanivadekar. and Dan Albaugh – while an unusual year kept us from truly getting to know one another, I'm confident you will make great and impactful findings during your time in the lab, and I cannot wait to see what you will accomplish.

A big thank you to the administrators and staff of the CNBC and MICV whose tireless work and dedication made my research possible. I'd also like to thank a great number of colleagues and professors throughout the Great Hall of Brain Science, the Math-Bio groups at Pitt, and the CNBC: Ryan Phillips, Youngmin Park, Faisal Baqai, Sandy Kuhlman, Allison Barth, Eric Yttri, Andreas Pfenning, Bard Ementraut, Brent Doiron, Rob Kass, Steve Chase, and DJ

Brasier – you all greatly influenced my research and learning in these past years. Thanks as well to the professors during my years in undergrad who took me under their wing and fostered my initial growth as a young researcher – John Donoghue, Carlos Vargas-Irwin, Andrey Rzhetsky, and Jerome Sanes – as well as a number of professors who particularly inspired my research and growth through our conversations and their courses – Elie Bienenstock, Chris Moore, and John Stein.

On the education front, I must finally go back even further to the incredible teachers I've had throughout my life – you may not have influenced this work directly, but you completely shaped who I am as a person and gave me the knowledge and strength to be who I am today: Karen Crowe, who nurtured my curiosity when it mattered most, Catherine Crow, who kept that wonder and excitement of learning burning throughout my younger years, Doc Aronson, who showed me the power of persuasion, Anders Lewis, who showed me the power of storytelling, Kristen Lapierre-Small, who helped me truly find my written voice, and Lyubov Shmidt, who helped me build the mathematical foundation and intuition that underlies everything in my work to this day. You all went above and beyond to imbue in me the wisdom that makes up the fiber of who I am, and I am incredibly grateful to have had the opportunity to learn from you.

Finally, to those closest to me – my parents, Jill and Don Whalen, who always believed in me and nurtured my love of learning. You ensured I got the best education I possibly could and that I had every resource I needed for success, and this achievement is a culmination of that support. And to my friends outside of science who have supported me along the way: Virginia Lyon, you are the brilliant, ever compassionate constant in my life who I can always count on. Thank you for always being there. Craig and Jen Corlis, you are two of the most generous people I have ever met, and I truly thank you for the supportive community of friends your gregariousness has built. To Jen Gentzel, Floris van Doorn, Erich Wilkerson, Lynn and Josh Speakman, Shawn Doremus, Kath Kyruchkova, Ann Bridge, Victoria Tatsumi and Katie Kim – you each helped me immensely in your own ways through these five and a half years, in part or in whole. Thank you all for your support.

And to you reading this now – thank you. This thesis is far from perfect. It contains many holes to be filled in and avenues to be investigated further, and those require insight I was not able to find. For whatever purpose you are reading this, whether to gain a deeper understanding of the topic at hand or to locate a single detail or idea, I hope you will find something valuable in this document. In the realm of basic science, a colleague like you trying to extend or utilize my research in even the smallest way is the most impactful achievement I could hope for, so thank you for taking the time to try to do so.

TABLE OF CONTENTS

1	Introduction.....	1
1.1	Connections between dopamine depletion and PD	2
1.2	Parkinsonian neurophysiological changes	4
1.3	Parkinsonian neural oscillations	7
1.3.1	Beta oscillations.....	7
1.3.2	Delta oscillations.....	10
1.4	Summary and aims of dissertation	11
2	Delta Oscillations Indicate Severity of Dopamine Depletion and Motor Dysfunction.....	13
2.1	Introduction.....	14
2.2	Materials and Methods.....	16
2.2.1	Animals.....	16
2.2.2	Stereotaxic surgery	16
2.2.3	Drugs.....	18
2.2.4	<i>In vivo</i> recordings.....	19
2.2.5	Histology.....	19
2.2.6	Data pre-processing.....	20
2.2.7	Oscillation detection and visualization.....	21
2.2.8	Neural measures	23
2.2.9	Behavioral testing and metric.....	24

2.2.10	Linear regression	24
2.2.11	Decision tree regression	25
2.2.12	Movement analysis	26
2.2.13	Time series regression.....	27
2.2.14	Quantifying neural phase lags.....	28
2.2.15	Statistical tests.....	29
2.3	Results.....	29
2.3.1	Dopamine depleted mice exhibit 0.5–4 Hz spike oscillations in SNr units	29
2.3.2	Phase shift analysis distinguishes delta oscillations and neural noise.....	30
2.3.3	Delta, not beta, oscillations in SNr units are a marker of dopamine depletion	31
2.3.4	Oscillations predict dopamine depletion severity and behavior better than other physiological measures of dysfunction	35
2.3.5	Oscillations are modulated by movement in a unit-specific manner	39
2.3.6	Delta oscillations arise immediately following loss of either MFB transmission or D2 receptor activation	40
2.3.7	Delta oscillations appear in depletion throughout the indirect pathway.....	42
2.3.8	Two populations of delta oscillating SNr units lead oscillations in motor cortex	42
2.3.9	M1 is not required for delta oscillations in SNr	45
2.3.10	SNr neurons exhibit consistent non-zero pairwise phase lags.....	47
2.4	Discussion	48
2.4.1	A novel method to distinguish oscillations from noise.....	49
2.4.2	Relationship to previous studies on Parkinsonian oscillations	50
2.4.3	Mechanisms of generation.....	52
2.4.4	Relationship between oscillations and motor dysfunction.....	53
2.5	Acknowledgements.....	54
3	Propagation of Delta Oscillations in a Biophysical Model of the GPe-SNr Network	56

3.1	Introduction	56
3.2	Materials and Methods	59
3.2.1	Biophysical model of SNr neurons	59
3.2.2	Simulated GPe spike trains	61
3.2.3	Fitting GPe phase lag distributions	63
3.2.4	Connection architecture	63
3.2.5	Simulations and analysis	64
3.2.6	Measuring irregularity with C_{V2}	64
3.2.7	Identifying oscillating neurons	65
3.2.8	Quantifying model fit	65
3.2.9	Clustering	66
3.3	Results	66
3.3.1	A model with partially segregated pathways matches <i>in vivo</i> recordings	66
3.3.2	A simpler, “competitive” model also matches <i>in vivo</i> recordings	70
3.3.3	Imperfectly synchronous GPe oscillations propagate and entrain phase lags in SNr	72
3.3.4	The power of oscillatory inputs from GPe and SNr define the AP and IP clusters	73
3.4	Discussion	75
3.4.1	Network architecture assumptions	75
3.4.2	Limitations	77
3.4.3	Model predictions and extensions	78
3.4.4	Propagation of imperfectly synchronous oscillations	80
3.5	Acknowledgements	81
4	Summary and Conclusion	82
4.1	Why do Parkinsonian oscillations vary across species?	83
4.2	How might delta oscillations lead to Parkinsonian symptoms?	85

4.3	Future directions for delta oscillations and SNr physiology.....	88
4.4	Final remarks.....	90
Appendix A		92
Bibliography		100

LIST OF FIGURES

Figure 2-1: Dopamine depletion leads to low frequency spiking oscillations in SNr units.....	30
Figure 2-2: A phase shift measure to distinguish oscillations from noise.	33
Figure 2-3: Dopamine depleted, but not control, SNr units exhibit phase-consistent delta oscillations, but no change in beta oscillations.	34
Figure 2-4: Delta oscillations predict severity of dopamine depletion.....	37
Figure 2-5: Movement in dopamine depleted animals modulates oscillations in a unit-specific manner biased towards attenuation.	38
Figure 2-6: Acute manipulations of MFB signaling or D2-receptors modulate oscillations.	41
Figure 2-7: Delta oscillations pervade the dopamine depleted, but not healthy, indirect pathway.	42
Figure 2-8: Delta oscillations define two SNr populations which both lead M1 oscillations.	44
Figure 2-9: M1 lesion does not disrupt oscillations in SNr	46
Figure 2-10: Delta oscillating SNr units exhibit non-zero phase lags.	47
Figure 3-1: Performance of models with segregated pathways.	69
Figure 3-2: Performance of the competitive model.	71
Figure 3-3: Model SNr neurons cluster based on presynaptic GPe and SNr delta power.	74

LIST OF FIGURES: APPENDIX A

Figure A-1: Unilaterally depleted animals exhibit a small number of delta oscillating units in the SNr of their intact hemisphere.	92
Figure A-2: Central delta oscillation frequency in SNr for each DD animal	93
Figure A-3: Power of SNr LFP beta oscillations is not affected by DD.	94
Figure A-4: Pairwise phase relationships corroborate the existence of two populations of oscillating units in dopamine depleted SNr.	95
Figure A-5 Poisson regression on spike trains corroborates consistent non-zero lags within SNr populations.	96
Figure A-6: Fitting simulated GPe spike trains.	97

LIST OF TABLES: APPENDIX A

Table A-1: Intrinsic current parameters for SNr biophysical model	98
Table A-2: Synaptic and miscellaneous parameters for SNr biophysical model.....	99

1 INTRODUCTION

Parkinson's disease (PD) is the second-most common neurodegenerative disorder, afflicting over ten million people worldwide (Marras et al. 2018). Treatments for PD exist, such as dopamine replacement therapy, in which drugs such as levodopa are given to replenish brain dopamine levels (Hornykiewicz 2010), and deep brain stimulation (DBS), in which a stimulating electrode is implanted in a dysfunctional locus in the patient's brain (Volkman 2004). While these treatments can be extremely effective, there are many drawbacks – levodopa loses its effectiveness over time alongside the advent of debilitating dyskinetic side effects (Cenci and Lindgren 2007), and the invasive surgery for DBS harbors its own potential dangers and complications (Beric et al. 2001; Constantoyannis et al. 2005).

A major roadblock toward improving treatment of PD are holes in our knowledge of the underlying neurophysiological changes that occur in PD and how treatments affect or mask these changes (McGregor and Nelson 2019). In studying such neurophysiological changes in the Parkinsonian brain, PD also provides a window into understanding dopamine, motor control, and neural dynamics, in both health and disease.

In this chapter, we will briefly review the literature surrounding these topics. First, we will look at the evidence linking PD and animal models of PD, with a focus on dopamine depletion. Then, we will examine the existing literature on neural changes in the brains of PD patients and animal models of PD, with a focus on abnormal oscillatory activity.

1.1 CONNECTIONS BETWEEN DOPAMINE DEPLETION AND PD

Parkinson's disease (PD) is a neurodegenerative disorder characterized symptomatically by progressively worsening akinesia, bradykinesia, rigidity, and tremor, as well as non-motor symptoms such as sleep disturbances, depression, and cognitive deficits (Chaudhuri et al. 2006; Poewe 2008; Sveinbjornsdottir 2016). In the brain, typically observed in post-mortem studies, Parkinson's disease is characterized by the loss of dopamine (DA) neurons (Naoi and Maruyama 1999) and the presence of Lewy body inclusions in the substantia nigra pars compacta (SNc) (Gibb and Lees 1988), a region which normally provides dopaminergic innervation to the basal ganglia primarily by its projections to the striatum through the medial forebrain bundle (MFB).

Animal models of Parkinson's disease typically aim to replicate this disease symptomology through disruption of dopamine signaling. Toxins such as 1-methyl-4-phenyl-1,2,3,6-tetrahydropyridine (MPTP), which is typically administered systemically in monkeys, or 6-hydroxydopamine (6-OHDA), which is injected directly into the SNc, MFB or striatum in rodents, model PD through ablating dopaminergic neurons, which leads to a significantly impaired dopamine depleted (DD) brain state. Reversible pharmacological treatments, such as the injection of reserpine or dopaminergic antagonists, disrupt dopamine's packaging and release from the presynaptic terminal (Leão et al. 2015) or its ability to activate postsynaptic dopamine receptors, respectively, thereby silencing or greatly decreasing dopamine signaling. Genetic models knockout or introduce mutations into genes such as *LRRK2*, *PINK1*, *parkin*, and *α -synuclein* which are implicated in heritable forms of PD; these mutations lead to a more progressive loss of dopamine neurons, more closely mimicking the etiology of PD in human patients (Dawson et al. 2010).

Many complications lead to difficulties synthesizing the results from experiments across different species and models of PD, and a rich literature exists comparing and contrasting the findings from extensive studies on these and other animal PD models (Blandini and Armentero

2012; Blesa et al. 2012; Jackson-Lewis et al. 2012; Schober 2004). For instance, toxin models can quickly lead to a profound dopamine depletion, and thus cause profoundly debilitating motor symptoms. However, this swift time course fails to replicate the progressive onset of symptomatology observed in patients and the progressive loss of dopamine occurring for years before symptoms even begin to appear (Willard et al. 2019). In contrast, genetic models typically deplete dopamine from the brain much more gradually which more closely mimics the time course seen in human PD patients. However, such models may never yield PD-like symptoms, due to both a depletion of dopamine which only reaches asymptomatic preclinical levels and the long length of time it takes to reach such levels of depletion (Blandini and Armentero 2012; Dawson et al. 2010). These factors allow for compensatory effects in the brain to mask the symptoms that might have appeared in a swifter depletion model.

This makes it difficult to relate the physiology of these models to behavioral or motor deficits. More complicated still is the selectivity of the model. Systemic toxins such as MPTP or reserpine cast a wide net, affecting systems beyond dopamine that may not be perturbed in such a way in clinical PD. In contrast, a targeted injection with 6-OHDA requires an invasive surgery, confounding the inflammatory changes known to occur in PD (McGeer and McGeer 2004; Whitton 2007) and requiring control surgeries to correct for this.

A successful study must choose the right model for the question at hand, and a well-rounded study could be best served by the use of multiple models with opposing confounds; the intersection of results across models can give a clearer picture of what aspects of neurophysiology truly represent changes in PD and which are merely side effects of the chosen model. It is through such an argument from observations across many animal models of PD that at least one common thread is clear: a profound loss of dopamine signaling leads to PD-like akinesia, bradykinesia and rigidity across species. While symptoms may not appear until a sufficient level of dopamine signaling loss occurs, a measurement which can be difficult to make and compare across models, a significant loss of dopamine signaling leads to progressively

worsening PD-like symptoms, and as such, DD and other manipulations to the dopamine system serve as our primary experimental window to the physiology of PD in this work.

1.2 PARKINSONIAN NEUROPHYSIOLOGICAL CHANGES

Given the causal relationship between dopamine loss in the basal ganglia and PD-like motor symptoms, there still remains an important missing causal link between these two events: how does dopamine loss affect signaling in the brain, and which, if any, of these changes in neural signaling lead to Parkinsonian motor symptoms? There is a vast and contentious body of literature addressing these questions (Galvan and Wichmann 2008; Hammond et al. 2007).

The rate model provides one of the earliest explanations for Parkinsonian dysfunction in the brain, which follows from observed firing rates increases in two basal ganglia nuclei, the globus pallidus interna (GPi) and subthalamic nucleus (STN), and decreased firing rates in the globus pallidus externa (GPe) in DD models of PD in monkeys and rats (Miller and DeLong 1987; Pan and Walters 1988; Soares et al. 2004; Wichmann et al. 1999).

The physiological explanation for these firing rate changes in DD come from simple wiring diagrams of basal ganglia nuclei. Striatal projection neurons (SPNs) make up the vast majority of neurons in the striatum, the main input nucleus of the basal ganglia, and typically express either D1 or D2 receptors. When dopaminergic tone is lost, the differing dopamine receptors on these populations of neurons cause their spontaneous firing rates to diverge – D1-expressing SPNs slow their firing, while D2-SPNs quicken. This leads to opposite firing rate changes in these populations' targets. Specifically, D1-SPNs form the “direct pathway” by directly inhibiting the main output nuclei of the basal ganglia, the substantia nigra pars reticulata (SNr) and GPi, and this loss of inhibition in DD increases their firing rates. Meanwhile, D2-SPNs form an “indirect pathway” to these output nuclei by first inhibiting the GPe, and a DD-induced firing rate increase in D2-SPNs slows GPe. GPe, in turn, projects to D1-SPNs' primary targets, SNr and GPi, and compounds the effects of disinhibition from D1-SPNs to further raise SNr and

GPI firing rates. Finally, these output nuclei more strongly inhibit their primary target, the thalamus, which now fails to sufficiently excite the motor cortex (M1) and other motor targets. As such, motor signals that would normally travel through the basal ganglia are dampened or shut off.

While elegant, this model oversimplifies basal ganglia physiology. While the dichotomy of D1-SPNs as direct pathway neurons and D2-SPNs as indirect pathway neurons is elegant, its cleanliness falls apart in both directions. A sizable population of SPNs coexpress D1 and D2 receptors (Deng et al. 2006; Surmeier et al. 1996), and a neuron's dopamine receptor expression does not perfectly predict its projection targets – D1-SPN axons make passing synapses in GPe (Cazorla et al. 2014), though these may specifically target the arkypallidal GPe population which does not project to SNr and GPI (Ketzef and Silberberg 2021). An explicit connection between basal ganglia firing rates and motor activity is also mired with mixed evidence. In the striatum, the story remains relatively clear – optogenetic excitation of D1-SPNs in mice leads to clear, time-locked increases in motor activity, whereas excitation of D2-SPNs leads to time-locked freezing behaviors (Freeze et al. 2013). Elsewhere in the basal ganglia, the story is muddled – optogenetic excitation or inhibition of GPe fails to yield any clear behavioral change, requiring careful consideration of cell types to explain behavioral effects (Mallet et al. 2016; Mastro et al. 2017).

In PD and DD, there are further complications. While GPe and GPI alter their firing in DD as predicted by the rate model, changes in SNr firing rates are inconsistent, with most studies showing no change due to DD (Seeger-Armbruster and von Ameln-Mayerhofer 2013; Wichmann et al. 1999). Surgical ablation of GPI through a pallidotomy in PD attenuates motor symptoms (Dogali et al. 1995; Lozano et al. 1995; Vitek et al. 2003), consistent with the theory that GPI's overactive output causes Parkinsonian motor dysfunction, but ablation of GPe does not induce Parkinsonism as would be predicted (Soares et al. 2004). Indeed, high-frequency DBS can ameliorate PD symptoms when targeted at either GPI or GPe (Chiken and Nambu

2016; Vitek et al. 2012), despite their opposite roles in the rate model, and STN DBS increases the firing rate of already overactive GPi neurons (Hashimoto et al. 2003) while GPi DBS in monkeys increases firing rates in motor thalamus (Anderson et al. 2003), neither of which fit with the predictions of the rate model. In humans, it is difficult to compare firing rates to those of healthy control subjects as these studies are performed during surgery, but compared to patients with dystonia, GPi firing rates in PD patients are higher in at least certain parts of GPi, as expected, but there is no difference in the firing rates in GPe (Levy et al. 1997; Starr et al. 2005; Tang et al. 2007) or in striatum (Valsky et al. 2020). Altogether, these conflicting results suggest that the rate model is at best insufficient to completely explain Parkinsonian motor symptoms.

Other changes in neural firing pattern may instead underlie Parkinsonian dysfunction. Increases in the irregularity of neural firing has been observed in rodent and monkey models of PD – namely, regions of the basal ganglia which typically fire in a pacemaking fashion with high discharge rates such as GPe and SNr begin to exhibit a more irregular, Poisson-like firing pattern in DD (Filion and Tremblay 1991; Seeger-Armbruster and von Ameln-Mayerhofer 2013; Wang et al. 2010). This irregularity may be due to a downregulation of hyperpolarization and cyclic nucleotide-gated (HCN) channels in DD; however, while upregulation of HCN channels to healthy levels in GPe neurons leads to resumed pacemaking, DD-induced motor deficits are unchanged (Chan et al. 2011a), suggesting that irregularity in BG neurons may be a side-effect of DD rather than a cause of its motor symptoms.

Excessive bursting activity – short periods of time where several spikes occur from a neuron in quick succession – is also associated with a Parkinsonian state (Lobb 2014). Increased incidence and duration of bursts has been observed in the STN, GPe and GPi of MPTP-treated monkeys (Bergman et al. 1994a; Wichmann and Soares 2006) and in PD patients (Gale et al. 2009; Hutchison et al. 1994), though, as before, it remains difficult to compare this activity in PD to that of healthy control subjects. Neural oscillations, which we

explore more in the following section, can be interpreted (or misinterpreted) as regularly occurring bursts of activity, and it is possible that results regarding one can be conflated with the other. However, bursts can be observed both alongside or without oscillations in a single neuron and are argued as being distinct neural properties in the Parkinsonian basal ganglia (Chan et al. 2011b; Kaneoke and Vitek 1996). The relationship between non-oscillatory bursting activity and PD symptoms remains unclear; levodopa has conflicting effects on bursting activity, reducing the number of bursts slightly in GPi while having no effect on GPe (Boraud et al. 1998), while the effects of the dopamine agonist apomorphine on bursting in PD patients are inconsistent (Hutchison et al. 1997; Levy et al. 2001).

1.3 PARKINSONIAN NEURAL OSCILLATIONS

A firing pattern which has gathered substantial evidence and explanatory power in PD research is increased power of neural oscillations in a variety of frequency bands. Neural oscillations can be measured in the local field potential (LFP), a more easily recorded signal comprising the sum of electrical activity from many nearby neurons and their synaptic input, or in the spiking patterns of individual neurons themselves. Neural oscillations are correlated with a large number of normal processes throughout the brain (Buzsáki and Draguhn 2004), such as memory encoding (Ward 2003), attention (Fries et al. 2001) and sleep (Steriade et al. 1993). However, abnormal increases or decreases of power in certain frequency bands are also associated with disease states, such as schizophrenia (Uhlhaas and Singer 2010), epilepsy (Englot et al. 2015), dystonia (Starr et al. 2005), and PD. Two frequency bands have received particular attention in PD: beta oscillations, and lower frequency delta or theta oscillations.

1.3.1 Beta oscillations

In the PD literature, abnormally high beta power is the most well-studied oscillatory phenomenon. Beta oscillations have been observed in the LFP of several basal ganglia nuclei, thalamus and M1, but in human studies, the most common loci of interest have been the

subthalamic nucleus (STN) and globus pallidus interna (GPi) as they are the most common regions for surgical recordings during implantation of a DBS electrode. Many studies have shown a high level of beta power in LFP recordings from the STN and GPi (Halje et al. 2019; Hammond et al. 2007; Jenkinson and Brown 2011) and a smaller number of studies have shown such oscillations in the spike trains of individual STN and GPi neurons as well (Du et al. 2018; Weinberger et al. 2006). When simultaneous recordings of STN and GPi are performed, there exists a strong beta band coherence between the two nuclei (Brown et al. 2001; Cassidy et al. 2002), and similar studies have shown STN beta coherence to EEG, MEG or ECoG recordings in M1 or premotor cortex (Hirschmann et al. 2011; Lalo et al. 2008; Williams et al. 2002), suggesting synchronization of these oscillations across many motor-related brain regions.

Dissecting the relationship between beta oscillatory power and PD symptom severity is a more complicated task, but many studies have provided correlative evidence for this relationship. In cases of asymmetric Parkinsonism where one side of the body is more significantly affected, beta oscillations are stronger in the STN of the more affected (contralateral) hemisphere (Shreve et al. 2017). When performing motor tasks, execution is typically slower during bouts of cortical beta (Gilbertson et al. 2005), and periods of time with higher STN beta power predict higher motor error scores (Ahn et al. 2020), though this is also the case for other frequency bands. On the other hand, studies show an increase in STN-M1 beta coherence during movement (Belova et al. 2020; Hirschmann et al. 2013), which complicates the simple idea of beta as an akinetic signal.

Beta oscillations also tend to weaken in the STN with treatments such as levodopa in a manner proportional to symptom reduction (Weinberger et al. 2006; Ray et al. 2008; Brown et al. 2001; Alonso-Frech et al. 2006; Kühn et al. 2006; Giannicola et al. 2010), though some studies show a levodopa-induced increase in cortical beta power through non-invasive EEG (Melgari et al. 2014) and MEG (Cao et al. 2020) recordings. Indeed, cortical beta may have a

complex relationship with beta oscillations in the basal ganglia – corticospinal and corticomuscular coherence in the beta band is abnormally low in patients with PD, and this coherence is heightened back to normal levels with levodopa (Brown 2007; Salenius et al. 2002).

Studies on DBS give similar results, lending credence to the relationship between beta oscillations and PD motor symptoms but also providing some confusing contradictions. The power of beta oscillations at a DBS stimulation site is a predictor for its effectiveness at that site (Boëx et al. 2018). Beta oscillations tend to weaken during stimulation (Kühn et al. 2006, 2008; McCairn and Turner 2015) but in other studies are unaffected (Rossi et al. 2008), decrease in some patients but not others (Giannicola et al. 2010), or return before symptoms reemerge (Foffani et al. 2006), complicating the relationship between DBS, symptom reversal and beta oscillations.

Similar oscillations are observed in some animal models of PD, though the literature is significantly more contentious. Strong oscillations at slightly higher frequencies (25-35 Hz) occur in 6-OHDA lesioned rats and are termed beta oscillations, while lower frequencies (8–15 Hz) are referred to as beta in MPTP-treated monkeys (McCairn and Turner 2009; Raz et al. 2000). In these models, however, the link between beta oscillations and motor symptoms is less clear. In studies tracking symptoms and STN beta power over several days, beta oscillations did not increase until after symptoms arose and plateaued, a result found in both monkeys (Leblois et al. 2007) and rats (Mallet et al. 2008), and there appears to be no consistent correlation between symptoms and beta power across animal subjects or as symptoms progress in individual subjects (Muralidharan et al. 2016). Conversely, beta power in animal models does not consistently decrease when symptoms are treated with STN DBS (McConnell et al. 2012). Furthermore, high STN beta power can occur in both Parkinsonian and healthy animals (Connolly et al. 2015), though the key difference between healthy and Parkinsonian animals may be longer bouts of beta oscillations rather than stronger or more frequent bouts (Deffains et

al. 2018). Attempts to artificially induce beta oscillations in these animals have not been sufficient to cause PD-like symptoms of akinesia (Swan et al. 2019), though such attempts have recapitulated nontraditional PD motor symptoms such as blink abnormalities (Kaminer et al. 2014).

Altogether, these studies demonstrate a strong correlative relationship between beta oscillations, PD, and its motor symptoms. However, the relationship between human beta oscillations and the oscillations defined as beta in animal studies may be tenuous, and some conflicting human studies, particularly regarding the relationship between beta oscillations and various PD treatments, raises questions on whether beta oscillations are the whole story behind Parkinsonian dysfunction.

1.3.2 Delta oscillations

While beta oscillations have achieved significant attention in the PD literature and success in explaining its pathophysiology, increased power in the delta band has also been observed in studies of PD patients. The delta band in cortex is typically defined as 1–4 Hz; here, we include studies considering oscillations as high as 6 Hz, which covers the wide range of slow oscillations observed in BG nuclei in both human and animal studies but remains distinct from the higher frequency beta oscillations discussed in the previous section.

High delta power has been observed in the STN, GPi and motor thalamus of PD patients in LFP recordings and, more often, in the firing patterns of individual spiking neurons or multiunit spiking activity (Du et al. 2018; Steigerwald et al. 2008; Zhuang et al. 2019). In STN LFP recordings, many patients exhibit both delta and beta band oscillations, but more patients exhibit only delta oscillations than only beta oscillations (Levy et al. 2002). Similarly in motor thalamus, delta oscillations occur in more recorded neurons than beta oscillations (Du et al. 2018).

Delta oscillations in PD have often been referred to as tremor oscillations due to their typical coherence with Parkinsonian tremor (Bergman et al. 1994b). However, tremor-oscillating

neurons can exhibit these oscillations with or without a coherence to Parkinsonian limb tremor measured through electromyography (EMG) (Du et al. 2018; Hurtado et al. 1999). Individual delta oscillating neurons may also phase in and out of coherence with EMG signals over the course of a recording (Hurtado et al. 2005). Notably, these oscillations' relationship to other PD symptoms such as akinesia and rigidity has not been investigated in either human or animal studies, though their connection has been hypothesized (Magnin et al. 2000).

Similar oscillations have also been observed in animal models of PD. In monkeys, oscillations as low as 3–7 Hz have been observed (Raz et al. 2000; Heimer et al. 2006; McCairn and Turner 2009), but these have mostly been viewed as an extension of the beta band. In anesthetized rodents, oscillations at even lower frequencies (0.5–4 Hz) are most prevalent (Tseng et al. 2001a; Walters et al. 2007; Parr-Brownlie et al. 2009; Aristieta et al. 2016), but these have been mostly discounted as artifacts of anesthesia or artificial respiration (Ruskin et al. 2002). Indeed, delta oscillations in the striatum of 6-OHDA-lesioned rats were shown to have high coherence to anesthesia-induced slow waves in motor cortex (M1) (Tseng et al. 2001b; Belluscio et al. 2003) and were weakened after cortical ablation (Magill et al. 2001), leading to the conclusion that these oscillations merely infiltrate the basal ganglia through M1 and are not relevant to the awake, behaving Parkinsonian animal. Because experiments investigating the presence of sub-beta band oscillations in awake, behaving Parkinsonian animals have not been performed, however, this theory is uncertain.

1.4 SUMMARY AND AIMS OF DISSERTATION

Our understanding of Parkinson's disease neurophysiology is rich but incomplete. It is clear that a loss of dopamine signaling in the basal ganglia leads to widespread neural dysfunction in basal ganglia nuclei and other movement centers in the brain such as M1 and motor thalamus; in particular, these regions experience a stark increase in their individual spectral power and coherence between regions in multiple oscillatory bands. However, a

number of unanswered questions remain. Which oscillatory bands are critical and causal to Parkinsonian motor dysfunction, and in which brain regions? If such abnormal patterning is causal to motor symptoms, how does it exert this influence? By what mechanism does a loss of dopamine lead to the appearance of these oscillations, and how do they propagate through the brain?

In this dissertation, we attempt to answer some of these questions, utilizing mouse models of Parkinson's disease and computational models derived from that experimental data. In Chapter 2, we characterize the oscillatory landscape of the dopamine depleted basal ganglia, with a focus on its main output nucleus in the mouse, the SNr. We also explore how these oscillations relate to motor symptoms and by what mechanisms they arise. In Chapter 3, we take a biophysical modelling approach to dissect how these oscillations propagate through the brain and lead to the unique neurophysiology we observe in the dopamine depleted SNr. In Chapter 4, we summarize our findings and future directions for these topics. We also discuss how our results relate to the overall literature and improve our understanding of Parkinson's disease and oscillatory dynamics.

2 DELTA OSCILLATIONS INDICATE SEVERITY OF DOPAMINE DEPLETION AND MOTOR DYSFUNCTION

Delta oscillations are a robust feature of basal ganglia pathophysiology in Parkinson's disease (PD) patients in relationship to tremor, but these oscillations' relationship to other Parkinsonian symptoms has not been investigated. While delta oscillations have been observed in mouse models of PD, they have only been studied in anesthetized animals, which suggests that the oscillations may be an anesthesia artifact and has limited the ability to relate them to motor symptoms.

In this chapter, we establish a novel approach to detect spike oscillations embedded in neural noise to study delta oscillations in awake, DD mice. We find that approximately half of neurons in the substantia nigra pars reticulata (SNr) exhibit delta oscillations in dopamine depletion and that these oscillations are a strong indicator of dopamine loss and akinesia, outperforming measures such as changes in firing rate, irregularity, bursting and synchrony. These oscillations are typically weakened, but not ablated, during movement. We further establish that these oscillations are caused by the loss of D2 receptor activation and do not originate from motor cortex, contrary to previous findings in anesthetized animals. Instead, SNr oscillations precede those in motor cortex (M1), and these neurons' relationship to M1 oscillations can be used as the basis for a novel classification of SNr into two subpopulations. These results give insight into how dopamine loss leads to motor dysfunction and suggest a reappraisal of delta oscillations as a marker of akinetic symptoms in PD.

2.1 INTRODUCTION

The oscillatory landscape of basal ganglia nuclei and motor cortical regions has been studied in patients with Parkinson's disease as well as in animal models of PD. While beta oscillations have received the most attention in studies, lower frequency delta oscillations appear prominently in both PD patients (Du et al. 2018; Levy et al. 2002; Steigerwald et al. 2008; Zhuang et al. 2019) and animal models under anesthesia (Aristieta et al. 2016, 2019; Tseng et al. 2001b, 2001a; Walters et al. 2007). These oscillations are often termed "tremor frequency" oscillations due to their typical coherence with Parkinsonian tremor (Bergman et al. 1994b), though neurons can exhibit these oscillations with or without this tremor coherence (Du et al. 2018; Hurtado et al. 1999), or in a more complex, time-varying fashion (Hurtado et al. 2005). Meanwhile, these oscillations' relationship to other PD symptoms such as akinesia and rigidity has not been investigated.

A major confound in animal studies of these low frequency oscillations in DD has been the use of anesthesia which, even in healthy animals, elicits a strong delta oscillation throughout cortex. Indeed, delta oscillations in the striatum of anesthetized 6-OHDA-lesioned rats were shown to have high coherence to anesthesia-induced slow waves in M1 (Tseng et al. 2001b; Belluscio et al. 2003) and were weakened after cortical ablation (Magill et al. 2001). This led to the conclusion that delta oscillations in DD are merely anesthesia-induced slow waves infiltrating the basal ganglia through M1's corticostriatal projections and are not relevant to the awake, behaving Parkinsonian animal.

No experiments have been performed exploring the oscillatory landscape of the basal ganglia in awake, DD mice. This fact, despite mice frequently being used as a model for PD, has led to a dearth of understanding of Parkinsonian oscillations in these animals and, critically, how they relate to movement and Parkinsonian motor symptoms.

One factor limiting these investigations, particularly at frequencies near or below 1 Hz, is the high levels of noise that contaminate low frequency signals, particularly during awake

recordings. So-called “1/f”, “pink”, or “flicker” noise is most prevalent at low frequencies and typically observed in LFP recordings but is also present in the spiking of individual neurons. This complication makes reliable detection of delta oscillations difficult with current methods, which in turn makes it difficult to relate these signals to Parkinsonian behavior and untangle their dynamics within individual regions and across the brain.

Here, we develop a method to reliably distinguish spike oscillations from noise and use this approach to characterize the oscillations we observe in DD mice. We focus on the SNr, the major output nucleus of the mouse basal ganglia which encodes motor information (Barter et al. 2015) and projects to downstream motor areas (Capelli et al. 2017; Roseberry et al. 2016). We demonstrate that delta (0.5–4 Hz), not beta, oscillations are the primary oscillatory feature in SNr neurons after loss of dopamine, and that the strength of delta oscillations is both predictive of an animal's overall level of motor dysfunction and correlates with akinesia on a moment-to-moment basis.

We show that, contrary to prior reports, delta oscillations in the SNr precede those in M1, and that M1 is not necessary for these oscillations to develop in the SNr. Moreover, the latency and sign of SNr neurons' relationship to oscillations in M1 subdivide SNr into two novel subpopulations. We also establish that a loss of D2 receptor activation is sufficient to immediately and reversibly generate both delta oscillations and PD-like akinesia in awake mice, suggesting a direct link between dopamine loss, delta oscillations, and Parkinsonian symptoms. Altogether, these results provide evidence that delta oscillations in basal ganglia neurons are a critical component of Parkinsonian pathology in DD mice and suggest that DD mice may be a valuable model of the low frequency oscillations seen in PD patients.

2.2 MATERIALS AND METHODS

2.2.1 Animals

All experiments were conducted in accordance with guidelines from the National Institutes of Health and with approval from the Carnegie Mellon University Institutional Animal Care and Use Committee. Male and female mice on a C57BL/6J background aged 8-15 weeks were randomly allocated into experimental groups (e.g. Control, Bilateral 6-OHDA, Reserpine, etc.), except insofar as to ensure that male and female mice were both represented in every group.

2.2.2 Stereotaxic surgery

2.2.2.1 Headbar implantation

Animals were anesthetized with 20 mg/kg ketamine and 6mg/kg xylazine and placed in a stereotaxic frame (Kopf Instruments). Anesthesia was maintained throughout surgery with 1.0-1.5% isoflurane. All coordinates were measured in mm with AP and ML measured from bregma and DV relative to the dural surface. The scalp was opened and bilateral craniotomies (for later probe insertion) approximately 1.5 x 1.5 mm in size were drilled over SNr (AP: -3.00, ML: ± 1.50), GPe (AP 0.00, ML: ± 2.12), or STN (AP: -1.70, ML: ± 1.52). A custom-made copper or stainless steel headbar was affixed to the mouse's skull with dental cement (Lang Dental). A well of dental cement was then built around the exposed skull (see *in vivo recordings*) and filled with a silicon elastomer.

2.2.2.2 Dopamine depletion

A hole was drilled on one (for unilateral) or both (for bilateral) hemispheres of the skull over the medial forebrain bundle (MFB, AP: -0.80, ML: ± 1.10). A unilateral infusion cannula (PlasticsOne) was slowly lowered into the brain 5mm below the dura. 1 μ L of 5 μ g/ μ L 6-OHDA (Sigma-Aldrich) or 0.9% saline was injected over the course of 5 minutes with a GenieTouch Hamilton syringe pump (Kent Scientific). The infusion cannula was left in place for 5 minutes

post-injection before being slowly retracted. For animals undergoing bilateral depletion, this process was repeated on the opposite hemisphere.

2.2.2.3 Cannula implantation

For experiments involving acute drug infusion into the MFB or gradual dopamine depletion with 6-OHDA, a bilateral guide cannula (Plastics One) was implanted (same coordinates as dopamine depletion) using dental cement (Lang Dental) and a dummy cannula was placed in the guide. Before infusion, the dummy was replaced with an infusion cannula and attached to the same Hamilton syringe pump as above. Gradually depleted animals were infused with 1 μ L of 0.75 μ g/ μ L 6-OHDA every 5 days (See Willard et al 2019 for full details).

2.2.2.4 ECoG connector implantation

For experiments involving electrocorticogram (ECoG) recordings, a male gold connector (Ampityco Electronics) was soldered to a stainless steel wire, and the connector was gently lowered above left or right motor cortex (M1, AP: +1.40, ML: \pm 1.00) such that the wire touched the dural surface then secured in place with dental cement (Lang Dental).

2.2.2.5 Aspiration lesions

For experiments involving M1 lesion, a craniotomy was drilled bilaterally over M1 (AP 0.0-2.5, ML 1.0:2.5) and the dura was removed. Using a 20-gauge suction tube (Miltex) attached to a vacuum source, we aspirated cortex to a depth of 2.1 mm on the medial side of the craniotomy gradually decreasing to 2.5 mm near the lateral side of the craniotomy, but leaving the most ventrolateral portion intact to preserve somatosensory cortex. In the anterior portion of the craniotomy, the mediolateral extent of the lesion was approximately 2.4–1.0 mm, becoming gradually less lateral to approximately 1.7–1.0 mm in the posterior portion. The craniotomy was periodically lightly rinsed with saline. We filled the lesioned space with triple antibiotic (bacitracin, neomycin, polymyxin) before sealing the craniotomy with a silicon elastomer (Smooth-On)

The size and location of lesions was confirmed post-hoc through imaging sections of the brain tissue (see Histology). Of the lesioned animals included in the study, two brains were sectioned sagittally and two coronally to get the best sense of the 3-dimensional extent of the lesions. We compared the sections to a mouse brain atlas (Paxinos Mouse Brain Atlas in Stereotaxic Coordinates, Second Edition) to ensure that M1 was entirely lesioned (two of the six animals which underwent aspiration were excluded at this point due to insufficient aspiration depth). In our endeavor to ensure that M1 was completely lesioned, some other brain regions were also partially lesioned. In 2 of the 4 animals, the cingulum was partially lesioned due to excessive aspiration ventrally, and a small portion of the dorsal striatum was erroneously removed contralateral to the recording site in one animal. Small portions of medial S1, particularly on the posterior edge of the lesion, and very small portions of the lateral edge of M2 were removed in each animal.

2.2.2.6 Post-operative care

Upon completion of surgery, animals were injected subcutaneously with 0.5 mg/kg ketofen and placed inside their cage half on/half off a heating pad to recover. Dopamine depleted animals were supplied with trail mix and moistened food to maintain weight and hydration, in addition to their usual food pellets and water bottles, and animals were tracked regularly to ensure proper health and weight.

2.2.3 Drugs

In addition to the drugs used above during surgery, animals were given the following drugs (Sigma-Aldrich, except when specified) dissolved in 0.9% saline (except when specified). For reserpine depletions, animals were injected i.p. daily for three days with 5 mg/kg reserpine in 2% acetic acid (diluted in 0.9% saline). For recordings involving dopamine agonists and antagonists, animals were injected i.p. during recording with either 0.4 mg/kg SCH22390, 3 mg/kg raclopride, 1 mg/kg SKF81297 (Tocris Biosciences), or 3 mg/kg quinpirole. Acute infusions into the MFB used 2% lidocaine.

2.2.4 *In vivo* recordings

Mice were head-fixed atop a free-running wheel (Heiney et al. 2014). After acclimation to head-fixation for ten minutes, the silicon elastomer was removed and craniotomies were cleaned with saline. Using a micromanipulator (Sutter Instruments), a linear microelectrode probe with sixteen channels spaced 50 μm apart (NeuroNexus) was lowered into the craniotomy at the coordinates listed above for SNr, GPe or STN. After the initial lowering, a ground wire was placed in saline in the dental cement well on the skull. Once the top of the nucleus (SNr, -4.0mm, GPe: -3.60mm, STN: -4.00mm from the top of the brain) was found and high firing rate units were observed, the probe was held stable for at least ten minutes prior to recording. Spiking (bandpass filtered for 150-8000 Hz, sampled at 40 kHz) and local field potential (bandpass filtered to 0.5-300 Hz, sampled at 1 kHz) recordings were collected through an OmniPlex amplifier (Plexon, Inc.) with common median virtual referencing. After recording for at least three minutes, the probe was lowered to obtain recordings from the full dorsal-ventral extent of the nucleus. Simultaneous to these recordings, the mouse's walking speed on the wheel was recorded using an optical mouse and fed to a TTL-pulser which was connected to the OmniPlex amplifier analog input. For ECoG recordings, the gold implant was connected to a headstage with a ground wire in saline on top of the skull. The headstage was connected to an amplifier (A-M Systems) with 1000x gain and 0.1–500 Hz bandpass filtering and this amplifier was connected to the OmniPlex amplifier analog input.

2.2.5 Histology

After recording, animals were sacrificed and perfused with 4% paraformaldehyde (PFA). The brain was extracted from the skull and stored in PFA for 24 hours then moved to a 30% sucrose solution for at least 24 additional hours. Tissue was sectioned using a freezing microtome (Microm HM 430; Thermo Scientific) and primary antibody incubations were performed on these sections at room temperature for 24 hours. A tyrosine-hydroxylase (TH) antibody (rabbit anti-TH, 1:1000; Pel-Freez) was used to confirm successful dopamine depletion

in 6-OHDA-depleted animals; animals required at most 15% TH fluorescence compared to controls on both hemispheres (for bilateral 6-OHDA injection) or the contralateral hemisphere (for unilateral 6-OHDA injection) to be considered for analysis. and an Iba1 antibody (rabbit anti-Iba1) for microglia activation was used to confirm probe location and guide cannula placement in animals undergoing infusion during recording. Epifluorescent images were taken at 10x magnification (Keyence BZ-X) and outlines of nuclei of interest were overlaid on the images (from Paxinos Mouse Brain Atlas in Stereotaxic Coordinates, Second Edition).

2.2.6 Data pre-processing

Spikes were manually sorted into single units using Offline Sorter (Plexon). For classification as a single unit, the following criteria were set: 1) principal component analysis of waveforms generated a cluster of spikes significantly distinct from other unit or noise clusters ($p < .05$), 2) the J3-statistic was greater than 1, 3) the Davies-Bouldin statistic was less than 0.5, and 4) fewer than 0.15% of ISI's were less than 2ms. In the case where a unit was lost during recording, it was only used in analysis for the time period when its spike cluster satisfied these criteria, and only if its cluster was present for at least three minutes. Data were then imported into MATLAB (MathWorks) in which all further analysis was performed using custom code except when specified.

Since units must fire quickly enough to exhibit an oscillation, only units with a firing rate greater than 5 Hz (over 95% of sorted units) were considered for analysis. As ECoG signals were occasionally corrupted for short time windows, generally due to muscle activity, we visually determined a noise threshold for each recording and zeroed any length of signal within 250 milliseconds of any data point whose absolute value exceeded that threshold. ECoG signals were then delta (0.5–4 Hz) bandpassed using a 2nd order Butterworth filter, except for analyses looking at higher frequency bands.

2.2.7 Oscillation detection and visualization

2.2.7.1 Renewal-Corrected Power Spectrum

For each unit, we downsampled its spike train to 1 kHz and split it into segments of 2^{12} ms, advancing from one segment to the next with time step size $\Delta s = 2^9$ ms. For each segment, we calculated its interspike interval (ISI) probability distribution, $P_0(t)$. We calculated $\hat{C}_0(\omega)$, the theoretical power spectral density (PSD) of a renewal process defined by $P_0(t)$ scaled by the number of spikes in the segment:

$$\hat{C}_0(\omega) = Re \left(\frac{1 + \hat{P}_0(\omega)}{1 - \hat{P}_0(\omega)} \right) n$$

where $Re(x)$ indicates the real part of x , $\hat{P}_0(\omega)$ indicates the Fourier transform of the ISI distribution in appropriate frequency units, and n is the number of spikes in the segment. This is a variant of a method presented previously for calculating $\hat{C}_0(\omega)$ analytically rather than approximating it through Monte Carlo shuffling simulations (Rivlin-Etzion et al. 2006).

We next calculated an estimate of the PSD of the spike train in that segment:

$$\hat{C}_\infty(\omega) = |FFT(x(t))|^2$$

where $x(t)$ is the mean-subtracted spike train in the segment, FFT is the fast Fourier transform (MATLAB function *fft*) and vertical bars indicate absolute value. Finally, we normalized this estimate to achieve the renewal-corrected PSD of a single segment:

$$\hat{C}(\omega) = \frac{\hat{C}_\infty(\omega)}{\hat{C}_0(\omega)}$$

and averaged $\hat{C}(\omega)$ values across segments to obtain the renewal-corrected PSD. All PSD's in this study have undergone this renewal-correction, but are simply referred to as PSD's for brevity.

2.2.7.2 Phase Shift

For the k th time segment, we calculated the uncorrected phase $\tilde{\phi}$ at each frequency:

$$\tilde{\phi}(\omega, k) = \tan^{-1} \left(FFT(x(t)) \right)$$

and made the following correction such that the phase of each frequency is defined relative to the start of the recording rather than the start of the segment:

$$\phi(\omega, k) = \text{mod}(\pi + (\tilde{\phi} - 2\pi\omega(k-1)\Delta s), 2\pi) - \pi$$

where *mod* is the modulus operator and Δs is the time step between adjacent segments (here, $2^9/1000$ seconds). In other words, for each frequency, imagine a perfect oscillator with zero phase at the start of the recording. For each segment, we determined what phase this oscillator would reach at the start of the segment and defined that phase to be zero for that segment. This correction ensures that a perfect oscillator would have the same corrected phase ϕ for every segment.

After computing the corrected phase of all segments, we approximated the time derivative $\phi_s(\omega, k)$ by computing the difference of phase across successive time steps and averaged over each difference to obtain the average absolute rate of phase shift:

$$\xi(\omega) = \frac{1}{N-1} \sum_{s=1}^{N-1} |\phi_s(\omega, k+1) - \phi_s(\omega, k)|$$

where N is the number of segments. For brevity, we refer to $\xi(\omega)$ as the phase shift.

2.2.7.3 Oscillation Detection

We detected oscillations in a two-step process by first seeking frequencies with high power and then determining whether these frequencies also had low phase shift.

To determine whether a unit reached statistically significantly high power at a particular frequency, we found each local maximum of $\hat{C}(\omega)$, defined as a value higher than its three neighbors on both sides, within the band 0.5–4 Hz (or 7–35 Hz for detecting beta oscillations). We then estimated a 99% confidence interval of renewal-corrected power from the region of $\hat{C}(\omega)$ between 250 and 500 Hz, correcting for multiple comparisons (Bonferroni correction) of all frequencies in the band of interest. A peak of $\hat{C}(\omega)$ was considered significant if it fell above this confidence interval.

As our second step, we determined if any frequency detected in the previous step had a significantly low phase shift. We estimated a 95% confidence interval of phase shifts from the region of $\xi(\omega)$ between 250 and 500 Hz, correcting for multiple comparisons (Bonferroni correction) if multiple frequencies were detected from the PSD. We concluded that an oscillation was present at a frequency with significant power if the phase shift at that frequency fell below this confidence interval.

2.2.7.4 Spike Spectrograms

For time frequency analyses, the process outlined in section 2.2.7.1: Renewal-Corrected Power Spectrum was modified to use segments of length 2^{13} ms with 2^{11} ms overlap to improve visualization. Rather than averaging over segments, the resultant matrix was smoothed with a 3x3 2-D gaussian filter and plotted as a normalized heatmap (MATLAB function *imagesc*). Due to the loss of fine frequency resolution at low frequencies, this procedure was only used on spike trains in which an oscillation was detected in the previous procedure.

2.2.8 Neural measures

Beyond oscillations, we investigated several other neural measures – firing rate, firing variability, bursts and synchrony. A unit's firing rate was defined as its number of spikes divided by the total time of recording. Variability was measured as the coefficient of variation (standard deviation divided by mean) of a unit's interspike intervals. Bursts were quantified using the Poisson surprise algorithm (Legendy and Salzman 1985) with a surprise threshold of 5, initial firing rate threshold of 200% of baseline calculated over the entire recording, and removal of any burst with fewer than 3 spikes.

To determine if two units were synchronous, we used the method and parameters outlined in Willard et al. 2019, which determines the fraction of synchronous spikes above chance after correcting for nonstationarity in a unit's firing rate (Willard et al. 2019). In brief, we windowed both spike trains into 12-second segments and zeroed the first and last four seconds of the segment taken from the second spike train. We performed cross-correlation with a

maximum lag of four seconds. Since this maximum lag is equal to the length of time zeroed on the second spike train, this ensures a constant number of non-zero-padded comparisons (n_c) at each lag, as opposed to traditional cross-correlation in which n_c is a function of lag. We divided the cross-correlogram for the segment by the mean value from 0.5–4 seconds on both sides, which allows the correlation's units to be interpreted as the fraction of spikes greater than chance at a given lag (where 1 = chance). We repeated this process on overlapping segments (time step = 4 seconds) and then averaged these results together to get the mean, nonstationarity-corrected cross-correlogram. We generated a 99% confidence interval from the data with lag ≥ 0.5 s (which is a reasonable null distribution due to n_c , and thus the variance of the correlation estimate, being held constant). We conclude that a pair is synchronous if its normalized cross-correlation at lag zero is larger than the upper boundary of this confidence interval.

2.2.9 Behavioral testing and metric

Full details on the behavioral testing and the principal component analysis (PCA) metric for gradually depleted animals can be found in Willard et al. 2019. In brief, PCA was performed on the following metrics from behavioral tests: mean speed in an open field, number of rears in 10 minutes in a small enclosure, total time spent traversing a pole task, and latency to fall on a wire hang task.

2.2.10 Linear regression

Linear regression was performed using ordinary least squares. To determine if a linear fit was statistically significant, we computed 1000 fits each using a random subsample containing 80% of the data. We computed a bootstrapped confidence interval of the slope of this linear relationship from the middle 99% of the slopes of these 1000 fits, and the relationship was considered significant if this interval did not include zero.

2.2.11 Decision tree regression

We sought to determine the relationship between dopamine loss, motor symptoms and neural firing by predicting animals' TH immunofluorescence (see *Histology*) and the first principal component (PC1) of their behavior (see *Behavioral Testing and Metric*) from four physiological measures (see *Neural Measures*) and prevalence of delta oscillations. Firing rate, CV and bursts/second were averaged across all neurons for each animal, synchrony was measured as the fraction of synchronous pairs of units, and oscillations were measured as the fraction of delta oscillating units. Because of the highly nonlinear nature of these parameters' relationships to dopamine loss and behavior (Willard et al. 2019), we used a variant of decision tree regression, a highly nonlinear regression method.

We built an individual tree on 80% of the data (20 animals) using the *fit* method of the `DecisionTreeRegressor` class in the `scikit-learn` package for Python to predict the percent of TH remaining (Y) from the above neuronal parameters (a set X). In brief, this method places all training data at the topmost node of a tree and calculates the mean squared error (MSE) of this node as if each animal's TH were estimated to be the mean TH of every animal at the node. We determined, for each parameter X, the threshold T that would most reduce the mean squared error (MSE) of the animals if they were to be estimated in two different sets depending on whether their value of X is "greater than" or "less than or equal to" T. We then found the parameter for which the best T most reduces that MSE and split the animals at that node into two new child nodes according to the identified threshold. We iteratively repeated this process at every node until all terminal nodes had two or fewer animals at them, at which point each terminal node is termed a "leaf" of the tree.

We tested the remaining 20% of the data (5 animals) using the `DecisionTreeRegressor` *test* method, which runs each animal through the tree (picking $>$ or \leq at each node as determined by the animal's data) until it reaches a leaf. The mean value of Y at each leaf is the

prediction for that animal. We computed the error of the tree as the root-mean-squared error (RMSE) of its 5 predictions.

We computed a forest of 1000 such trees through subsampling the data into training and testing sets (Monte Carlo cross-validation) and calculated the top and bottom 2.5 percentiles to approximate a 95% confidence interval for the forest. We generated an intercept-only forest (using no parameters in the training set) and oscillation-only forest (using only the fraction of oscillations and an intercept term in the training set) on the same 1000 bootstrapped training and testing sets.

The importance of each parameter was determined using a variant on permutation importance. For a given parameter and tree, consider the set S of values for that parameter in the test set. We produced pseudo-test data with every derangement of S (i.e. 5 animals \times 44 derangements of 5 values = 220 pseudo-test animals with shuffled data for one parameter). The difference between the RMSE of the real test data and the pseudo-test data is the importance of that parameter for that tree. To determine the parameter importance for the entire forest, we approximate a 95% confidence intervals as above from the 1000 trees.

A forest predicting the first principal component (PC1) of behavior instead of % TH remaining was computed in the same manner.

2.2.12 Movement analysis

To analyze how oscillations were affected by movement, we considered recordings during which the animal was both stationary and voluntarily walked or ran on the wheel for at least 8 FFT windows each. Windows were considered “rest” if there was no detected movement and were considered “movement” if there was at least two seconds of not necessarily consecutive movement in the window. Since noise in any individual unit’s spike train was typically consistent over time, we were able to directly compare each unit’s delta power during rest and movement. To do so, we took the mean of the renewal-corrected PSD’s computed for

these windows to generate the average rest and movement PSD's and identified the 0.5–4 Hz peak in each PSD.

2.2.13 Time series regression

To determine if SNr neurons have a significant lead/lag relationship with M1, we built a series of regression models predicting an M1 ECoG signal from the spiking of a single SNr unit at various lags. First, we binned the ECoG into 10ms bins and defined the dependent variable Y as the difference between adjacent ECoG measurements to reduce nonstationarity. We then built a 10th order autoregressive model of Y which served as the null model.

To incorporate SNr firing into the prediction, we calculated the spike density function (SDF) for an SNr unit by convolving its spike train with a Gaussian function with a standard deviation of 100 ms. We then aimed to determine which time shift of the SDF best improves the prediction of the ECoG. One might use a distributed lag model for this task, where the explanatory variables consist of the time shifted ECoG (autoregression) and all considered time shifts of the SNr SDF simultaneously in a single model, but the multicollinearity of the SDF at different time shifts can heavily bias the regression coefficients. Instead we assumed that, if a lag exists by which the unit firing influences the ECoG or vice versa, then there is only one such lag by which this influence occurs. Thus, we could build an individual model for each time shift of the SDF. Each model used the 10th order autoregressive terms and one SDF term shifted from between -100 and +100 bins (-1000 to +1000 ms) as its explanatory variables. We built 201 such models, which covers the entire range of lags at 1 bin increments.

To determine if a significant lead/lag existed, we found the best model as determined by its mean squared error (MSE). We then determined if the model at this lag was significantly better than the null autoregressive model by performing an F-test at $\alpha < 0.05$, correcting for 201 comparisons (Bonferroni correction). As choosing ECoG as the independent variable and using autoregressive terms from the past could introduce bias in favor of SNr predicting M1, we also performed these analyses using SNr as the independent variable (i.e. computing a null

autoregressive model for SNr spiking and then computing 201 models at distinct ECoG time shifts to compare to the null), and performed the same analysis as above but in backwards time (i.e. building an autoregressive model of the ECoG from future ECoG samples). These analyses gave very similar results to the original analysis but were omitted for brevity.

To predict neural firing from the spike train of a simultaneously recorded neuron, we used a similar procedure. Instead of the continuous ECoG signal, we used spike counts from an individual neuron as the response variable. We performed generalized linear regression with a log link function (i.e. Poisson regression) using the MATLAB function `glmfit`, which optimizes the coefficients using Fisher's scoring method. When reporting residuals for the generalized linear models, we used deviance residuals. Heatmaps of deviance residuals over time computed the residuals over a moving 5-second window with a step of 25 ms.

2.2.14 Quantifying neural phase lags

To quantify the oscillation phase lags between pairs of units, we first computed the SDF of each oscillating unit using a Gaussian filter with $\sigma = 50$ ms, a value long enough to smooth fast fluctuations in spiking but preserve lower frequency delta oscillations. For each pair, we performed cross-correlation using a moving window procedure to minimize the effects of nonstationarities in firing rate over the course of the recording. We used a window size of 20 seconds with a maximum lag of 4 seconds and zeroed the first and last 4 seconds of the one of the SDF's to ensure the correlation computation at each lag would have an equal amount of zero-padding. We then divided the cross-correlation by its mean at lags greater than 4 seconds so that the value at each lag could be interpreted as a fraction of the neuron's mean firing rate. This procedure was computed on every window with a moving window step size of 8 seconds then averaged together to obtain the final normalized cross-correlation between the two signals.

Since most data did not include an ECoG reference to determine the SNr neuron's identity (AP or IP), we determined that the pair was in the same population if their cross-correlation peak was closer to lag zero than their trough, and different populations if their trough

was closer to lag zero than their peak. We defined their relative phase as the absolute value of the lag at which this extreme occurred (whether peak or trough).

2.2.15 Statistical tests

Statistical tests were performed to establish if fractions of oscillatory units and fractional ECoG bandpowers were significantly different across conditions. For comparisons with two groups, a two-sample t-test was performed, unless data were paired before and after a manipulation (e.g. acute drug infusion), in which case a one-sample t-test was performed. For comparisons with multiple groups compared against a control group, a one-way ANOVA was performed, and if this reached significance at the $\alpha = 0.05$ level, a Dunnett's post-hoc test was performed to determine if there were individual differences comparing groups to control. Asterisks above comparisons in figures correspond to *: $p < 0.05$, **: $p < 0.01$, *** $p < 0.0001$.

2.3 RESULTS

2.3.1 Dopamine depleted mice exhibit 0.5–4 Hz spike oscillations in SNr units

We recorded single units from the substantia nigra pars reticulata (SNr) of awake, head-fixed mice (Figure 2-1A–B) that had been bilaterally dopamine depleted with 6-OHDA or injected instead with saline. To investigate oscillations in the spiking activity of single units, we first examined spike trains and their autocorrelograms for the full extent of recordings (regardless of motor activity). In control animals, units typically fired in a regular, pacemaking pattern, indicated by a fast oscillation in their autocorrelograms which corresponded to the interspike interval of pacemaking and flattened within 20-100 ms (Figure 2-1C). In contrast, units in bilaterally dopamine depleted animals exhibited autocorrelograms that showed much slower oscillations between 0.5 and 4 Hz that remained autocorrelated for several seconds, visible in the raw spike trains as peaks and troughs or pauses in firing (Figure 2-1D). The units tended to exhibit oscillations around a particular frequency in the 0.5 – 4 Hz range that was

consistent for oscillating units within the animal but differed between animals. These slow oscillations were never observed in the autocorrelograms of units from control animals.

2.3.2 Phase shift analysis distinguishes delta oscillations and neural noise

First, we sought to reliably quantify these oscillations in DD mice. Neural noise is more prevalent in awake than anesthetized animals, and typically manifests in a power law fashion (called “pink” or “flicker” noise) such that it is dominant in low frequencies. Since the oscillations we observe in SNr units in DD were in the range typically tainted by pink noise, we could not reliably detect them using standard approaches based solely on the power spectral density or transformations of it. Specifically, random peaks in the power spectral density atop pink noise, or the pink noise itself, can easily be misidentified as an oscillation of interest (Figure 2-2C)

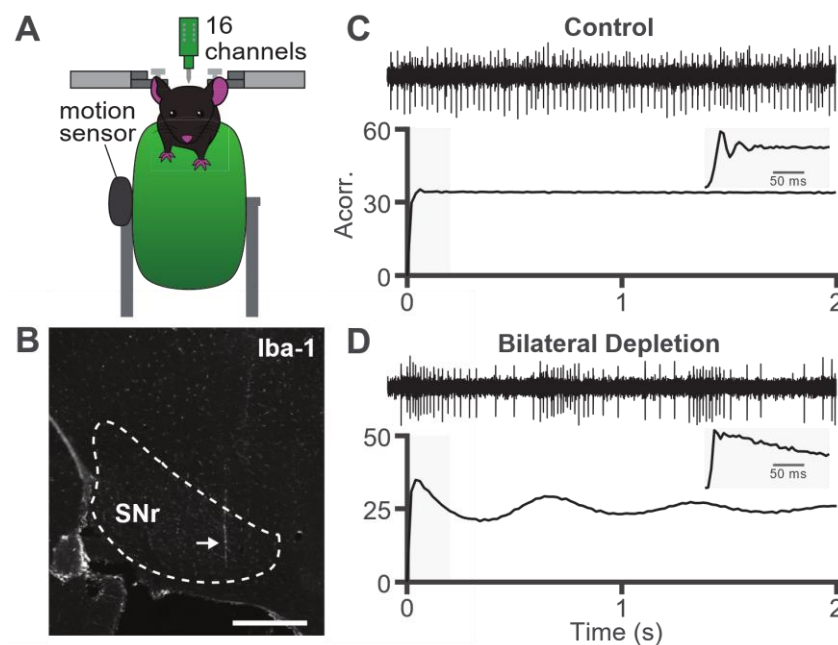


Figure 2-1: Dopamine depletion leads to low frequency spiking oscillations in SNr units.

A. Schematic of recording setup. Mice were head-fixed atop a free-running wheel with attached movement sensor and single units were recorded with a 16-channel probe. **B.** Example sagittal slice with IBA immunofluorescence showing location of the recording probe in SNr. Dotted line indicates approximate location of target nucleus, arrow indicates probe location. Scale bar = 500 μ m. **C.** Two seconds of an example SNr unit firing from a control animal (top) and the unit's autocorrelation (bottom). Inset is zoomed into the first 200 milliseconds of the autocorrelation using a smaller bin size. **D.** Same as **C** for a bilaterally dopamine depleted animal.

To overcome false positive detections, we used both the power and phase information provided by the short time Fourier transform to identify oscillatory components of spike trains with consistent phase over time (see Methods). By requiring that an oscillation have both high spectral power and low phase shift (Figure 2-2A), we successfully distinguished the oscillations of interest embedded in pink noise from the noise itself (Figure 2-2B). Notably, spike trains that exhibit a relatively flat autocorrelation but have delta peaks in their PSD are successfully disregarded as oscillators when phase shift analysis is applied (Figure 2-2C).

2.3.3 Delta, not beta, oscillations in SNr units are a marker of dopamine depletion

Using this detection method, we observed that very few SNr units from control animals exhibit an oscillation in the 0.5–4 Hz range (2 of 85 units pooled across animals), whereas in each bilaterally dopamine depleted animal, 33–92% of units exhibited significant delta oscillations (117 of 226 units pooled) three days after depletion (Figure 2-3A). Without using the phase shift criterion, a much greater number of units were flagged as oscillating, particularly in control mice (28% of units vs 2% after phase shift correction, Figure 2-3B), despite these units having a nearly flat autocorrelation as in Figure 2-2C. To determine whether these oscillations remained stable at longer time points after depletion, we recorded from the SNr of unilaterally depleted mice 2-4 weeks after depletion. We found that a significant proportion of SNr neurons still exhibited delta oscillations at these later time points (22–82% for each animal, 48 of 83 units pooled), suggesting that these oscillations are a stable feature of basal ganglia pathophysiology following dopamine depletion. A small number of units on the contralateral side of the lesion also exhibited delta oscillations (0–19% for each animal, 7 of 72 units pooled) (Figure A-1).

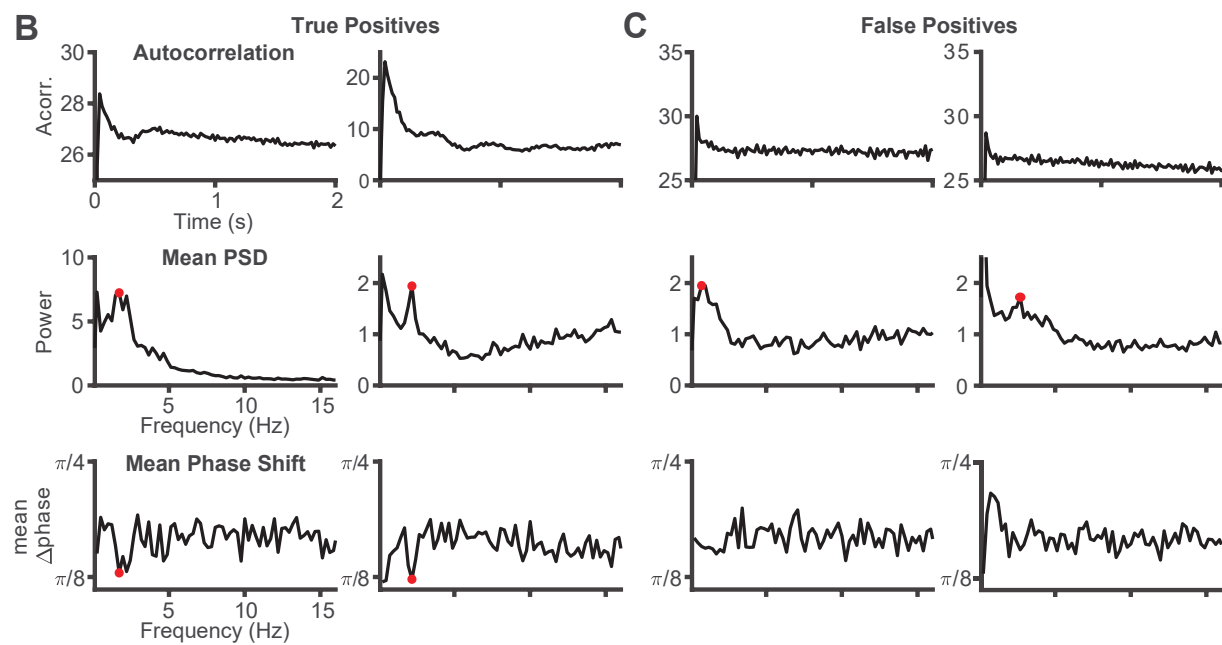
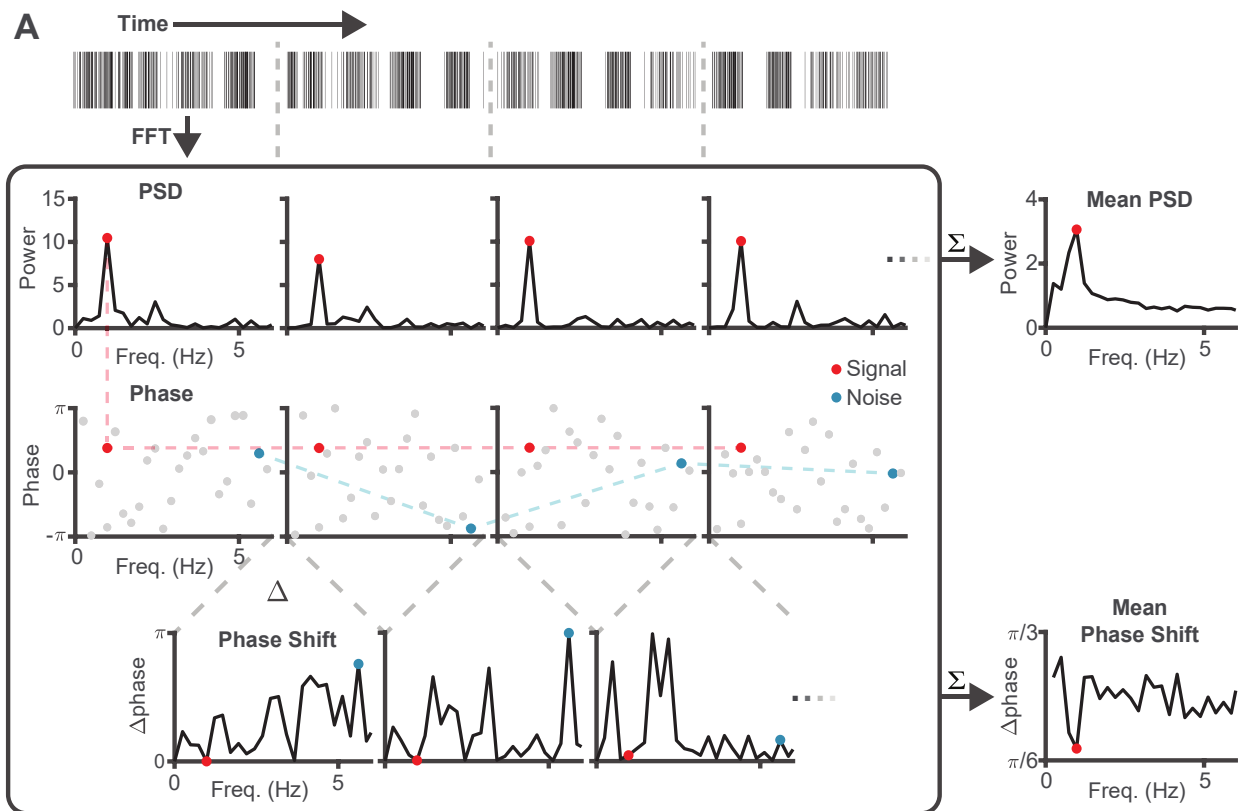


Figure 2-2: A phase shift measure to distinguish oscillations from noise.

A. Diagram of the phase shift oscillation detection method. A spike train is divided into overlapping windows (1st row) and its Fourier transform is computed (corrected for its interspike interval distribution, see Methods). We identify statistically significant peaks in the 0.5–4 Hz range (compared to a control 100–500 Hz range) in the averaged power spectral density (PSD) across all windows (2nd row) and label the oscillation phase (3rd row) at that frequency. Notice while the peak frequency (red) has consistent phase across windows, an arbitrary noise frequency (blue) has inconsistent phase. We take the absolute circular difference of phases at each frequency (4th row) and compute whether the frequency identified in the power spectrum also has statistically significantly lower phase difference than the control band. A spike train which has both a significant spectral peak and significant phase difference trough at the same frequency is labeled oscillating. **B.** Data from two example oscillating units. Top: Autocorrelation exhibiting oscillations. Middle: Significant peaks (red dots) in the PSD surrounded by pink noise. Bottom: The phase difference at these detected frequencies is significantly lower than control frequencies. **C.** Same as **B** but for two units whose autocorrelation appears non-oscillating yet which have a peak in their PSD and which would be “false positive” detections if only PSD’s were analyzed without considering phase shift.

To ensure that delta oscillations were not merely an immune or inflammatory side effect of the injected toxin or cell death, we treated a cohort of animals intraperitoneally with reserpine, a compound that blocks the vesicular monoamine transporter 2 (VMAT2) complex from packaging monoamines into vesicles. This yielded a monoamine (including dopamine) depletion without any intracranial injection or cellular death and produced akinetic symptoms similar to those observed in bilateral 6-OHDA depleted mice. When we recorded three days after the start of daily reserpine injections, these animals exhibited a high proportion of slowly oscillating units in the SNr (33–100% for each animal, 74 of 119 units pooled), similar to bilaterally depleted animals (Figure 2-3A).

Pooling all DD animals together (bilaterally and unilaterally 6-OHDA depleted and reserpine-treated), we saw that each animal typically exhibited oscillations tightly centered around a frequency specific to that animal. The intrinsic frequencies across animals extended over the full 0.5–4 Hz range we have defined for delta oscillations, with a mode between 1–2 Hz (Figure A-2)

Given the prevalence of beta oscillations in the PD and PD animal model literature, we sought to determine if these animals’ SNr units also exhibited beta oscillations. We defined a wide frequency range for beta oscillations, 7–35 Hz, in order to fully encompass the definition of beta oscillations across humans (typically 13–30 Hz) and common model species (monkeys

typically at 7-13 Hz and rats typically at 13-35 Hz) thereby ensuring that we did not miss beta oscillations due to a species-specific difference in the frequency band. We saw no increase in the fraction of beta oscillating units after any form of dopamine depletion, with or without our phase shift criterion (Figure 2-3C–D). We also looked analyzed the SNr LFP signal, as beta oscillations are more typically associated with the LFP rather than individual spike trains, but found no significant change in LFP beta power between DD and control mice (Figure A-3). Taken together, our results suggest that delta, not beta, oscillations are the primary oscillatory feature in the SNr of awake, DD mice.

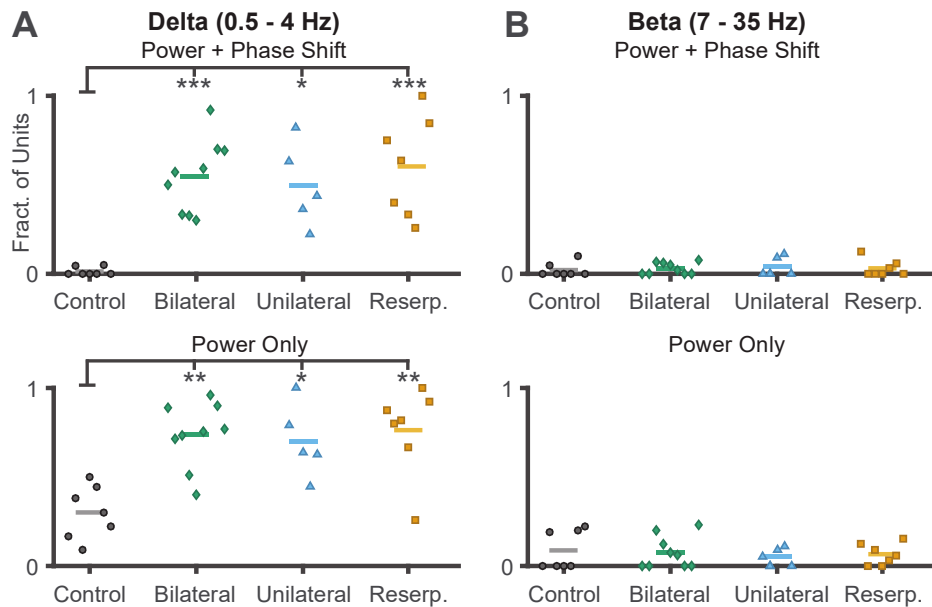


Figure 2-3: Dopamine depleted, but not control, SNr units exhibit phase-consistent delta oscillations, but no change in beta oscillations.

Fraction of oscillating units from each animal in control conditions (black circles, $n = 7$) or various methods of dopamine depletion – bilateral 6-OHDA (green diamond, $n = 9$), unilateral 6-OHDA (blue triangle, $n = 5$), or systemic reserpine (orange square, $n = 7$). Lines indicate mean. **A.** Delta (0.5–4 Hz) oscillations detected using both PSD peak and low phase shift criteria. ANOVA: $p = 5.206 \times 10^{-5}$; bilateral: $p = 9.506 \times 10^{-5}$; unilateral: $p = 0.00172$; reserpine: $p = 5.908 \times 10^{-5}$, Dunnett's post-hoc test. **B.** Same as **A** but using only the spectral power criterion. ANOVA: $p = 4.668 \times 10^{-4}$; bilateral: $p = 5.645 \times 10^{-4}$; unilateral: $p = 0.00601$; reserpine: $p = 5.794 \times 10^{-4}$. **C–D.** Same as **A–B** but for beta (7 – 35 Hz) oscillations. With phase shift, ANOVA: $p = 0.8936$; without phase shift, ANOVA: $p = 0.8908$.

2.3.4 Oscillations predict dopamine depletion severity and behavior better than other physiological measures of dysfunction

To understand how delta oscillations relate to the severity of dopamine depletion, we used an existing dataset of SNr recordings from mice gradually depleted to varying levels of dopamine loss through successive small injections of 6-OHDA (Willard et al. 2019). In this data, we looked at the relationship between an animal's fraction of units exhibiting a delta oscillation and its level of dopamine neuron loss (as measured by striatal tyrosine-hydroxylase (TH) immunoreactivity). Performing a linear regression to predict %TH remaining from oscillation fraction showed a relatively strong ($r^2 = 0.5267$) and significant ($p < 0.01$ from a bootstrapped 99% confidence interval, see Methods) relationship between dopamine loss and the fraction of oscillating units (Figure 2-4A).

Since striatal TH immunoreactivity is not a perfect indicator of Parkinsonian symptoms, we also used these measures to predict motor behavior. Prior to *in vivo* recordings, these animals were given a series of behavioral tests to measure their mobility, dexterity, and strength (see Methods & Willard et al., 2019), and we performed principal component analysis on the results of these tests to get a single measure – the first principal component (PC1) – of their motor deficits. A linear regression predicting PC1 from the fraction of oscillating units illustrated a similarly strong and significant relationship (Figure 2-4B, $r^2 = 0.6406$, $p < 0.01$).

Besides oscillations, many other neural measures in the basal ganglia have been suggested as correlates of dopamine depletion severity – most commonly, changes in firing rate, firing regularity, burstiness, and synchrony between units. To see how delta oscillations compare to these measures in reliably predicting dopamine depletion severity, we built a set of statistical models to predict %TH in each animal from five physiological parameters measured from single units in the SNr: 1) median firing rate, 2) median coefficient of variation (CV) of interspike intervals (ISIs), 3) median rate of bursts, as measured from the Poisson surprise test, 4) fraction of significantly synchronous pairs of units, and 5) fraction of units with significant 0.5–

4 Hz oscillations. Due to the highly nonlinear relationship between the first four of these measures and dopamine depletion severity (Willard et al. 2019), we performed a series of nonlinear regressions on this data by building 1000 decision trees from randomly selected sets of 20 (out of 25) animals, excluding the remaining 5 animals as a testing set for each tree (Figure 2-4C). We estimated a 95% confidence interval of mean squared errors (MSE's) from these 1000 trees and showed that a tree built from these parameters predicts TH significantly better than a naive intercept-only model (Figure 2-4D).

To determine how each parameter informs the model, we shuffled the testing data for that parameter and calculated how much this loss of information increased the MSE of the model (the 'importance' of that parameter). We then estimated 95% confidence intervals for the importance of each parameter (see Methods). The fraction of oscillating units was the only parameter whose confidence interval did not extend below zero (Figure 2-4E), suggesting that, when the model is built to include oscillations, they are the only parameter that provides reliably predictive information. In other words, while other parameters may provide information, that information is redundant when the fraction of oscillating units is known.

To confirm this in another manner, we rebuilt the models using the same cross-validated training and testing sets as above using only a single parameter at a time or using all of the parameters except oscillations. The first four parameters fall outside (FR) or on the edge (CV ISI, Burst and Sync) of the full model confidence interval, but the model with all four parameters performs better than any individual parameter (Figure 2-4D), confirming results seen previously (Willard et al. 2019). However, the model built using only oscillations as a predictor is, on average, better than any other model including the combined parameter model, providing further evidence that other physiological parameters are not additionally informative when oscillations are considered.

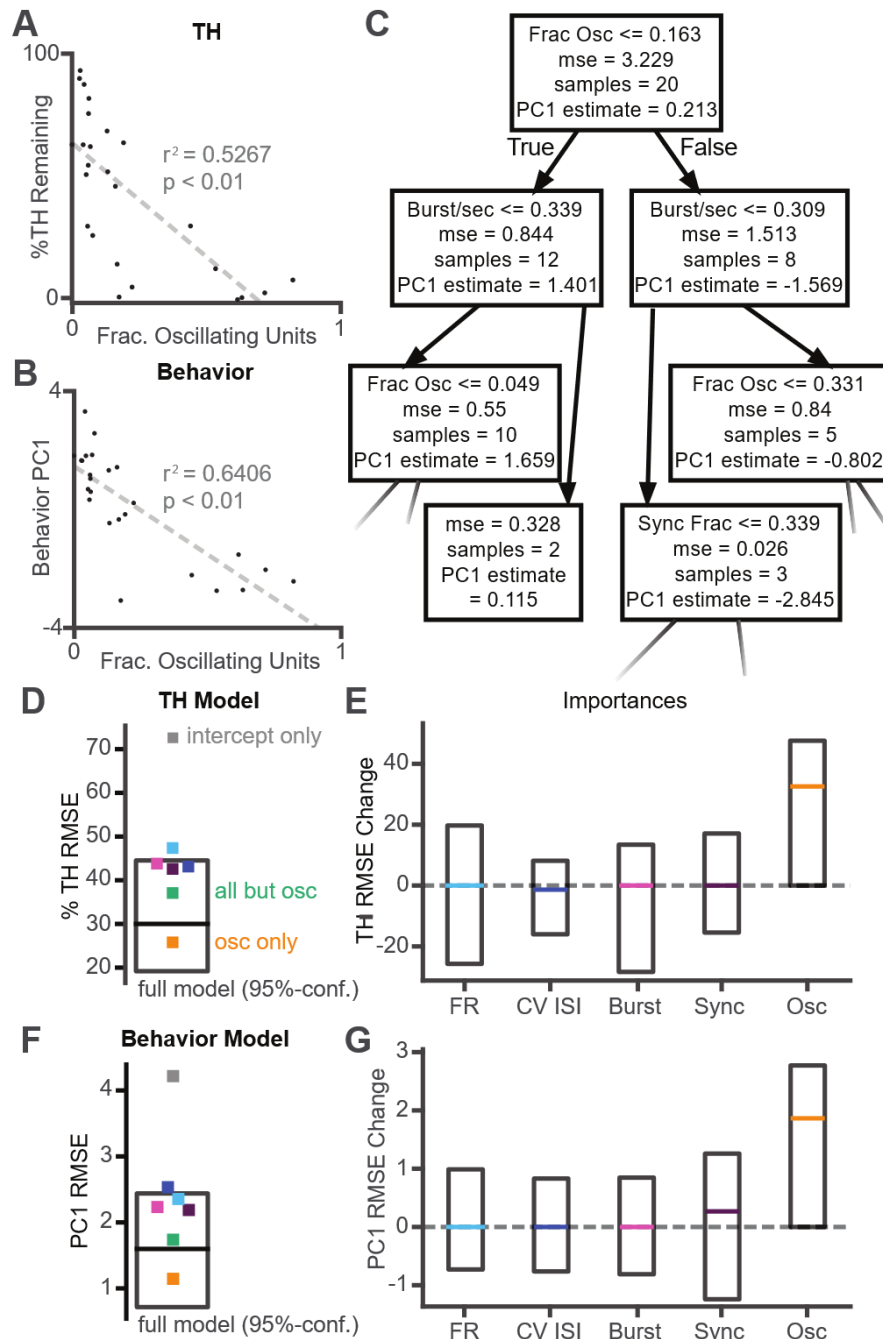


Figure 2-4: Delta oscillations predict severity of dopamine depletion.

A. Scatterplot showing relationship between levels of remaining striatal TH and fraction of oscillating SNr units in animals ($n=25$) gradually dopamine depleted to different severities. Each dot denotes one animal, dashed line is the least squares fit. **B.** Same as **A** showing relationship between the first principal component (PC1) of several behavioral metrics (see methods, more negative indicates more dysfunctional) and the fraction of oscillating SNr units. **C.** The first three rows of one example decision tree predicting striatal TH from SNr neural properties (firing rate, irregularity, burstiness, synchronicity and fraction of delta oscillating units). **D.** A 95% confidence interval of MSE from 1,000 trees predicting TH. Each square is the MSE of the median model trained using a subset of parameters (grey: intercept-only, i.e. no parameters; light blue: firing rate; dark blue: CV of interspike intervals; pink: bursts/second; purple: mean synchrony across pairs; yellow: fraction of delta oscillating units; green: all parameters except fraction of delta oscillating units). **E.** Middle 95 percentile (box) and median (colored line, same color scheme as in **D**) of feature importances (permutation importance, see Methods) for each neural measure in the TH model computed from 1,000 trees. Dotted line indicates zero importance. **F–G.** Same as **D–E** for the model predicting PC1 of behavior.

Using the same procedure as above to predict PC1 of the animals' behavior, we found very similar results to those predicting TH levels – namely, firing rate, irregularity, burstiness and synchrony provide some information in predicting behavior, particularly when considered together. However, when the fraction of oscillatory units is included in the model, it is the only important variable, and is significantly so, in predicting motor dysfunction (Figure 2-4F–G).

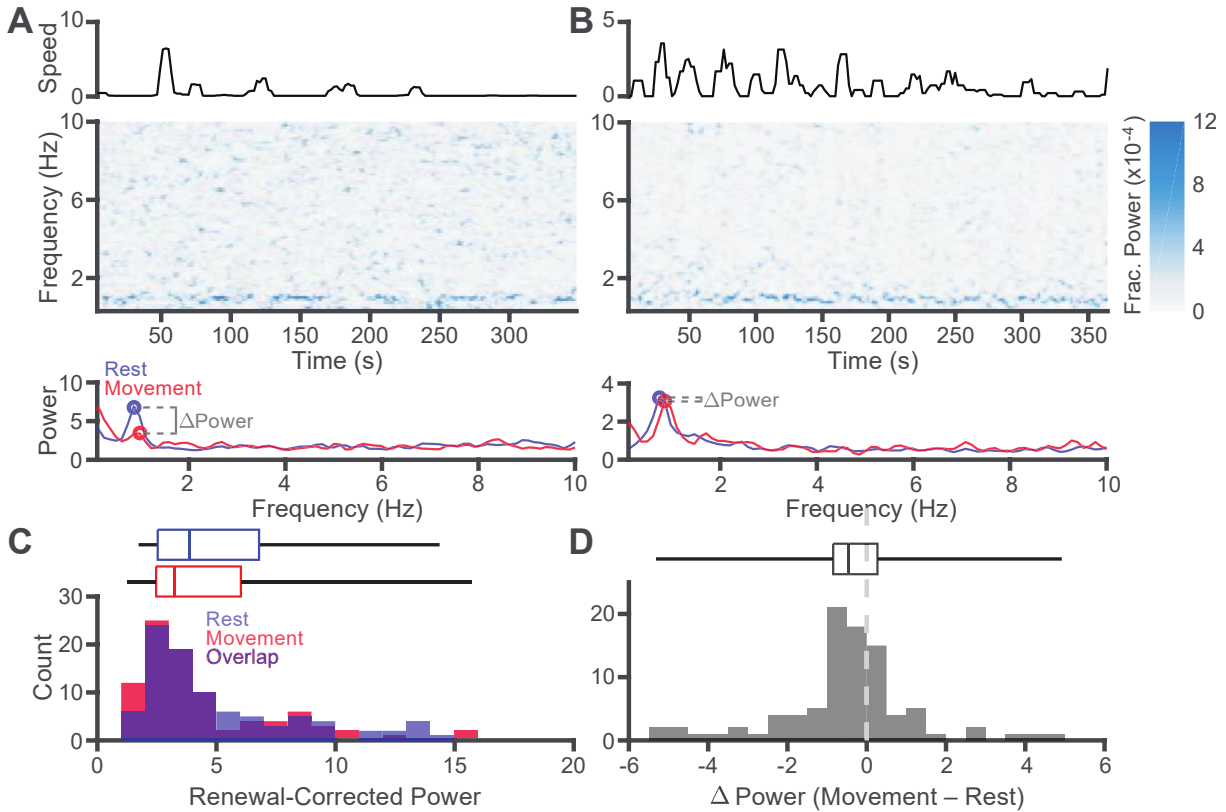


Figure 2-5: Movement in dopamine depleted animals modulates oscillations in a unit-specific manner biased towards attenuation.

A. Example unit with an oscillation negatively modulated by movement. Top: smoothed movement trace of mouse walking on wheel during recording. Middle: spike spectrogram illustrating an oscillation attenuating during movement bouts. Bottom: PSD's of the unit above averaged over windows containing only rest (black) or movement (red). Δ Power illustrates the power difference used in **D** to summarize the data. **B.** Same as **A** for a unit whose oscillation is unaffected by motor activity. **C.** Top: boxplot of the average power of all units from 6-OHDA-depleted animals with a significant oscillation (computed across the whole trial) during rest (black) and movement (red). Vertical line indicates median, box indicates 25th – 75th percentile, whiskers indicate minimum and maximum. Bottom: Histogram showing full distribution of delta power during rest and movement, with overlap in purple. Note that since these are renewal-corrected PSD's, a value of 1 indicates no power at that frequency compared to chance (see Methods). **D.** Same as **C** for the paired difference (movement – rest) for all units in **C**. Dashed line indicates zero difference. $p = 0.0076$, one-sample t-test for non-zero mean.

2.3.5 Oscillations are modulated by movement in a unit-specific manner

Because of known associations between slow oscillations and rest states or drowsiness, we proceeded to check whether the oscillations observed in DD animals would be attenuated during movement bouts. To test this possibility, we examined how delta oscillations differed during periods of movement and rest. Acutely depleted animals spent no more than 4% of their recording time moving and several did not move at all, but gradually depleted animals (to <15% TH remaining) moved up to 10% of their recording time on average, a distribution similar to that of control animals. Since we saw no difference in how units responded during movement activity between acutely and gradually depleted animals, we pooled these animals for this analysis to increase the number of units recorded during movement bouts.

To quantify how delta oscillations relate to bouts of movement, we analyzed units recorded when the animal underwent periods of both rest and movement and separately analyzed the oscillatory power of each SNr unit during these two behavioral states. We found that many units exhibited decreased oscillatory power during movement (Figure 2-5A), but other units exhibited little to no change (Figure 2-5B) or even increased power during movement. Pooling all units together, we found a wide distribution of power shifts when comparing movement to rest with a small but statistically significant (approximately 10% on average) decrease in oscillatory power during movement (Figure 2-5C-D). Overall, during movement 53.9% of SNr units decreased their delta power by at least 10%, whereas only 19.8% increased their delta power by at least 10%. This result suggests that oscillations do not completely preclude motor activity and oscillatory power can even strengthen in some units during movement, but on average, SNr oscillations in DD mice are weakly attenuated during motor activity. Moreover, these low frequency oscillations are not seen exclusively in rest or inactive states in DD animals.

2.3.6 Delta oscillations arise immediately following loss of either MFB transmission or D2 receptor activation

The mechanism behind these delta oscillations is unclear, but they could arise due to a wide range of immediate biophysical changes in the basal ganglia after dopamine depletion or emerge more slowly through plasticity or compensation. To determine this time course, we recorded from the SNr of healthy animals while acutely infusing lidocaine (a voltage-gated Na⁺ channel blocker) into the medial forebrain bundle (MFB), the same injection site for 6-OHDA in our other experiments, to quickly disrupt MFB transmission. We found that oscillations arose in the SNr within 2 minutes of the start of lidocaine infusion (before infusion ended) and waned within ten minutes after the end of infusion, mirroring the time course of akinesia observed during the experiment (Figure 2-6A-C). This result is consistent with the similarly rapid onset of slow oscillations produced by TTX infusion to the MFB under anesthesia (Galati et al. 2010) and demonstrates that low frequency oscillations arise in the SNr almost immediately after loss of MFB transmission, ruling out long-term mechanisms for their generation.

To determine whether the loss of dopamine signaling is causal to the onset of delta oscillations, we recorded from the SNr of healthy animals before and during the systemic injection of a D1-receptor (D1R) antagonist (SCH233890) or a D2-receptor (D2R) antagonist (raclopride). While both drugs caused reduced movement on the wheel, only the D2R antagonist led to the development of oscillations in the SNr (Figure 2-6D-F). We then performed the converse experiment, injecting a D1R agonist (SKF81297) or D2R agonist (quinpirole) systemically into bilateral DD animals. Similarly, while both led to highly increased motor activity (though highly dyskinetic in the case of D1 agonism), only the D2R agonist injection attenuated delta oscillations in the SNr (Figure 2-6G-I). This suggests that low frequency oscillations are mediated purely due to a loss of action on D2Rs and are not affected by D1Rs.

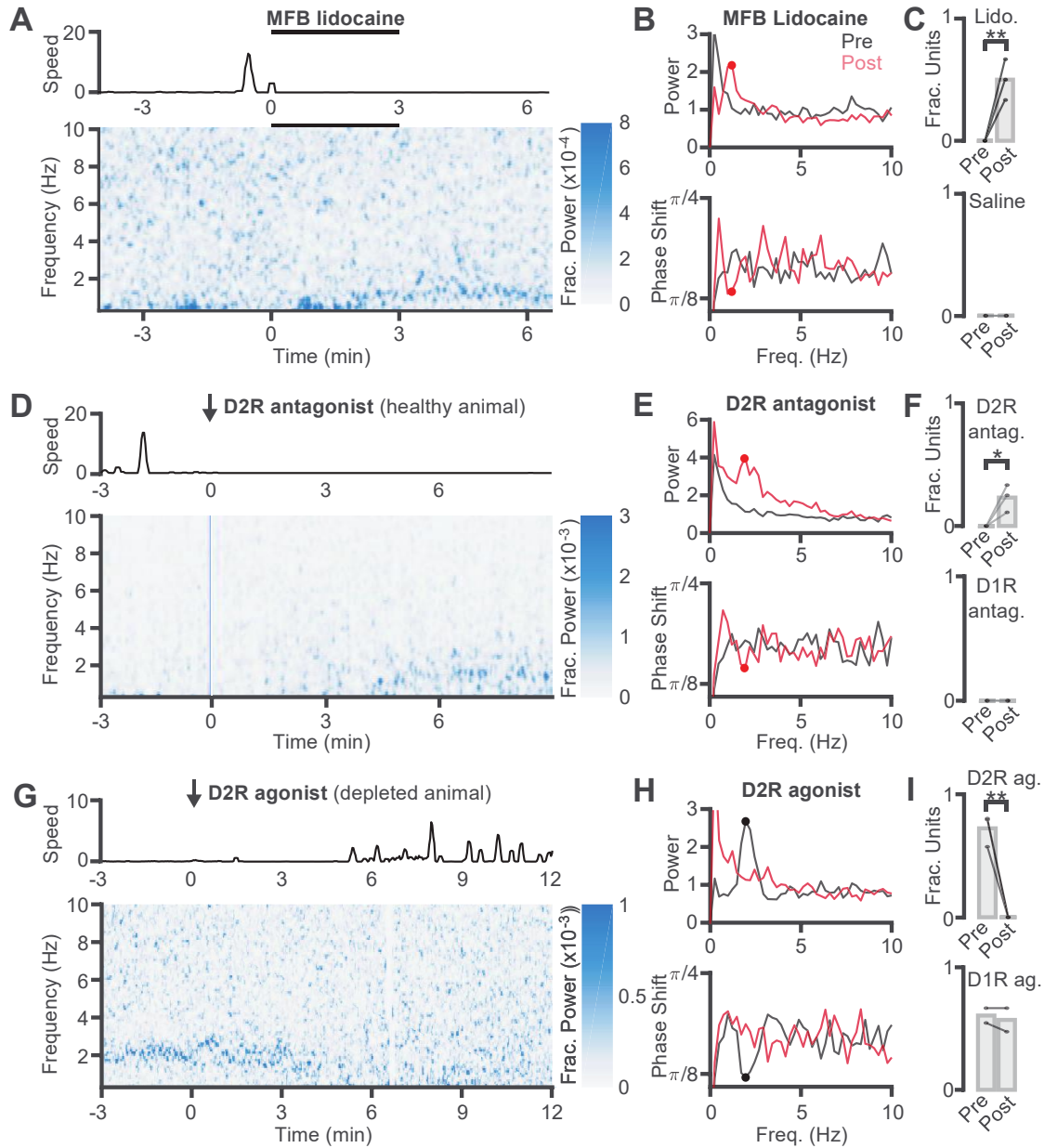
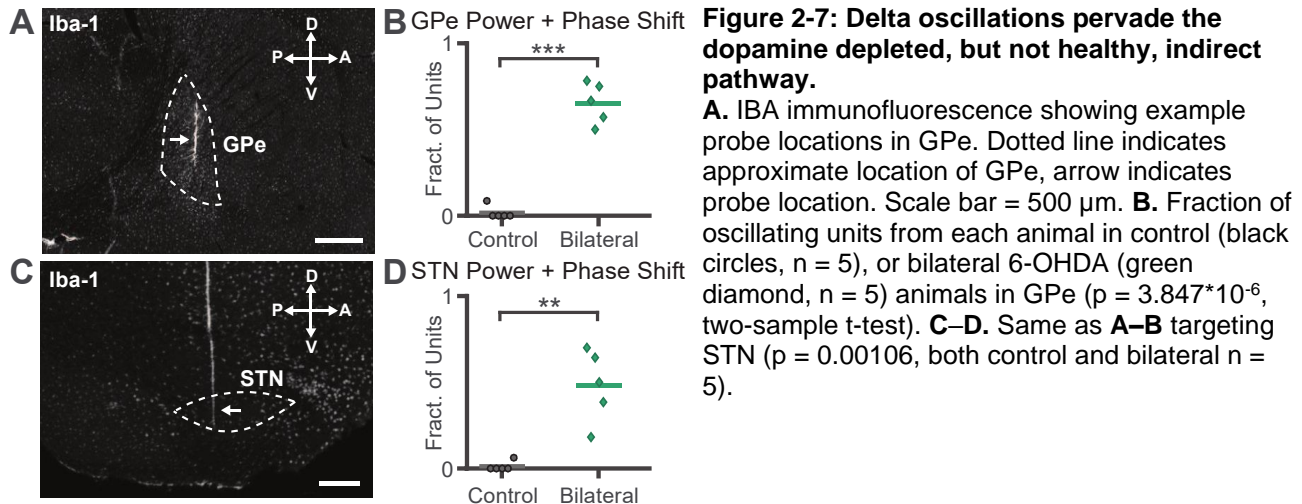


Figure 2-6: Acute manipulations of MFB signaling or D2-receptors modulate oscillations.

A. Effects of lidocaine infusion into the MFB of healthy mice. Top: Speed of mouse on running wheel during lidocaine infusion (black bar). Bottom: Spike spectrogram of an example SNr unit during the same infusion as above. **B.** Top: PSDs from the same unit before (left) and after (right) lidocaine infusion. Bottom: Phase shift plots corresponding to the above PSDs. A dashed line from the detected oscillation in the right PSD (red dot) connects to the same frequency in the corresponding phase shift plot. **C.** Fraction of oscillating units from all animals before and after lidocaine (top, $n = 3$, $p = 0.00219$) or saline (bottom, $n = 2$, $p = 1.000$) infusion into the MFB. Each dot is one animal, bars indicate mean, and lines connect the same animal before and after infusion. **D–F.** Same as **A–C**, but for systemic injection of a D2R antagonist (raclopride, $n = 3$, $p = 0.0233$) compared to a D1R antagonist (SCH233890, $n = 2$, $p = 1.000$). **G–I.** Same as **D–F**, but for systemic injection of a D2R agonist (quinpirole, $n = 3$, $p = 8.686 \times 10^{-4}$) compared to a D1R agonist (SKF81297, $n = 2$, $p = 0.7455$) in DD animals.



2.3.7 Delta oscillations appear in depletion throughout the indirect pathway

Since the indirect pathway of the basal ganglia is a primary location of D2R-expressing neurons, we posited that oscillations may also be present elsewhere in the indirect pathway. We thus recorded from healthy and dopamine depleted globus pallidus externa (GPe) (Figure 2-7A) and subthalamic nucleus (STN) (Figure 2-7C), two reciprocally connected nuclei in the indirect pathway that both project heavily to SNr. We found a similar pattern of oscillatory activity across units in the GPe (40–80% of units in each animal, Figure 2-7B) and STN (15–70% of units in each animal, Figure 2-7D) after dopamine depletion, whereas only 1 of 111 total GPe and 1 of 63 STN units exhibited oscillations in the healthy state.

2.3.8 Two populations of delta oscillating SNr units lead oscillations in motor cortex

Previous literature suggests that oscillations in the dopamine depleted basal ganglia arise due to input from oscillating neurons in motor cortex (M1) under anesthesia (Tseng et al. 2001b). However, since we have shown that these oscillations arise from antagonism on D2R's, a receptor more prevalent in the basal ganglia than M1, a possible alternative in awake animals is that these oscillations arise first in the basal ganglia and then entrain M1.

To distinguish between these possibilities, we sought to characterize oscillations in M1 of DD animals and determine the phase lag between M1 and SNr oscillations. We recorded an electrocorticogram (ECoG) in M1 while simultaneously recording from single units in SNr

(Figure 2-8A). Compared to healthy controls, the M1 ECoG of DD animals exhibited a large increase in delta oscillations and reduction in theta (4–7 Hz) oscillations, which are typically seen in the cortex of healthy mice (Tort et al. 2018) (Figure 2-8B–C).

Determining the relationship between two oscillating signals from their phases is a difficult task – if the phase of one perfect oscillator slightly leads that of a second perfect oscillator, it is impossible to distinguish whether the first leads the second at a short lag or if the second leads the first at a long lag. However, neural oscillations do not match the activity patterns of perfect oscillators, but have profiles that vary across periods and highly varying period lengths that are merely centered on a range of values. While analyses in the frequency domain average out these fluctuations, we can perform an analysis in the time domain specifically on units already determined to exhibit delta oscillations to characterize whether fluctuations in neural firing lead or lag the same fluctuations in M1 (Figure 2-8D).

To quantify this relation, we performed a series of Granger causality regressions which predict changes in M1 ECoG based on its own history (the null, autoregressive model) or by additionally including SNr spiking information from a single unit. For each unit, we computed 201 separate models predicting M1, each using SNr spiking information at a different lag between -1 (i.e., past spikes) and +1 seconds (i.e., future spikes). Aligning the lag coefficients of the models for a single unit illustrates a periodicity in their values that matches the oscillation period (Figure 2-8E-F).

We computed the mean squared error (MSE) of each model at each lag and considered the lag that minimized MSE. To quantify whether this model significantly outperforms the purely autoregressive ECoG model, we performed an F test on the two models, correcting for multiple lag comparisons (Figure 2-8E-F). We find that 51 of 63 of oscillating units in SNr predicted changes in the ECoG significantly better than the null autoregressive model, suggesting that there is significant correlation between SNr and M1 at a consistent time lag.

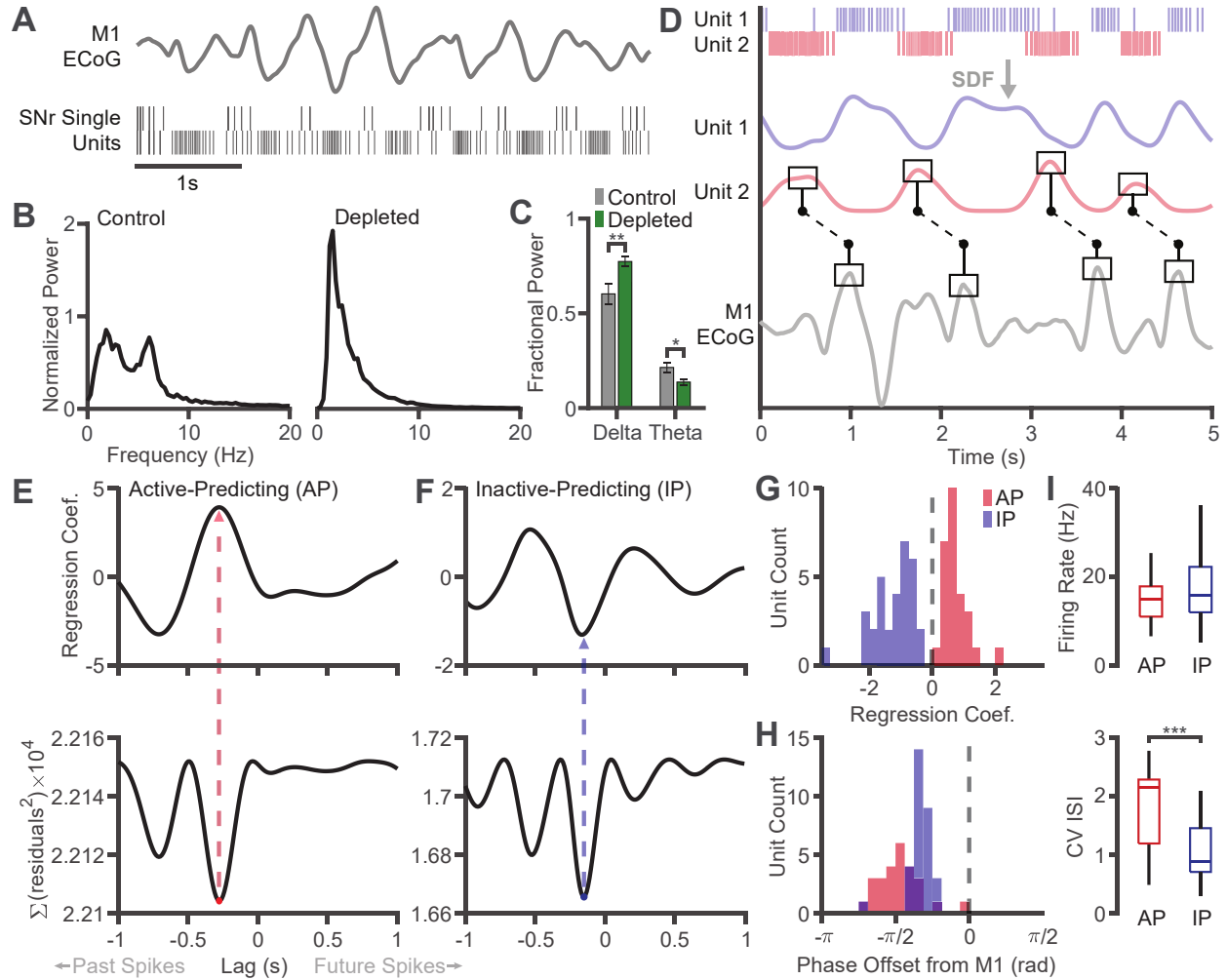


Figure 2-8: Delta oscillations define two SNr populations which both lead M1 oscillations.

A. Example simultaneous M1 ECoG and spike trains from two SNr units exhibiting coherent oscillations. **B.** Example M1 ECoG power spectra from control (left) and bilaterally depleted (right) animals. Power spectra were normalized to their total 0.5-100 Hz power and multiplied by 1000 for visualization. **C.** Fractional delta and theta band power in M1 ECoG across all control ($n = 8$) and acutely depleted ($n = 9$) animals. Bars indicate mean, error bars indicate standard error ($p = 0.00818$ for delta, 0.0173 for theta, two-sample t-test test). **D.** Example data demonstrating SNr predicting M1. Top: 5 second rasters from two simultaneously recorded SNr units. Middle: spike density functions (SDF) of the above SNr rasters of matching colors. Bottom: Simultaneously recorded M1 ECoG. Lines between the bottom two panels illustrate M1 exhibiting peaks at a consistent time lag after the peak of an SNr SDF, even amidst variance in oscillation period length. **E.** Example regression results predicting M1 ECoG from an “active-predicting” (AP) SNr unit. Top: Regression coefficients for each individual lag. Negative lag corresponds to SNr oscillations leading M1. Bottom: MSE of regression results using each lag. The red dot indicates that the model using that lag significantly outperforms an autoregressive model of the ECoG (F-test, $p < 0.05$ correcting for multiple lag comparisons). The dotted line to the upper panel lands at a peak in the coefficients, defining the unit as “active-predicting”. **F.** Same as **E** for an “inactive-predicting” (IP) SNr unit, whose significant lag is labeled in blue. **G.** Summary histogram of regression coefficients from all oscillating SNr units recorded simultaneously with M1 ECoG ($n = 59$). Counts are colored as in **D–F** based on their regression coefficients (red: positive, blue: negative, dashed line at zero), which define their type (AP or IP). **H.** Same units colored as above grouped by the phase offset at which they best predict the M1 ECoG (as in **E–F**, negative phase offsets correspond to SNr oscillations leading changes in M1). **I.** Boxplots comparing the firing rate (top) and coefficient of variation of interspike intervals (bottom) of AP (red) and IP (blue) units. Wilcoxon rank sum test, FR: $p = 0.4371$; CV ISI: $p = 3.449 \times 10^{-5}$.

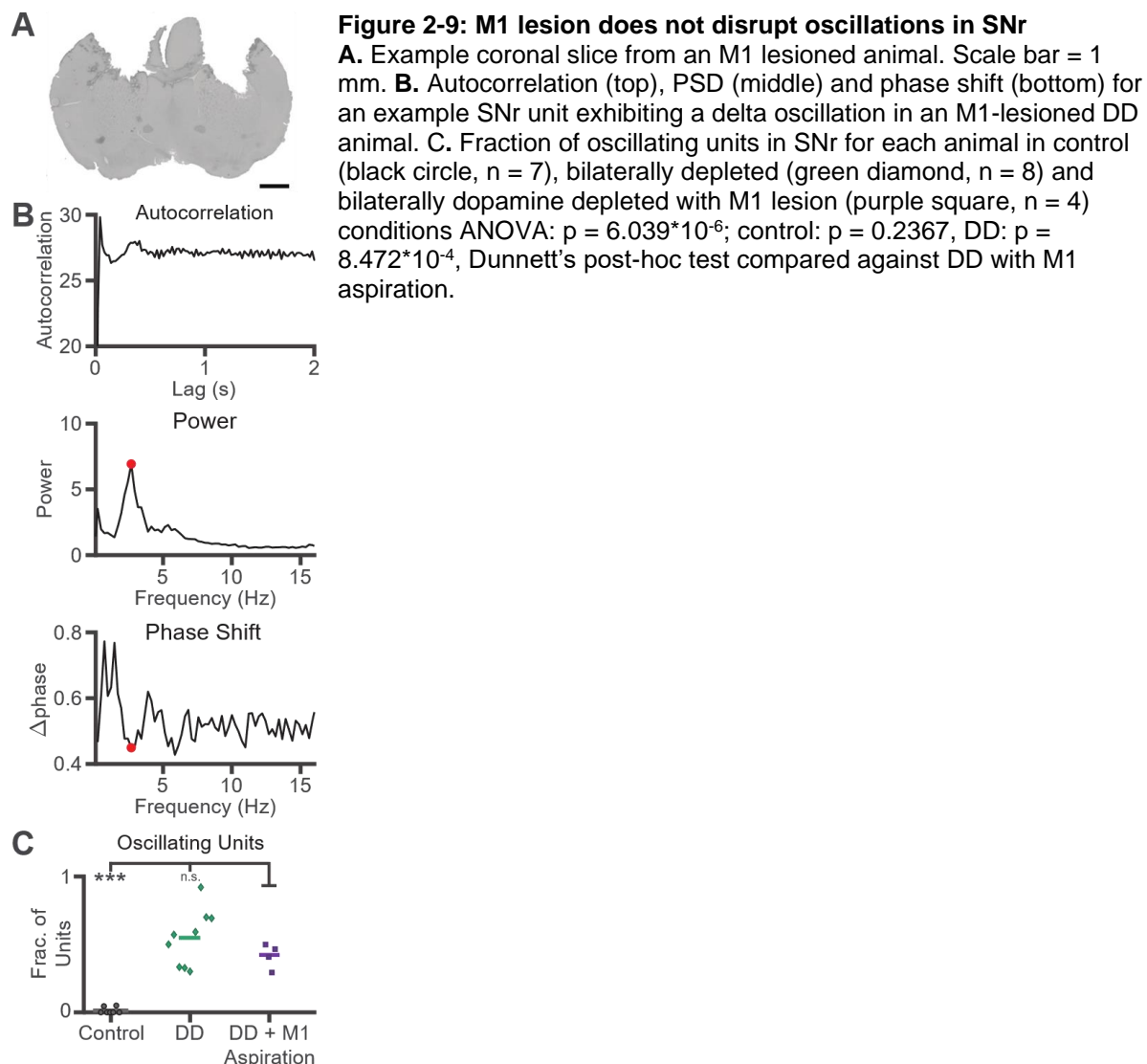
When analyzing the regression coefficients at these significant lags, we found a clear bimodal distribution of units determined by whether the active or inactive phase of their spike oscillation predicted positive deflections in M1 (Figure 2-8G). We term these “active-predicting” (AP) and “inactive-predicting” (IP) units, and examples of each can be seen in Figure 2-8D-F, We see further evidence of these two distinct populations through cross correlation analysis of SNr unit pairs (Figure A-4).

When clustering units based on their phase lag relative to M1, SNr units also organize into a bimodal distribution, with one mode dominated by AP units and the other by IP units. (Figure 2-8G). Critically, all significant lags were negative – that is, SNr spikes from both populations of SNr units consistently predicted future changes in the ECoG, but not the inverse (Figure 2-8H). The relative timings of these signals suggest an order in which oscillations propagate through the SNr and cortex - AP units enter their active phase (increase firing), then IP units enter their inactive phase (decrease firing or pause), and finally M1 enters its active phase. More specifically, AP units increase firing 0.24 ± 0.06 (mean \pm standard deviation) periods before M1’s active phase (corresponding to 180 ± 45 ms for a 1.5 Hz oscillation), and IP units decrease firing 0.16 ± 0.02 periods (120 ± 15 ms for a 1.5 Hz oscillation) before M1’s active phase. These results suggest a consistent timeline of oscillatory dynamics by which two oscillating populations in SNr both dynamically predict M1 activity.

To determine if AP and IP units exhibit different firing properties, we compared their firing rates (FR) and the coefficient of variation of their interspike intervals (CV ISI). We saw no significant difference in firing rates, but AP units exhibited a significantly higher CV ISI than IP units (Figure 2-8I). This is primarily due to the units’ behavior during their inactive phase – IP units tended to slow down whereas AP units tended to pause completely.

M1 is not required for delta oscillations in SNr

The results of our regression analysis suggest that oscillations in SNr are not caused by M1, but rather that oscillations in the SNr precede and predict those in M1. To test this hypothesis, we performed M1 aspiration lesions in DD mice (Figure 2-9A) and recorded units from SNr. SNr units in the DD + M1-lesioned mice had similar oscillations to those DD mice without M1 lesions (Figure 2-9B). These mice had a significantly higher fraction of oscillating units than control animals, but there was no difference between DD animals with or without an M1 lesion (Figure 2-9C). These results provide additional evidence that M1 is a recipient, not the source, of delta oscillations in dopamine depletion.



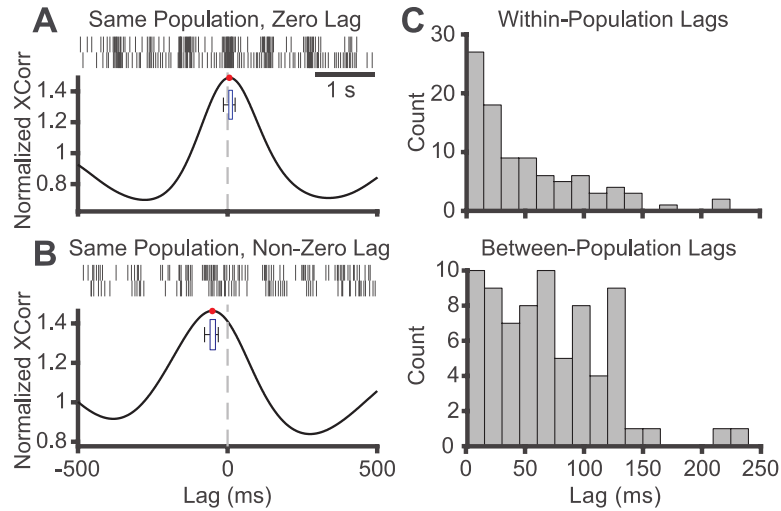


Figure 2-10: Delta oscillating SNr units exhibit non-zero phase lags.

A. Top: Example rasters from a pair of simultaneously recorded SNr units exhibiting an in-phase relationship. Bottom: Normalized cross-correlation of the above two units. The red dot indicates the peak of the cross-correlation at 6 ms. The inset boxplot shows the variability of the peak location measured at each overlapping 20-second window over which the cross-correlogram was computed (box is 25–75th percentile, whiskers extend to minimum and maximum). Note that the boxplot extends across the zero line (dashed gray line). **B.** Same as A for a second pair of units indicating a consistently non-zero lag (mean peak at 51 ms). **C.** Top: Histogram summarizing the mean pairwise phase lags (zero line to nearest extreme point, red dots in A and B) for all pairs of units whose extreme point closest to zero lag was a peak. Bottom: Same as top for all pairs of units whose extreme point closest to zero lag was a trough.

2.3.9 SNr neurons exhibit consistent non-zero pairwise phase lags

Having determined the phase lags between SNr neurons and M1, we considered whether such lags exist between individual SNr neurons, both within and between the AP and IP populations. To analyze this, we performed a cross-correlations analysis of the SDF's of simultaneously recorded SNr neurons. Specifically, we performed sequential cross-correlations with a moving window and normalized the cross-correlogram at each step (see Methods); this both reduced the effect of nonstationarities on the resulting mean cross-correlogram and allowed us to observe if the lags at which peaks or troughs occurred in the cross-correlogram varied over time.

We computed these cross-correlograms for every pair of simultaneously recorded SNr neurons and found pairs which had in-phase relationships with lags centered near zero (Figure 2-10A), as well as nearly in-phase relationships with lags centered at small delays (typically

<100 ms, Figure 2-10B). Critically, many of these relationships were consistently non-zero across all computed windows – that is, the two units exhibited a consistent lead-lag relationship at a consistent time lag. We also computed these pairwise relationships using a Poisson regression method and plotted the residuals of the best fit over time to confirm that these lead-lag relationships for individual neurons were consistent across the full recording time (Figure A-6).

We considered all units whose cross-correlograms had a peak closer to lag-zero than a trough to be from the same population (either both AP or both IP) and found that their distribution of lags peaked at zero with a median lag of 34 ms and a long tail extending out to a maximum 213 ms lag. Conversely, we considered all pairs whose cross-correlograms had a trough closer to zero to be from opposite populations (one AP, one IP) and found a wider distribution with median 61 ms and maximum 233 ms, indicating longer average lags between neurons of opposite populations (Figure A-6C). This additional time lag when comparing between populations on average is consistent with the tendency for AP neurons to lead IP neurons.

2.4 DISCUSSION

We have demonstrated that delta (0.5–4 Hz), not beta (7–35 Hz), oscillations are the predominant oscillatory feature in basal ganglia neurons in awake, dopamine depleted mice, including during movement, and that the fraction of units exhibiting these oscillations is a good marker of dopamine loss and motor deficits. These results are consistent with data from the human PD literature demonstrating that delta oscillations are the dominant or only oscillatory feature in some PD patients (Du et al. 2018; Levy et al. 2002). We further show that these oscillations arise from a loss of action on D2 receptors and that, contrary to conclusions drawn from anesthetized experiments, motor cortex is not required for their generation but rather follows the oscillations evident in the basal ganglia.

2.4.1 A novel method to distinguish oscillations from noise

Although several studies demonstrate the presence of delta oscillations in the LFP (Levy et al. 2002; Priori et al. 2004) and single units (Steigerwald et al. 2008; Du et al. 2018; Zhuang et al. 2019) of PD patients, many more studies ignore oscillations in this band completely. Difficulties in detecting these oscillations may contribute to this lack of attention. Most studies examining oscillations in PD patients investigate the LFP, not individual spiking units, and the intrinsic low frequency noise of LFP signals makes reliably detecting oscillations in the delta range difficult. Even when it is possible to record from single units, we have demonstrated that low frequency noise can make it difficult to reliably detect these spiking signals as well.

To reliably detect low frequency spike oscillations in awake animals, we have introduced phase shift as a novel detection technique which utilizes phase information typically discarded from the Fourier transform. Phase shift measures the local stationarity of a signal composed primarily of one frequency – a perfect sine wave would have zero phase shift and high power, but a sine wave with a phase that randomly advances would have high phase shift while maintaining high power. This measure can distinguish our signal of interest – a single oscillatory signal that shifts in phase only gradually or rarely – from low frequency pink noise, a phenomenon that is not restricted to a single frequency and in which phase components measured at individual frequencies may shift rapidly between adjacent windows.

Note that, in all spectral analysis in this chapter, a rectangular window was used rather than a tapered window more typically used in modern signal processing applications. We chose a rectangular window for two reasons. First, window choice involves a tradeoff between discrimination of nearby peaks (frequency resolution) and detection of smaller peaks in the PSD. The rectangular window maximizes frequency resolution, and since our signal of interest is typically near a lower frequency peak due to pink noise, this window ensures that these signal and noise peaks are not smoothed together and conflated. Second, multiplication with a window function manifests as a convolution (i.e., smoothing) in the frequency domain. The phase shift

signal is weak compared to that of the PSD, and the smoothing that occurs due to a tapered window confounds this signal and compromises detectability. For other applications of phase shift where the former requirement (high frequency resolution) is not necessary, it may be wise to use perform two separate Fourier analyses – using a tapered window function such as the Hamming window to compute the PSD, while maintaining a rectangular window for the computation of phase shift.

2.4.2 Relationship to previous studies on Parkinsonian oscillations

In PD research, much of the oscillation literature has focused on the beta band (Hammond et al. 2007; Jenkinson and Brown 2011). Here, we demonstrate dopamine loss and PD-like symptoms in mice without the presence of beta oscillations in basal ganglia neurons or LFP. One recent study has demonstrated beta oscillations in the basal ganglia of parkin knockout mice, a model of early stage PD (Baaske et al. 2020); however, this model does not lead to any PD-like motor dysfunction or dopamine loss, and to our knowledge, beta oscillations have not been linked to either of these phenomena in mice. Instead, our study indicate that delta oscillations are an important signal in the DD basal ganglia in mice and track the progression of akinetic motor symptoms. While beta oscillations are not present in DD mice, this does not discount this oscillatory band from playing an important role in PD. Instead, we suggest that delta oscillations observed in Parkinsonian patients may contribute to Parkinsonian dysfunction alongside beta oscillations, or may be a primary driver of motor symptoms in the subset of patients with delta but without beta oscillations (Du et al. 2018; Levy et al. 2002).

The low frequency oscillations that we observe resemble those seen in anesthetized DD mice and rats, although oscillations in awake settings are generally noisier. Importantly, by performing these experiments in awake mice, we rule out concerns that oscillations in the basal ganglia are simply entrained by anesthesia-induced oscillations from cortex (Tseng et al. 2001b; Belluscio et al. 2003) or by artificial respiration devices (Ruskin et al. 2002). Instead, we see that oscillations in the basal ganglia arise even during wakefulness and in fact lead and predict

oscillations in M1. While we can rule out one causal direction (M1 to SNr) being solely responsible for the propagation of these oscillations through the basal ganglia and cortex, it is difficult to know whether SNr entrains M1 directly or if both SNr and M1 are entrained by a common source. While we have demonstrated that M1 is not necessary for these oscillations, it is likely that feedback loops between M1 and several basal ganglia nuclei allow both systems to shape the dynamics of these oscillations.

By referencing SNr oscillations to M1, we distinguish two populations of oscillating SNr neurons. These populations and how they are defined share similarities with the Type-A (TA) and Type-I (TI) populations observed in GPe whose discharge is high and low, respectively, during the active phase of M1 oscillations (Mallet et al. 2008). While active-predicting (AP) and inactive-predicting (IP) SNr neurons may be viewed as analogous to TA and TI GPe neurons respectively in terms of their timing relative to M1, the analogy does not extend to several other properties. First, the granularity of our regression analysis illustrates that AP and IP neurons are not simply active or inactive during the active phase of the M1 oscillation but begin discharging (AP) or slowing down (IP) 100–300 ms before the active component of the M1 oscillation. To our knowledge, a precise timing analysis of TA and TI neurons with M1 oscillations has not been performed to determine if a similar phenomenon occurs in GPe. Second, SNr AP and IP neurons are approximately equal in number, whereas TI neurons are the prevailing population in GPe (72% TI, 17% TA) (Mallet et al. 2008). Lastly, GPe TA neurons fire significantly slower than TI neurons; we see no such difference here, although we do observe a difference in firing pattern. The TA and TI populations of GPe neurons were later shown to have anatomical (Corbit et al. 2016; Mallet et al. 2012), genetic (Abdi et al. 2015), and functional (Gage et al. 2010; Mallet et al. 2016) differences, forming the prototypic (TI) and arkypallidal (TA) populations. AP and IP neurons may exhibit such differences as well upon further study.

2.4.3 Mechanisms of generation

A previous study demonstrated that delta oscillations in anesthetized mice arise immediately after loss of dopamine signaling through the MFB (Galati et al. 2010), a finding that we have replicated here in awake mice. This fast onset (<2 minutes) contrasts with the typical longer timescale associated with beta oscillations in dopamine depletion (Mallet et al. 2008). We further show that these oscillations arise due to a loss of D2R activation and can be ablated in DD animals through D2R agonism. It is unclear where the D2 receptors responsible for this ablation are located, but the high density of D2R's in the striatum make it a strong candidate. Lack of D2R activation causes a wide array of biomolecular changes within D2R-expressing neurons, including the opening of NMDA (Higley and Sabatini 2010; Wang et al. 2012) and L-type calcium channels (Hernández-López et al. 2000), which have been shown to be involved in membrane potential and calcium oscillations, respectively, in other circuits (Guertin and Hounsgaard 1998).

In addition to striatum, another candidate for the generation of delta oscillations in dopamine depletion is the STN-GPe loop. While often associated with beta oscillations (Mallet et al. 2008; Nevado-Holgado et al. 2014; Pavlides et al. 2012; Wei et al. 2015), this loop was originally implicated in generating much lower frequency oscillations (0.8 – 1.8 Hz) in cultured neurons (Plenz and Kital 1999), a phenomenon that has been demonstrated subsequently in computational models (Terman et al. 2002; Modolo et al. 2008). The slow rates associated with the dynamics of T-type calcium channels and of some after-hyperpolarization currents have been shown to contribute the generation of oscillations and could explain the low frequency of these oscillations as well (Devergnas et al. 2015).

Delta oscillations are a common feature of non-REM sleep and arise throughout cortex through oscillations involving thalamocortical relay neurons. Thalamic delta oscillations arise from the interplay of HCN and low threshold T-type Ca^{2+} channels in thalamocortical neurons when they are hyperpolarized (Steriade et al. 1993), which occurs in part due to decreased

levels of acetylcholine in thalamus (Jones 2005). While there may be many mechanisms by which delta oscillations are generated in the brain, the neurotransmitter systems and intrinsic currents critical for the generation of sleep oscillations play important roles in the basal ganglia and may be useful avenues for investigating the oscillations we observe in this study. For instance, cholinergic interneurons in the striatum express D2R's (Maurice et al. 2004), and HCN channels are prevalent in BG regions such as GPe (Surmeier et al. 2005).

Delta oscillations have previously been observed in mouse barrel cortex phase-locked to respiration (Ito et al. 2014), and while it is not clear why loss of action on D2 receptors would cause this rhythm to leak into the basal ganglia, it is one possible mechanism by which these oscillations could arise from a rhythm already present in the nervous system. Whether or not the oscillations we observe are generated within the basal ganglia or entrained from another source (which may have a physiological function elsewhere in the brain), we have demonstrated that the emergence of these oscillations in the basal ganglia correlate strongly with akinesia, suggesting that they become pathological once they emerge in these nuclei.

2.4.4 Relationship between oscillations and motor dysfunction

Of those studies that examine low frequency oscillations in PD patients, many consider only their relationship to tremor, seeing primarily units with positive correlation to EMG signals during tremor bouts but also units with no such correlation (Hurtado et al. 1999; Du et al. 2018), or a correlation which changes in time due to phase slips in the unit's oscillation (Hurtado et al. 2005). No study, to our knowledge, has investigated low frequency oscillations in relationship to other PD symptoms. Here, we have established a strong relationship between delta oscillations, dopamine loss, and akinetic dysfunction in mice. Further research and re-examination of existing patient data could elucidate a role for delta oscillations in predicting or causing PD motor deficits in humans.

When comparing the strength of delta oscillations between periods of rest and movement, we found that delta oscillations weakened on average during periods of movement,

but occasionally strengthened and were rarely ablated completely. In contrast, an animal's fraction of oscillating SNr units was a strong predictor of the animal's overall motor dysfunction. We see the discrepancy between the strength of these results to be due primarily to a difference of timescale – the long timescale of predicting overall motor activity versus the short timescale of individual motor bouts. We suggest that delta oscillations on average represent a decreased probability to engage in motor activity, but for individual motor bouts, other parallel or further downstream motor circuits could override the akinesia-promoting delta signal. We also note the difficulty of correlating oscillations with movement bouts, which can be shorter than a single period of a delta wave. The long window size necessary to quantify oscillations in our movement analysis means that some windows containing movement activity (and thus labeled as movement) still contain periods of rest, which may dilute the relationship we have observed.

While we cannot demonstrate a causal link between oscillations and motor dysfunction in this work, it is notable that the emergence of delta oscillations in the SNr from multiple experimental manipulations is consistently paired with a time-locked and commensurate reduction in motor activity, and that motor activity dynamically attenuates (though does not ablate) delta oscillations in a majority of SNr neurons as Parkinsonian mice shift between motor and resting states. These results suggest a reappraisal of delta oscillations as a potential cause or marker of motor dysfunction in Parkinson's disease patients that could be an underappreciated target for PD therapies.

2.5 ACKNOWLEDGEMENTS

Thanks to Rachel Bouchard, Hyun Young Park, Jenna Schwenk and Christen Snyder for help with tissue processing and immunohistochemistry. A large thanks as well to Amanda Willard who collected the data from gradually dopamine depleted animals, assisted in the creation of Figure A-3, and provided valuable insight and guidance throughout the data collection process. Thanks finally to Dr. Robert S. Turner for code that served as a scaffold for oscillation analysis

and burst detection, as well as for fruitful analytical discussions at this work's early stages. This work was supported by NSF awards DMS 1516288 (AHG, JER), 1724240 (JER), and NIH awards R01NS101016, R01NS104835, and R21NS095103 (AHG), and F31NS101821 (TCW). This chapter was adapted primarily from (Whalen et al. 2020).

3 PROPAGATION OF DELTA OSCILLATIONS IN A BIOPHYSICAL MODEL OF THE GPE-SNR NETWORK

In the previous chapter, we showed that delta oscillations are a strong and robust signal which arise in the Parkinsonian substantia nigra pars reticulata (SNr) after dopamine depletion (DD) and are a useful predictor of motor dysfunction. However, a key question remains – once dopamine has been depleted, what causes delta oscillations to arise in the SNr? In this chapter, we take a computational approach to model a subset of basal ganglia circuitry and suggest that delta oscillations may not arise within the SNr alone, but can arise through entrainment by the globus pallidus externa (GPe). We propose a network architecture which, through simulation, generates firing patterns in model SNr neurons which match those measured *in vivo* solely through inhibition from oscillating GPe neurons and fellow SNr neurons. In particular, we see the spontaneous generation of active-predicting (AP) and inactive-predicting (IP) neural populations whose firing patterns match observations *in vivo*. These results demonstrate how delta oscillations can propagate through the basal ganglia despite imperfect oscillatory synchrony in the source node, narrowing down potential targets for the source of delta oscillations in DD and giving further insight into the dynamics of SNr oscillations.

3.1 INTRODUCTION

Delta oscillations in the SNr are a strong signal and predictor of motor dysfunction in the Parkinsonian mouse basal ganglia. However, the SNr is not the only nucleus which exhibits delta oscillations in DD. Within the basal ganglia, GPe and subthalamic nucleus (STN) neurons

also strongly modulate their firing rate at a delta frequency in DD conditions, and electrocorticogram (ECoG) signals in motor cortex (M1) exhibit a strong delta component due to DD. With all of these brain regions oscillating at a similar frequency, it is unlikely that they each develop this firing pattern completely independent of each other. Instead, one of two scenarios is likely: 1) delta oscillations arise in a single region of the brain in DD and propagate throughout the basal ganglia and M1 (and potentially unexplored additional regions) through synaptic connections, or 2) delta oscillations arise in several regions of the brain in DD, but connectivity between independently oscillating regions amplifies and entrains downstream regions based on the particular oscillating patterns of the presynaptic population(s). Depending on the region, either of these hypotheses could be true – for example, each basal ganglia nucleus may oscillate individually and be entrained by its presynaptic partners, but M1 may require input from the basal ganglia (directly or indirectly) in order to oscillate at all.

In either scenario, the synaptic connectivity between oscillating regions likely plays a major role in shaping these oscillations. In Chapter 2, we demonstrated through simultaneous recordings of the SNr and M1 that SNr oscillations dynamically predict oscillations in M1, strongly suggesting that M1 is entrained by SNr or that the delta oscillations in M1 are directly caused by those in SNr. However, the propagation of these oscillations between basal ganglia nuclei has not been studied.

We also demonstrated in Chapter 2 that delta oscillations are directly tied to action on dopamine D2 receptors – systemic antagonism of D2 receptors causes delta oscillations in the healthy SNr, while D2 agonism in DD conditions ablates the SNr oscillations. D2 receptors are present throughout the basal ganglia, but are especially prevalent in the striatal neurons which initiate the indirect pathway. It is feasible, then, that oscillations arise in the indirect pathway and arrive at SNr through connections from GPe.

However, the oscillation phase distributions we observe *in vivo* make propagation more complicated. It is intuitive that oscillations in the brain would propagate most effectively when

each input to the postsynaptic population is synchronous, as in synfire chains (Abeles 1982) except on the timescale of the oscillation, not necessarily on the timescale of individual spikes. That is, when comparing the oscillatory rate function for two neurons in a presynaptic population, the two would most effectively entrain a common downstream target if they share identical phases. In both GPe and SNr, this phase synchrony is not present. There are, of course, near-antiphase populations of neurons within these nuclei – prototypic (TI) and arkypallidal (TA) in GPe (Abdi et al. 2015; Mallet et al. 2008, 2012), AP and IP in SNr – but even within these populations, individual neurons’ oscillations lead and lag one another. It is unclear if or how effectively a network with such imperfect synchrony may allow for oscillatory propagation.

We aim to test whether it is possible for GPe to entrain a delta rhythm in SNr neurons in a computational model of the SNr receiving input from simulated GPe spike trains. Specifically, we seek to determine if there exists a GPe-SNr circuit architecture which can reproduce our experimental observations from Chapter 2 – namely, the near-antiphase AP and IP populations in the SNr and their intrinsic firing patterns and phase relationships. The successful architecture we find suggests that a competitive process for GPe and SNr synaptic formation on the somas of SNr neurons is sufficient to allow for the spontaneous generation of AP and IP populations when inhibited with oscillatory GPe input. Despite phase lags in GPe, oscillations arise as expected in the two SNr populations with inherited phase lags which match experimental data. These results suggest that SNr need not develop its own intrinsic oscillations in DD but can instead inherit them from other basal ganglia nuclei. We also generate hypotheses to test the validity of this model of oscillatory propagation to further narrow down where delta oscillations may arise, a critical detail in targeting the source of these oscillations for potential PD treatments.

3.2 MATERIALS AND METHODS

3.2.1 Biophysical model of SNr neurons

We used the conductance-based biophysical model of SNr neurons from (Phillips et al. 2020) with small modifications noted below. Parameters were originally adapted from (Abbott et al. 1997; Corbit et al. 2016; Xia et al. 1998) or tuned from experimental data in (Connelly et al. 2010; Zhou et al. 2008), except where otherwise noted.

Each neuron is modelled with a synaptic and dendritic compartment with respective membrane potentials V_S and V_D governed by the equations

$$C_S \frac{dV_S}{dt} = -I_{Na} - I_{NaP} - I_K - I_{Ca} - I_{SK} - I_{leak} - I_{GABA}^S - I_{DS}$$

$$C_D \frac{dV_D}{dt} = -I_{TRPC3} - I_{SD} - I_{STN}$$

where C is that compartment's membrane capacitance and each I is an ion current: a fast (I_{Na}) and persistent (I_{NaP}) Na^+ current, delayed rectifying K^+ current (I_K), Ca^{2+} current (I_{Ca}), Ca^{2+} -activated K^+ current (I_{SK}), leak current (I_{leak}) in the somatic compartment, and a transient receptor potential channel 3 current (I_{TRPC3}) in the dendritic compartment. I_{DS} and I_{SD} are coupling currents representing the current flow from the dendritic to somatic compartments and vice-versa. I_{GABA}^S denotes the synaptic current due to projections from simulated GPe neurons (see below) and local connections from other SNr neurons. I_{STN} denotes a transient excitation from STN whose neurons synapse primarily on dendrites in the SNr (Kita and Kitai 1987) which is included in lieu of spiking STN neurons. Each current is governed by the following equations:

$$I_{Na} = g_{Na} \cdot m_{Na}^3 \cdot h_{Na} \cdot s_{Na} \cdot (V_S - E_{Na})$$

$$I_{NaP} = g_{NaP} \cdot m_{NaP}^3 \cdot h_{NaP} \cdot (V_S - E_{Na})$$

$$I_K = g_K \cdot n_K^4 \cdot h_K \cdot (V_S - E_K)$$

$$I_{Ca} = g_{Ca} \cdot m_{Ca} \cdot h_{Ca} \cdot (V_S - \ln \left(\frac{[Ca]_{out}}{[Ca]_{in}} \right) E_{Ca})$$

$$I_{SK} = g_{SK} \cdot m_{SK} \cdot (V_S - E_K)$$

$$I_{leak} = g_{leak} \cdot (V_S - E_{leak})$$

$$I_{GABA}^S = g_{GABA}^S \cdot (V_S - E_{GABA}^S)$$

$$I_{DS} = g_C \frac{C_S}{C_S + C_D} \cdot (V_S - V_D)$$

$$I_{TRPC3} = g_{TRPC3} \cdot (V_D - E_{TRPC3})$$

$$I_{SD} = g_C \frac{1}{1 - \frac{C_S}{C_S + C_D}} \cdot (V_D - V_S)$$

$$I_{STN} = g_{STN} \cdot (V_D - E_{glut})$$

where each g is the current's maximum conductance, E is the current's reversal potential, and each m , h and s is a gating variable governed by an equation of the type

$$\frac{dx}{dt} = \frac{x^\infty - x}{\tau_x}$$

where x is an m , h or s gating variable of a particular current, x^∞ is the gate's steady state and τ is the gate's time constant, governed by the following equations

$$x^\infty(V) = (1 + e^{-(V-x_{1/2})/k_x})^{-1}$$

$$\tau_x(V) = \tau_x^0 \frac{\tau_x^1 - \tau_x^0}{e^{(\tau_{1/2}^x - V)/\sigma_x^0} + e^{(\tau_{1/2}^x - V)/\sigma_x^1}}$$

where all variables besides V are constants.

An exception is the Ca^{2+} -gated SK channel, whose m gate is governed by

$$m_{SK}([Ca]_{in}) = \left(1 + \left(\frac{k_{SK}}{[Ca]_{in}}\right)^{n_{SK}}\right)^{-1}$$

where k_{SK} is the half-activation calcium concentration and n_{SK} is the Hill coefficient. The intracellular Ca^{2+} concentration $[Ca]_{in}$ is governed by

$$\frac{d[Ca]_{in}}{dt} = -\alpha_{SK} \cdot I_{Ca} - \frac{[Ca]_{in} - [Ca]_{min}}{\tau_{Ca}}$$

where α_{SK} is a constant relating current with the rate of change of $[Ca^{2+}]_{in}$, τ_{Ca} is the time constant for calcium efflux through Ca^{2+} pumps, and $[Ca]_{min}$ is the minimum calcium

concentration at which these pumps are active. The parameters for this equation were adapted from (Xia et al. 1998).

The synaptic conductance g_{GABA}^S is governed by

$$\frac{dg_{GABA}^S}{dt} = -\frac{g_{GABA}^S}{\tau_{GABA}^S} + W_{GABA}^{GPe} \cdot D \cdot \delta(t - t_n) + W_{GABA}^{SNr} \cdot \delta(t - t_m)$$

where τ_{GABA}^S is the synaptic decay time constant, W is the synaptic weight matrix from either GPe or other SNr neurons, δ is the delta (impulse) function, and $t_{n,m}$ is the presynaptic spike times for GPe and SNr, respectively. D is a scale factor for short-term synaptic depression governed by (Abbott et al. 1997)

$$\frac{dD}{dt} = -\frac{D_0 - D}{\tau_D} + -\alpha_D \cdot (D - D_{min}) \cdot \delta(t - t_n)$$

We tuned two of the parameters to match differences in DD and control (non-DD) conditions. g_{TRPC3} in the model was tuned to match the findings in (Zhou et al. 2008) – that is, under Na^+ channel block, blockade of TRPC3 channels yields a 10 mV hyperpolarization of the membrane potential. Since activation of D1 receptors is required for the opening of TRPC3 channels in SNr (Zhou et al. 2009), g_{TRPC3} was set to 0 in DD conditions.

g_{STN} was tuned such that the firing rate of SNr neurons in the full network model in DD conditions would match the mean firing rate observed *in vivo* in DD. Since electrophysiological data from chapter 2 indicated a 50% increase in mean STN firing rates in control compared to DD conditions, this value was scaled by 1.5 in the control model.

3.2.2 Simulated GPe spike trains

Rather than simulating GPe neurons, we generated artificial spike trains to serve as input to the SNr model neurons. In DD, GPe spike trains were of two types, Poisson or oscillating. Both types are modelled as inhomogeneous Poisson processes with rate function $\lambda(t)$. In Poisson spike trains, that rate function is

$$\lambda(t) = \begin{cases} 0 & t - T \leq t_{refrac} \\ \lambda_c & t - T > t_{refrac} \end{cases}$$

where t_{refrac} is the absolute refractory period and λ_c is the baseline firing rate which was fit to the mean firing rate of GPe neurons recorded in Chapter 2. Since the median GPe firing rate did not differ significantly in control and DD animals (34.47 Hz in control compared to 33.09 Hz in DD, $p = 0.803$, Wilcoxon rank sum test), λ_c was set to 34 Hz and was unchanged between control and DD simulations.

Oscillating spike trains have a rate function as follows:

$$\lambda(t) = \begin{cases} 0 & t - T \leq t_{refrac} \\ \lambda_c + f_{osc}(t, A, \omega) & t - T > t_{refrac} \end{cases}$$

where $f_{osc}(t, A, \omega)$ is a periodic function of time t , frequency ω chosen as 2 Hz to be near the median delta frequency observed in our GPe units, and amplitude A chosen such that a spike train would have a 1 Hz firing rate at its trough.

Since the delta oscillations we observe in the SNr are not perfect sine waves but rather modelled better as oscillatory processes with up and down states, we chose f_{osc} to be a square wave with unequal up and downstate durations; that is

$$f_{osc}(t, A, \omega) = \begin{cases} \frac{A}{2} & \text{mod}(t, \frac{1}{\omega}) \leq \frac{u}{\omega} \\ -\frac{A}{2} & \text{mod}(t, \frac{1}{\omega}) > \frac{u}{\omega} \end{cases}$$

where u is the fraction of each period spent in the upstate. To fit an appropriate value for u , we analyzed the oscillation shapes of GPe neurons recorded in Chapter 2. We included only neurons with detected oscillations and whose firing rates exceeded 20 Hz to ensure that no arky pallidal neurons were included, as they do not project to SNr (Abdi et al. 2015; Mallet et al. 2012). For each neuron, we computed its spike density function (SDF) by convolving the spike train with a Gaussian filter with $\sigma = 50$ ms; this produces a smooth instantaneous firing rate function, but one which is coarse enough such that delta oscillations can still be seen. We then computed a moving mean $m(t)$ of the SDF with a rectangular window of 5 seconds to obtain a

mean firing rate over a much longer timescale, but short enough to change along with long-timescale nonstationarities in firing rate (Figure A-6A). We then computed the fraction of time F for which $sdf(t) > m(t)$, and found the median F across all neurons to be approximately 0.55. Thus, we chose the upstate to comprise 55% of the period while the downstate comprises the remaining 45%.

In the control model, we generated spike trains with a more regular firing pattern, mimicking the firing patterns observed in the healthy GPe. All neurons in the control model fired spikes with an interspike interval of $1000/F \pm 2$ ms, where F is their pre-determined firing rate in Hz, and the ± 2 ms jitter was sampled randomly from a uniform distribution.

3.2.3 Fitting GPe phase lag distributions

Like SNr, oscillations in GPe neurons can exhibit non-zero delays relative to one another. To incorporate these delays into our model, we computed the pairwise phase lag distribution for GPe (Figure A-6B), as done in Chapter 3 for SNr. In order to simulate a population of neurons with phases such that this distribution was maintained, we sought to estimate the distribution of individual phases from this pairwise phase lag distribution. We assumed that the phases are normally distributed following $N(\theta, \sigma)$ and sought to estimate σ . The pairwise phase lags we measured can be considered the absolute difference of two independent samples from $N(\theta, \sigma)$, which means they follow a half-normal distribution $H(0, \sqrt{2}\sigma^2)$. The best fit to the pairwise distribution gives an estimate of $\sigma = 34.6164$ ms. At the start of each simulation, a GPe neuron's phase was chosen from this distribution, resulting in a pairwise phase distribution similar to the one observed experimentally (Figure A-6B).

3.2.4 Connection architecture

We chose populations of 100 SNr neurons (50 in each of Population A and B when applicable) and 100 GPe spike trains (50 in each of the oscillating and Poisson populations when applicable). Equally sized populations were chosen because the number of neurons in

SNr *in vivo* is approximately equal to the number of GPe neurons which project there (Simmons et al. 2020).

Each SNr neuron received four (in the basic and partially segregated models) or an average of four (in the competitive model) connections from both GPe and other SNr neurons, as real SNr neurons receive a small number (approximately two to six) of unitary connections from GPe (Simmons et al. 2020) and an average of four from other SNr neurons (Higgs and Wilson 2016). While the large strength of these connections is likely due to many synapses from a single presynaptic neuron forming on the postsynaptic neuron (Simmons et al. 2020; Smith and Bolam 1989), we modelled these nests of boutons as a single, strong synapse from each presynaptic cell.

3.2.5 Simulations and analysis

Code to simulate the biophysical network was written in C++. Differential equations were evolved using Euler's method with a timestep of 0.05 ms. Simulations were run for a total of 50 simulation seconds, and the first three seconds were discarded. Results from the simulation were imported into MATLAB for analysis.

3.2.6 Measuring irregularity with CV_2

Since real spike trains have a greater degree of nonstationarity than those in our simulations, we used the CV_2 measure of irregularity (Holt et al. 1996) which computes the coefficient of variation (CV) over a moving window of two interspike intervals (ISI's) thereby correcting for nonstationarities in firing rate. Specifically, we compute the CV for all pairs of adjacent ISI's and compute this distribution's mean:

$$CV_2 = \frac{1}{N} \sum_{i=1}^N \frac{2|\Delta t_{i-1} - \Delta t_i|}{\Delta t_{i-1} + \Delta t_i}$$

where Δt_i is the length of the i th ISI and N is the number of adjacent pairs of ISI's in the spike train.

3.2.7 Identifying oscillating neurons

Oscillations in single neurons were detected using the same procedure as in section 2.2.7: Oscillation detection and visualization, requiring that oscillations passed both the power and phase shift criteria. Although the forcing frequency in our simulations was known to be 2 Hz, our oscillation detection algorithm remained agnostic to this information.

Since we did not simulate motor cortex, we could not define AP and IP units in the same manner as in Chapter 3. Instead, we compared the phases of SNr oscillations with those in GPe. We computed an SDF of the sum of all GPe neurons' spike trains and calculated the cross-correlation of this mean GPe signal with each SNr neuron which exhibited a delta oscillation. Beyond their relationship to M1, a defining feature of the AP population is that it, on average, leads IP units *in vivo*. Since the only way in our simulations for an oscillation in SNr to become approximately in phase with GPe oscillations would be through a bisynaptic (GPe to SNr to SNr) or higher multisynaptic connection, we defined IP neurons as those whose GPe SDF cross-correlation peak was closer to zero lag than their trough, and AP neurons as those whose trough was closer to zero lag than their peak. To lend evidence to our assumption, we ran a simulation of the "basic" model with no GPe phase delays (so lead-lag relationships could be easily identified) and confirmed that every neuron defined as AP through this process led every neuron defined as IP. We also confirmed that the AP lead bias remained in our final model (the competitive model, Figure 3-2E) While our assumption appears accurate, the units in this section may be more accurately referred to as putative AP and IP units; we primarily drop the "putative" modifier for brevity.

3.2.8 Quantifying model fit

To compare the model results to experimental data, we computed means and two-sided 95% confidence intervals for several metrics on the data, such as the firing rate of SNr neurons and the fractions of neurons which exhibited an oscillation. Confidence intervals were computed in one of two ways:

1. The fraction of non-oscillating, AP and IP neurons each follow a binomial distribution $B(p_g)$ with the assumption that each recorded neuron's identity is independent of all others. For each group (AP, IP, or non-oscillating), p_g represents the probability that a neuron is a member of that group. We estimated a 95% confidence interval around the sample mean for each group using the analytic Clopper-Pearson method implemented in the MATLAB function `binofit`.
2. For all other measures where an analytic estimate was not possible, we computed 1000 bootstrapped samples and calculated the statistic being estimated (e.g. mean, CV), then used the 2.5th and 97.5th percentile from all samples as the confidence interval.

3.2.9 Clustering

Cluster analysis of AP and IP neurons was performed using an unsupervised k-means algorithm with $k=2$. The boundary between clusters was defined as the line orthogonal and equidistant from the two cluster centroids. Distance from each point to the boundary was defined as the shortest path to the boundary (i.e. a line orthogonal to the boundary).

3.3 RESULTS

3.3.1 A model with partially segregated pathways matches *in vivo* recordings

We sought to test the hypothesis that the features of SNr oscillations observed in our data can be explained by SNr inheriting its oscillatory pattern from its GPe inputs. That is, we sought to determine if there exists a reasonable GPe-SNr architecture that replicates our observations in Chapter 2. To investigate this, we built networks of 100 biophysically realistic SNr neurons receiving input from a population of 100 simulated GPe spike trains and compared the results of these simulations to *in vivo* data from SNr.

To start, we built a model with a simple architecture restricted in such a way that two antiphase populations were likely to form. We simulated GPe spike trains split into two populations – 50 Poisson trains and 50 trains spiking with an underlying 2 Hz oscillation (see

Methods). Then, we initialized 100 SNr neurons split into equal populations A and B – Pop. A received synaptic input only from oscillating GPe neurons and Pop. B SNr neurons, whereas Pop. B received input only from Poisson GPe neurons and Pop. A SNr neurons (Figure 3-1A). Synaptic connectivity was determined randomly at the start of the simulation – as such, each SNr neuron received the same number of synapses, but each GPe train and SNr neuron did not necessarily make an equal number of synaptic connections.

To compare the model results with real data, we first looked at the power of oscillations for each neuron in each population (AP or IP) as defined by their relationship to GPe (see Methods) and compared these to the delta powers of AP and IP neurons recorded *in vivo* (Figure 3-1B-C). Note that the underlying oscillations in our simulations are stationary (i.e. they are exactly a function of time, so their autocorrelation does not decay at long lags), whereas oscillations in the experimental setting have an autocorrelation which decays to zero after a few periods. As such, it is difficult to compare raw power values between the simulations and experimental data, and thus we will scale these values to make better quantitative comparisons later in this chapter.

Qualitatively, the results of this simulation show a clear AP/IP dichotomy, which is determined completely by the neuron's identity in the network architecture – those in Pop. A receiving oscillatory inhibition from GPe make up the AP population, while those receiving Poisson inhibition from GPe and thus inheriting their oscillations only from SNr connections make up the IP population. The AP neurons also have greater power than the IP neurons, as seen *in vivo*. However, the distributions of power differ from those seen *in vivo*, with no overlap between the AP and IP power distributions.

To quantify the fit of our model to experimental data, we checked whether the SNr spike trains in our simulation fell within a 95% confidence interval of metrics derived from real SNr data in three categories: basic firing properties, size of oscillatory populations, and properties of oscillations (Figure 3-1D).

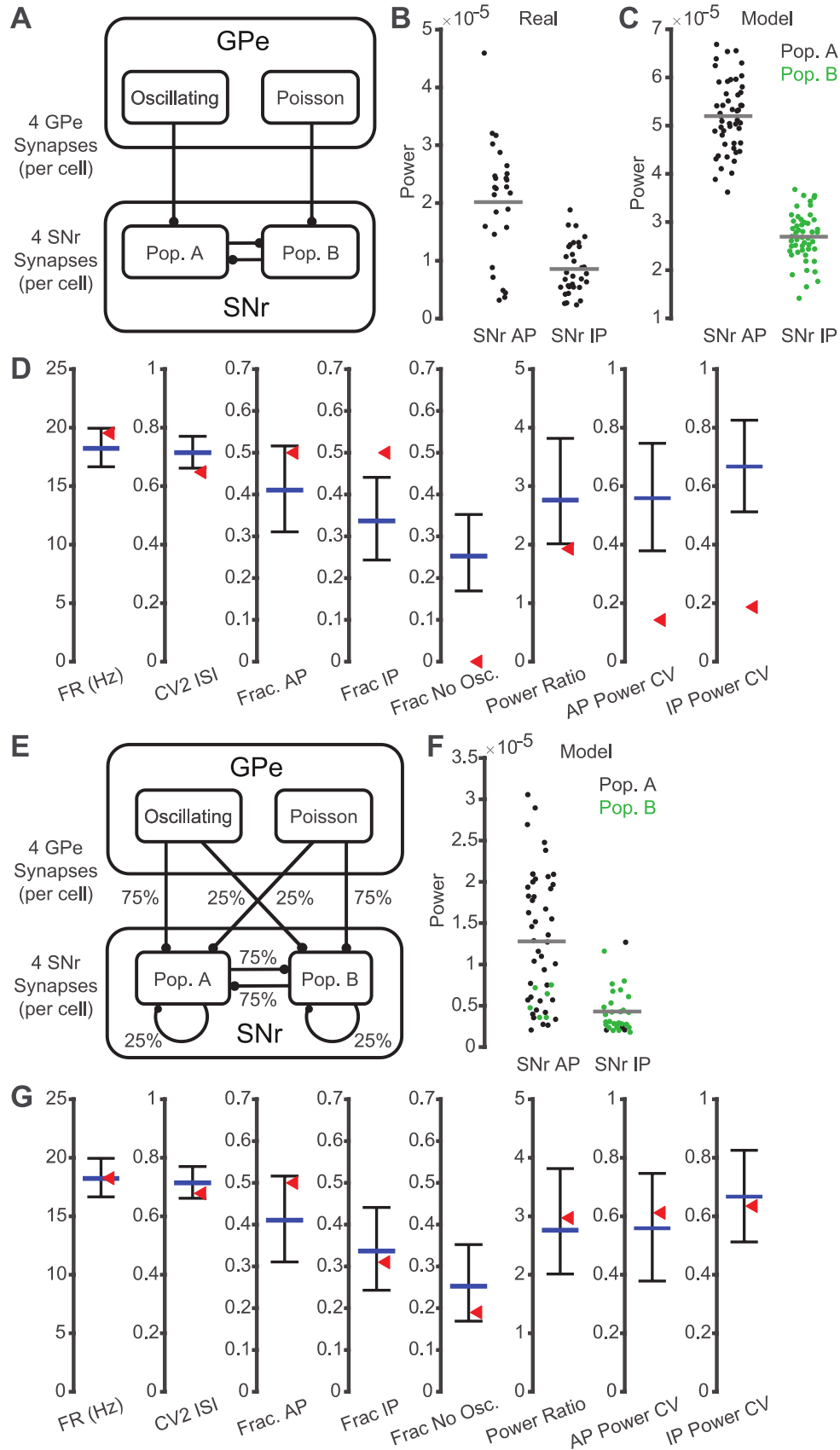


Figure 3-1: Performance of models with segregated pathways.

A. Architecture for the “basic” model, where two SNr populations receive entirely distinct GPe inputs (one oscillating, one Poisson) and only project to each other. **B.** Delta power of each neuron *in vivo* in the AP and IP SNr populations. **C.** As in B, but from the results of a simulation of the basic model. Black dots are neurons from Population A from the architecture in Panel A, green dots are neurons from Population B. **D.** Performance of the basic model on measures derived from *in vivo* data. Each bar is a bootstrapped or analytically derived confidence interval (see Methods) and each red arrow is the model’s results computed from all simulated SNr neurons. FR: mean firing rate (Hz); CV2 ISI: mean CV₂ of interspike intervals; Frac AP/IP/No Osc: fraction of neurons in the AP, IP, or non-oscillating populations. Power Ratio: ratio of the mean delta power of all AP neurons to the mean power of all IP neurons. AP/IP Power CV: CV of the distribution of AP/IP delta powers. **E.** Architecture for the “partially segregated” model, which extends the basic model to include probabilities of connections crossing over from the population they would normally project to. **F-G.** Same as C-D for the results from the partially segregated model.

For basic firing properties, we looked at firing rates and regularity of firing measured using CV2, a measure of irregularity which corrects for nonstationarities in firing rate over time. In this initial model, the neurons were significantly more regular (CV2 closer to zero) than in the experimental data.

We next looked at the putative identities of neurons – active-predicting (AP), inactive-predicting (IP) or non-oscillating. In this case, the differences from experimental data were stark – since each neuron’s identity is determined exactly by which of Pop. A or B it was assigned to, there are exactly 50 AP and 50 IP neurons with no non-oscillating neurons. Because of this, the results fail to replicate experimental data here.

Finally, we looked at properties of the AP and IP neurons. Since it is difficult to directly compare oscillatory powers between experiments and simulations, we computed a mean power ratio between the two populations, defined as the ratio between the mean power of all AP neurons in the simulation and the mean power of all IP neurons at the forcing frequency from GPe, as this ratio should cancel out the differences in stationarity between the experimental and simulated data. This model matches experimental data in that AP neurons are stronger than IP neurons, but significantly less so than *in vivo*. We also computed the CV of powers in each population to determine if the variability of oscillation strengths across neurons in each population matched the real data. In the basic model, there was significantly less variability in oscillation strength in both populations than *in vivo*.

This basic model's primary deviation from experimental data is in the variability of its oscillations – all neurons within a population oscillate at similar strengths, whereas neurons *in vivo* have more varied oscillations or no detectable oscillations at all. As such, we extended this model to add additional noise by relaxing its strict connectivity rules. Instead of all Pop. A neurons receiving input only from oscillating GPe neurons and Pop B. SNr neurons, we included a “crossover probability” such that 25% of Pop. A's GPe synapses instead came from Poisson neurons and 25% of SNr synapses were from other Pop. A neurons. This was mirrored in Pop. B; 25% of GPe synapses were now from the oscillating population and 25% of SNr synapses were from Pop. B. We termed this the “partial segregation model” (Figure 3-1E).

This model distributes neurons into AP and IP populations with much more realistic delta power distributions (Figure 3-1F). Notably, a neuron's fate was not determined completely by whether it was in Pop. A or B as was the case in the basic model – by chance, some Pop. A neurons have an IP relationship to GPe rather than the expected AP relationship, and vice-versa for Pop. B. This model also performed significantly better quantitatively, as each of the properties we measured fell within the confidence intervals derived from experimental data (Figure 3-1G). The small number of crossover connections led to weaker oscillations in some neurons, thereby increasing the breadth of oscillation strengths seen in each population and leading to some neurons which had no detectable oscillation due to their combination of synaptic inputs.

3.3.2 A simpler, “competitive” model also matches *in vivo* recordings

While it fits experimental data better than the basic model, the partial segregation model still assumes the existence of two anatomically distinct populations in SNr which are biased to receive particular patterns of connectivity from GPe and fellow SNr neurons. To relax this assumption, we considered an architecture which could potentially allow for such a dichotomy through natural heterogeneity. This model has a single heterogenous population of SNr neurons which receive a total of 8 synapses, each with equal likelihood to arise from a GPe or fellow SNr

neuron. We term this the “competitive model”, as GPe and SNr (randomly) compete for synapses on each neuron (Figure 3-2A). With this model, we posited that the neurons which, through random chance, had a high level of inhibition from GPe would form the basis of the AP population and those with a high level of inhibition from those AP neurons would form the IP population, while neurons receiving more balanced input would fall to one side or the other through more complicated multisynaptic dynamics or not oscillate at all.

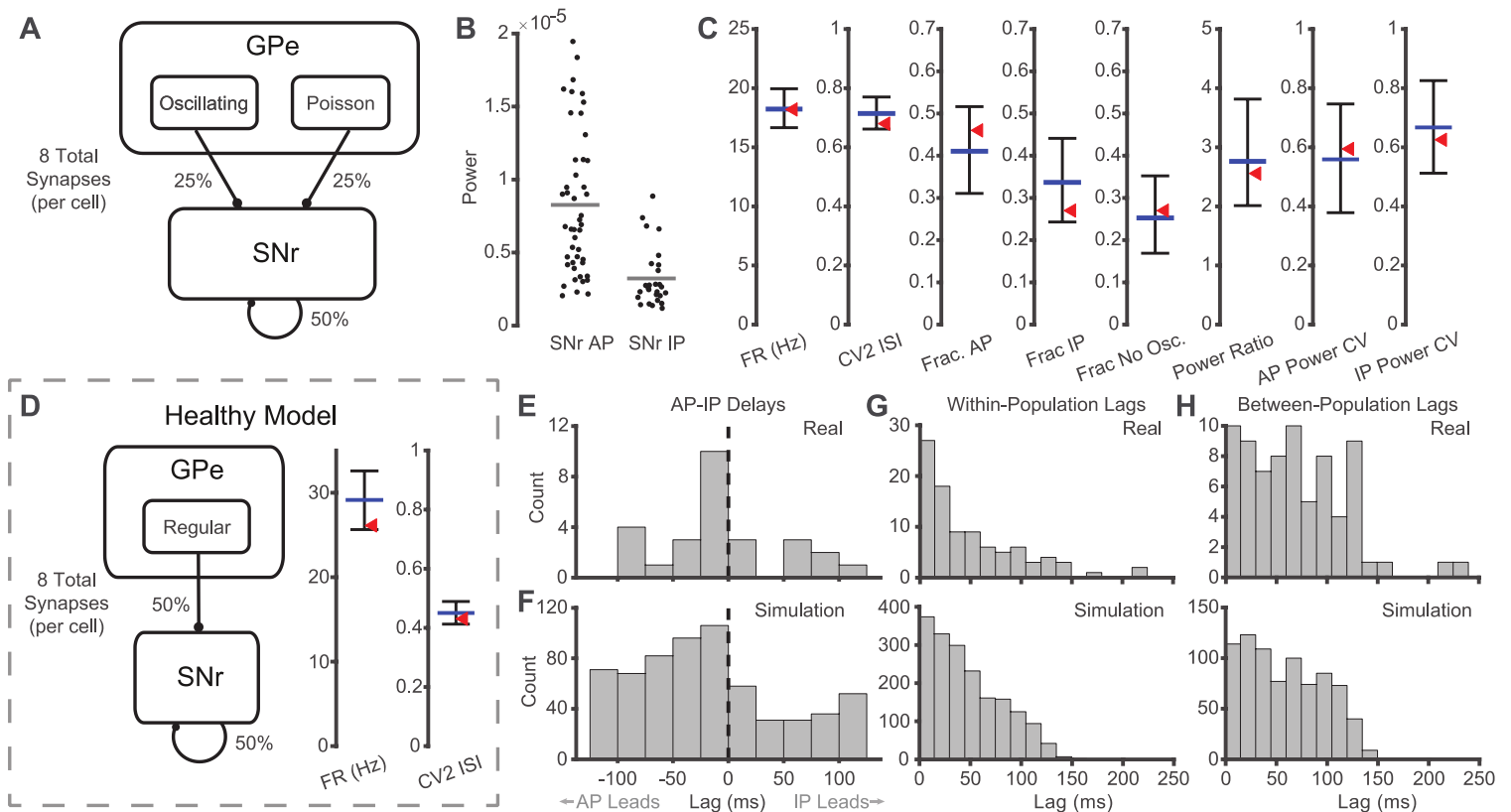


Figure 3-2: Performance of the competitive model.

A. Architecture for the “competitive” model, where the number of GPe and SNr synapses are not fixed but each SNr neuron’s fixed number of synapses have an equal chance of arising from GPe or SNr. **B.** Delta power for each neuron in the AP and IP populations from a simulation of the competitive model. **C.** Performance of the competitive model on measures derived from *in vivo* data, see Figure 3-1C. **D.** Left: Architecture of the healthy version of the competitive model where all oscillating and Poisson GPe neurons are replaced with pacemakers. Right: Same as C, but only comparing to measures from control *in vivo* data and only looking at measures which do not depend on the presence of delta oscillations. **E.** Analysis of AP/IP lead-lag relationship. Histogram of the phase lags between all pairs of simultaneously recorded AP and IP neuron pairs *in vivo*. Counts on the left indicate AP leading IP. **F:** Same as E for the results of the competitive model. **G.** Analysis of broader lead-lag relationships. Top: histogram of the absolute phase lags between all pairs of neurons in the same population (putatively AP vs. AP or IP vs. IP). Bottom: same as top-left for the results of the competitive model. **H.** Same as G for all pairs of neurons in opposite populations (putatively AP vs IP).

Simulations of the competitive model showed similar results to the partial segregation model, in that it demonstrated a reasonable distribution of delta powers in the AP and IP populations (Figure 3-2B) and all quantitative measures fell within the confidence intervals determined from *in vivo* data (Figure 3-2C).

Having identified a model which both fit the basic properties of the data and had a reasonably simple and realistic architecture, we asked if a version of this model which didn't exhibit features of dopamine depletion would reasonably fit our control *in vivo* data. As such, we made three modifications to the competitive model: 1) Instead of oscillating and Poisson spike trains, all simulated spike trains from GPe were approximately pacemaking (see Methods); 2) the passive TRPC3 current was tuned up to match experimental data (Zhou et al. 2008, 2009); 3) tonic STN excitation was tuned up to match our *in vivo* data. Without further tuning, the results of this model matched the expected firing rates and variability observed *in vivo* in healthy animals (Figure 3-2D). As such, this model of competitive synaptic allocation in SNr from GPe and other SNr neurons matches our SNr data in both the control and DD conditions.

3.3.3 Imperfectly synchronous GPe oscillations propagate and entrain phase lags in SNr

Next, we sought to delve deeper into some of the dynamics of the competitive model in DD. First, we investigated the phase delays between neurons within and between AP and IP populations. A feature of the AP/IP dichotomy is that oscillations in AP neurons tend to lead those in IP neurons (Figure 2-8). Since we do not have an M1 reference signal in the model as we did in some of our *in vivo* data, we attempted to replicate this finding using the cross-correlations between spike trains from individual neurons (see Methods). Using all of our labeled pairs of simultaneously recorded AP and IP neurons, we see a clear bias towards AP neurons leading simultaneously recorded IP neurons (Figure 3-2E, $p = 0.0179$, Wilcoxon signed rank test). In our results from the competitive model (in which we can simulate many more pairs

of simultaneously recorded neurons), we see a similar bias toward the AP population leading IP neurons (Figure 3-2F, $p = 4.490 \cdot 10^{-13}$).

We also compared the more general distributions of within-population and between-population distribution of pairwise phase lags. In our experimental data, both distributions peaked at zero as expected. While the within-population distribution has a sharper peak in the real data than in our simulation (indicating that our simulation has slightly inflated lags over the real data), the distributions are not significantly different from one another (Figure 3-2G, $p = 0.2850$, two-sample Kolmogorov-Smirnov test). Similarly, the between-population distributions in both the real and simulated data are wider than the within-population distributions, and the simulation is again not significantly different from the real data (Figure 3-2H, $p = 0.1443$). As such, this model replicates the phase delays evident in the DD SNr network, though may be biased slightly towards longer delays.

3.3.4 The power of oscillatory inputs from GPe and SNr define the AP and IP clusters

Finally, we sought to more deeply understand the dynamics leading to the distinct AP and IP populations in our competitive model. Since the number of synapses that each SNr neuron receives from either population (GPe or SNr) follows a unimodal binomial distribution, we might expect a continuous spectrum of oscillatory profiles, with a large number of non-oscillating neurons receiving a near equal number of GPe and SNr synapses while neurons on the tails of this distribution express a strong AP or IP oscillation. However, the large number of strongly oscillating AP and IP neurons suggests that the neurons' intrinsic dynamics and synaptic interactions may combine to separate units into the more distinct AP and IP classes.

To investigate this idea, we plotted each neuron's sum of synaptic weights from GPe against its sum of weights from SNr. As expected, these two measures have an inverse relationship as dictated by the competitive nature between the number of GPe and SNr synapses on a single neuron. Additionally, we see that AP neurons tend to receive more GPe input while IP neurons tend to receive more SNr input, as expected. Note that each neuron's

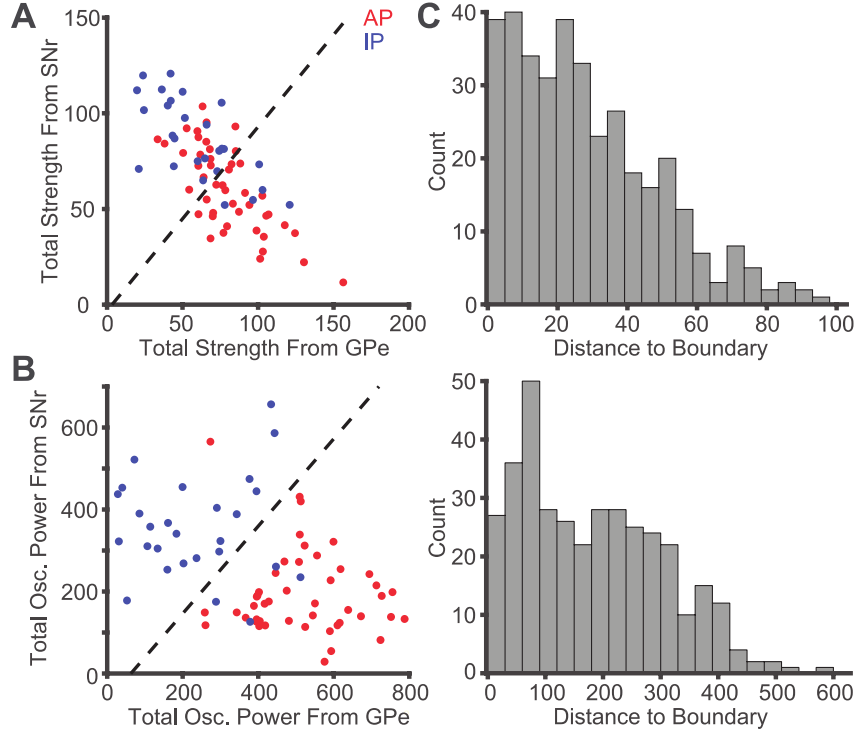


Figure 3-3: Model SNr neurons cluster based on presynaptic GPe and SNr delta power.

A. Scatterplot of AP (red) and IP (blue) neurons based on their total synaptic strength from other SNr and GPe neurons. Dashed line is a boundary based on the kmeans clustering algorithm with $n = 2$, used as a comparison against the clusters in panel B. **B.** Same as A, except plotting the total 2 Hz power ($\Sigma[2 \text{ Hz power} * \text{synaptic strength}]$) from SNr and GPe. **C.** Distance from each neuron to the kmeans boundary for panel A (top) and B (bottom), totaled over 5 runs of the competitive model with different randomly instantiated connections and strengths. The non-zero peak in the bottom panel indicates a separation of clusters from the boundary.

placement on this scatterplot is determined completely by the random setup of the network, as no synaptic weights are changed during the simulation. As such, there is an expected binomial-like density of points along the $y = -x$ line.

Next, we weighed each synaptic weight by its oscillatory power at the forcing frequency (2 Hz) to visualize the total oscillatory power each neuron receives from GPe and SNr synapses. Here, we see the AP and IP neurons separate into more distinct clusters. Using the kmeans (with $k=2$) clustering algorithm, we derived a boundary that best separates the two clusters and found that only 4 neurons were mislabeled (i.e., an AP neuron in the IP-dominant cluster or vice-versa). Most notably, we noticed an unexpected level of separation between these two clusters. To quantify this, we computed the distance from each point to the boundary

and found its distribution not centered at zero. As a comparison, we performed the same kmeans clustering and distance computation on the strength scatterplot in *Figure 3-3A* and found a distance distribution centered at zero, as would be expected from this visually unimodal 2-D distribution. This lack of neurons in this area between clusters is surprising, as it is not clear how the presynaptic oscillatory powers received by each neuron would dichotomize to leave this area sparse unlike what we observe in the strength scatterplot. Nevertheless, this demonstrates that the neurons in this model undergo an unexpected bifurcation into two mostly distinct AP and IP populations.

3.4 DISCUSSION

In this chapter, we have demonstrated that GPe oscillations are sufficient to entrain oscillations in SNr that mimic those observed *in vivo*. This is possible in a network architecture which explicitly defines SNr subdivisions by their distinct synaptic connectivity patterns, where neurons tend to (but do not always) fall into AP or IP-like phase relationships based on which of the two subdivisions they are in. However, we show this dichotomy is also possible through a simpler and less assumptive model wherein SNr and GPe compete for a limited number of synapses on each SNr soma. With small, realistic changes to this model to simulate a healthy state, we show that the model exhibits firing rates and patterns that match what we observe in healthy control mice, lending further credence to the realism of our model. We have also demonstrated that, despite their imperfect synchrony, delta oscillations in GPe are able to propagate to downstream targets and generate realistic phase distributions in SNr.

3.4.1 Network architecture assumptions

Our initial model assumed two anatomically distinct populations of SNr neurons receiving connections from specific types of GPe and SNr cells. Specifically, we assumed that oscillating and Poisson neurons in GPe are each biased toward distinct projection targets in SNr, and that these two SNr populations primarily project to one another rather than to

themselves. Experimentally, there is clear evidence of topographical pathways through the basal ganglia, including the GPe-SNr pathway, which are segregated by the higher order processes they are associated with – motor, limbic, or associative (DeLong and Wichmann 2010; Yelnik 2002). However, the topography is likely more complicated, continuous or convergent than the two discrete populations we present in this model (Foster et al. 2020; Nakano 2000). Given our results in Chapter 2 demonstrating the connection between delta oscillations and motor symptoms, it is possible that oscillations may be restricted primarily to motor pathways in the basal ganglia while not penetrating limbic or associative pathways, which could lend credence to our built-in dichotomy, although there is no direct evidence for this. However, even if two distinct GPe-SNr pathways exist as we have modelled them here, it is unlikely that the two SNr populations would be more likely to project to each other rather than back to themselves, and this is a critical detail for our basic and partially segregated models' oscillatory behaviors. As such, we consider these initial models a proof of concept for how realistic oscillations could form in such a system, but not necessarily a realistic model of the GPe-SNr network.

In contrast, our competitive model does not rely on any of these assumptions. Instead, the only architectural assumption is the existence of competition between GPe and SNr neurons for forming and maintaining synapses on SNr somas. While there is no direct evidence of this to our knowledge, other examples of similar synaptic competition exist. For example, synaptic scaling occurs in many regions of the brain to approximately balance a neuron's output (although this has primarily been studied at excitatory rather than inhibitory synapses) (Turrigiano 2008), and nascent synapses may be pruned if nearby synapses are particularly active (Lo and Poo 1991). Notably, SNr neurons tend to exhibit large nests of synapses all arising from the same presynaptic neuron (Simmons et al. 2020; Smith and Bolam 1989); this redundancy may explain the atypical strength of these connections onto SNr, and could also increase synaptic competition if there is simply not enough physical space for more synaptic

neurons. While studies have looked closely at the synaptic connectivity from GPe to SNr and within SNr (Higgs and Wilson 2016; Simmons et al. 2020), no study has looked at the relationships between these connections and whether strong inhibition from one source affects the probability of receiving strong inhibition from the other. A study directly testing whether levels of inhibition from GPe and SNr on a single SNr neuron are inversely correlated, as we have predicted here, would lend credence to our proposed model of delta propagation to SNr through GPe.

3.4.2 Limitations

In comparing the results from models to real data, we ran statistical tests or derived confidence intervals to determine if the simulated results were statistically indistinguishable from the real data in a classical statistical sense. We caution strongly, however, that our failure to reject the null hypothesis that our simulation produces distributions which are the same as those observed *in vivo* is not an acceptance of that null hypothesis. Such a claim can, in fact, never be proven, as even two samples from identical distributions will never have precisely the same mean (or any test statistic of interest). For the purposes of this study, we consider these classical techniques sufficient to claim that our model reasonably matches the experimental results.

As with any computational model, certain aspect of realism must be sacrificed, both for the simplicity of building the model and in interpreting its results. We used a conductance-based model of SNr neurons which grounds this model in biological realism based on the known ionic currents driving these neurons' electrochemical dynamics and allows them to be well fit to experimental data. However, even this relatively realistic model requires many simplifications. We included only two compartments, one somatic and one dendritic, which neglects features like dendritic computation and variable or even failed propagation of action potentials down an axon. While we include short-term synaptic depression, longer term plasticity is neglected, due both to the complexity this would induce in the model and a lack of experimental understanding

of plasticity in the SNr. Since it is not clear how delta oscillations initially arise in the basal ganglia, our choice to force these oscillations in artificial GPe spike trains allows us to study the propagation of oscillations to and within SNr. While we attempted to fit our artificial oscillations to data from GPe, features such as nonstationarities in oscillatory power, frequency and firing rate were not modeled, and could affect the propagation and integration of these oscillations in SNr.

While we use the term “competitive model” for the connection architecture we propose, we caution that the particulars of such synaptic competition have been ignored here. We assume that there is limited space for the large synaptic nests that are made on SNr somas (Simmons et al. 2020; Smith and Bolam 1989), and we begin the model at a state in which that limited space has already been allocated to GPe and SNr neurons. The endpoint of this inferred competition can be tuned in the model by adjusting the probability that a unitary connection arises from GPe rather than SNr, but the details of how that underlying competition might occur in the brain are not considered. In biological neurodevelopment, such competition could exist in many forms, with synapses being formed, pruned, strengthened, and weakened through a number of activity-dependent plasticity mechanisms (Fino et al. 2005; Thoenen 2000), or the synapses could genuinely be distributed in a simple random fashion. The details of such development and plasticity in the SNr are not known, but do not affect the endpoint of the system that we are modeling here.

Despite these limitations and simplifications, we find that our model is a good fit to our data in the particular questions we are investigating in this chapter. In order to truly determine the usefulness of this model, however, it is important to tie its results to predictions that can be verified experimentally and test its veracity.

3.4.3 Model predictions and extensions

A major conclusion of our work is that oscillations in GPe are sufficient to recreate the oscillations we observe experimentally in SNr. This hypothesis could be tested by comparing

the oscillatory power in SNr neurons before and after the ablation of GPe. We caution, however, that while GPe may be sufficient to entrain SNr in this way, it may not be the only nucleus doing so – delta oscillations in the STN could also play a role in entraining SNr. As such, an ablation of GPe could silence delta oscillations, but it could also merely weaken them, adjust their patterning, or have little to no effect if only a single oscillating nucleus projecting to SNr is needed to effectively entrain it.

As such, a clear next step for this model would be the inclusion of STN. Adding a nucleus with oscillations that have a shorter upstate (approximately 30% of the period compared to GPe's 55%) and are projected via excitatory synapses could considerably change the dynamics that emerge when GPe and STN's signals are integrated in SNr. Our simulations suggest an architecture of balanced inhibition such that individual neurons receive an approximately equal sum of strong GABAergic inhibition, whether through synapses from GPe or other SNr neurons – similarly, the addition of STN could suggest rules by which STN may innervate SNr neurons, such as a balanced level of excitation across all SNr neurons or a competitive level of innervation with D1 neurons from striatum, since both nuclei tend to synapse onto dendrites.

Additionally, certain newly discovered aspects of GPe and SNr physiology could have significant implications if included in this model. While GPe is canonically an inhibitory nucleus, it has been shown to have both inhibitory and excitatory effects in SNr (Freeze et al. 2013; Phillips et al. 2020) which may be due to a shift in the chloride reversal potential due to high chloride influx from a large amount of GABAergic tone from SNr's many sources of inhibitory input (Phillips et al. 2020). Such shunting or excitatory effects of GPe could greatly shift how effectively it propagates oscillations to SNr, especially in a model in which chloride dynamics are allowed to dynamically shift E_{Cl} . A sufficiently depolarized E_{Cl} also allows for the spontaneous emergence of delta oscillations in a network of interconnected SNr neurons (Phillips et al. 2020). While these oscillations are much weaker than those we see *in vivo*, exhibiting only

approximately a 2 Hz difference between peak and trough compared to the complete cessation of firing observed in many SNr neurons *in vivo*, this intrinsic drive to oscillate at a delta frequency under certain conditions could make SNr more effective at amplifying oscillations it is entrained to by other nuclei or be the source of these oscillations that are amplified within SNr by other biophysical mechanisms or through a multisynaptic loop as has been observed in the generation and amplification of beta oscillations in other computational models of basal ganglia circuitry (Corbit et al. 2016; McCarthy et al. 2011).

We find the separation of neurons into mostly distinct AP and IP populations in the competitive model surprising, as it is not clear how the dichotomous clusters in Figure 3-3 form. Here, we are looking at the total power of oscillatory activity each neuron receives – that is, its presynaptic profile – and it is unclear how the AP and IP neurons could shape their presynaptic profile in such a way except through a subtle and complicated multisynaptic network within SNr. We posit that, through the random connectivity and strengths randomly determined at the start of the simulation, mini circuits within SNr allow, for example, an AP neuron to effectively entrain the neurons which synapse onto it, or neurons which synapse onto other nearly synchronous neurons in the AP population (and similarly in the IP population). Simulated experiments controlling the connectivity of individual neurons could help to better understand the phenomena occurring here – for instance, if we specifically instantiate a test neuron whose presynaptic profile falls in this between-cluster region, will it be fated to move out of this region into one of the clusters? Such experiments may illuminate some of the interesting dynamics that can spontaneously arise through random connectivity and may be critical for synchronization in PD or other emergent phenomena in the brain.

3.4.4 Propagation of imperfectly synchronous oscillations

A particularly interesting result is the effective entrainment of SNr by GPe despite the imperfect synchrony of GPe oscillations. Within the prototypic GPe population, we observe pairwise delta phase differences as large as 100 ms, a much larger delay than we had

expected. We posit that delayed oscillations at the same frequency could still effectively integrate in a single SNr neuron in a manner which causes oscillatory firing merely by changing the shape of the resultant oscillation – for instance, in the case of square wave oscillatory profiles, oscillations with a large delay integrated in the same SNr neuron may simply change the relative durations of the neuron’s up and down states while still allowing the delta oscillation to express.

These long delays may hint at why delta oscillations are such a strong feature in DD, and perhaps in the brain as a whole. A 20 ms delay between two neurons undergoing a 1 Hz oscillation still keeps them approximately in phase, covering only 1/50 of their cycle. Yet, the same delay in, for example, a 25 Hz oscillation gives these neurons an antiphase relationship. If lags of this size are a common feature of neural oscillations regardless of the oscillation frequency, a group of neurons oscillating at the same high frequency would essentially tile the phase space, so the integration of these signals in downstream neurons would undergo destructive interference, making the propagation of these high frequency oscillations difficult. This suggests that delta oscillations may be particularly robust to the natural variability in relative timing across neurons within a population, and could help explain why they are such effective synchronizers, able to entrain the entire cortex during slow-wave sleep and, indeed, extend throughout the basal ganglia as we have established in DD.

3.5 ACKNOWLEDGEMENTS

Thanks to Ryan Phillips for providing the C++ code upon which the model in this chapter was based, as well as helpful discussions regarding our changes and tuning of the finished model. This work was supported by NSF award 1724240 (JER) and NIH awards R01NS101016, R01NS104835, (AHG), and F31NS101821 (TCW).

4 SUMMARY AND CONCLUSION

Through a thorough analysis of oscillatory activity in dopamine depleted mice, we have shown that delta oscillations are a robust neural signal of motor dysfunction in the SNr and across other basal ganglia nuclei. These oscillations correlate with Parkinsonian motor deficits and track the timeline of akinesia induced by D2R antagonists in healthy mice and the rescue of motor function in DD mice with D2R agonists.

The relationship between the oscillations we observe in SNr neurons and in M1 defines two novel SNr subpopulations: those whose firing predicts upcoming active states in M1, and those pauses or troughs predict active states in M1. This dichotomy mimics one of the defining features of the prototypic and arypallidal population in GPe, and studies which establish other analogies to these GPe subpopulations could help to uncover the roles of distinct cell types in SNr as has been done in striatum (Albin et al. 1989; DeLong 1990) and GPe (Mallet et al. 2012; Mastro et al. 2014).

The predictive nature of both AP and IP SNr population activity on future M1 states (100–300 ms later) suggest that these oscillations arise in the basal ganglia and propagate to other motor centers of the brain like M1, and we have shown through a computational model how these oscillations can effectively propagate within the basal ganglia in a way which matches *in vivo* data. This lends credence to the hypothesis that the delta oscillations we observe may arise from a single source in the basal ganglia, though it remains unclear which nucleus this is and the exact mechanism by which they arise.

4.1 WHY DO PARKINSONIAN OSCILLATIONS VARY ACROSS SPECIES?

The complete lack of beta oscillations in our recordings, in both LFP and individual neurons, was surprising. An argument could be made that, through some unknown mechanism, the delta oscillations we observe in DD mice are merely a slowed down beta oscillation: since beta oscillations already vary widely in frequency across species (roughly 13-30 Hz in humans, 20-35 Hz in rats, 8-15 Hz in monkeys), it is possible that an even greater slowdown of beta oscillations is occurring in mice. We would argue against this hypothesis for two reasons. First, since rats and humans exhibit both delta and beta oscillations in DD and PD respectively, it is more likely that the delta oscillations we observe in mice are mimicking the similar oscillation observed in these subjects, rather than the concurrent but much faster beta oscillations. Second, the delta oscillations we have measured exhibit a closer relationship to the timeline of motor symptoms than the beta oscillations observed in animal models of PD – delta oscillations arise immediately and along with symptoms in DD or acute D2R antagonism and attenuate along with symptoms when treated with D2 agonists, but beta oscillations in rats and monkeys require longer to arise and do so after symptoms first appear (Leblois et al. 2007; Mallet et al. 2008).

It is perplexing that DD in mice could replicate such profound Parkinsonian symptoms without bearing its signature beta oscillations, which are seen, in some form, in other animal models of PD. However, our expectation of such an elegant connection between disease states across species may have been naïve. Animal research is based on the expectation that certain aspects of physiology will be conserved to some extent across species – effective biological systems within organisms have evolved and been maintained because changes to them would be naturally selected against. The unnatural or rare states we study in disease research do not follow these conservation rules – there is no direct evolutionary pressure to conserve how a diseased system will perform.

Of course, disease states are a product of their surrounding physiology. In PD, for instance, the physiology of the basal ganglia determines how it will react to a loss of dopamine, and many aspects of this physiology are conserved between humans and model species. But, changes which could have minimal effect on BG physiology in health could lead to drastically different outcomes when dopamine is lost – the evolutionary pressure conserving similarity in disease states is almost entirely indirect. We should thus expect significantly more genetic drift in regard to disease states than healthy states, which would lead to, on average, an even smaller coherence between model species and humans in disease than we see in health.

Does this mean our use of animal models for studying diseases is fundamentally doomed? Clearly not, as decades of successful translational research have shown – our understanding of disease states across the entirety of human biology has been valuably informed by animal models, and countless treatments have graduated from bench to bedside. Instead, this tenet – that we should expect lower conservation across species in disease states than in health – recommends a certain humility in interpreting our models. We should not be surprised when aspects of disease physiology are changed or completely absent in animal models, and when we see physiological similarities, we should attempt to verify that these phenomena really do play similar roles in the disease states across species.

Delta oscillations, we hope, are one of these useful similarities between DD mice and patients suffering from PD, but further research is needed to make such a confirmation. The relationship between delta oscillations and motor symptoms, both predicting overall dysfunction and dynamically predicting periods of akinesia, are a hopeful indicator that the similar appearing oscillations in PD patients may play a similar role, but until such a hypothesis has been directly tested as it has been for beta oscillations, it remains a conjecture. We are hopeful that methodological tools such as the use of phase shift will make it easier to identify these slow oscillations amidst the high levels of low frequency biological noise present in both awake animals and human subjects and thus make such studies easier to pursue.

There may even be scientific benefits to the poor evolutionary conservation we expect (and, in the case of PD models, observe) in disease states. The existence of beta oscillations in DD rats but not DD mice, despite similar physiology, constrains which facets of BG physiology may be necessary for beta oscillation generation. A missing or altered ion channel in a BG nucleus, for instance, could have little effect on BG functioning in health, but may be responsible for the generation of beta oscillations in rats or their absence in mice. By comparing physiology in these species, we may find clues to the biophysical causes for beta oscillations, which can then be the target of directed experiments and potential disease-modifying interventions.

4.2 HOW MIGHT DELTA OSCILLATIONS LEAD TO PARKINSONIAN SYMPTOMS?

In chapter 2, we established two correlations between delta oscillations and motor deficits in DD mice. First, the fraction of neurons exhibiting a delta oscillation in SNr is correlated with the level of motor dysfunction in a barrage of standard behavioral tests. Second, delta oscillations in individual SNr neurons are weakened, though not completely ablated, during periods of movement. Such findings of course do not prove causality, and it would be difficult to do so in this situation. One could perform an experiment in which delta oscillations are electrically or optogenetically induced in a population of neurons to determine if this patterning is sufficient to cause PD-like motor deficits, but it would be difficult to accurately mimic the dynamics of these oscillations in DD. For instance, if we were to optogenetically excite or inhibit SNr neurons at a delta frequency, we would not be respecting the AP/IP dichotomy that arises in DD, or the small phase differences that exist within these populations. If these nearly antiphase populations with rich phase relationships are critical to the development of motor symptoms, such an experiment may erroneously conclude that delta oscillations are not causal to Parkinsonian deficits merely due to a limitation of our experimental procedures. This may be why analogous experiments inducing artificial beta oscillations have failed to replicate motor symptoms (Swan et al. 2019).

Aberrant patterning in BG spike trains is typically hypothesized to induce symptoms by sending an undesired “stop” signal to downstream motor networks, effectively “jamming” these circuits and rendering them unable to properly integrate motor plan information or output desired motor sequences (Rubin and Terman 2004; Turner and Desmurget 2010). Evidence from pallidotomy studies reinforce this idea – the complete removal of the aberrantly firing GPi greatly improves motor symptoms (Dogali et al. 1995; Lozano et al. 1995; Vitek et al. 2003), with only minor side effects involving learning of new motor skills (Obeso et al. 2009; Turner and Desmurget 2010). The question then becomes, what feature of delta oscillations could cause them to be a jamming signal?

Answering this question requires an understanding of how BG output usually transmits information to downstream targets. Synapses made by GPi and SNr typically exhibit short-term synaptic depression (Uno et al. 1978), as neurotransmitter-filled vesicles cannot be replenished quickly enough to cause significant neurotransmitter release and binding after every individual spike by these high-frequency firing neurons. Depending on the exact timescale of recovery from short-term depression at these synapses, delta oscillations could be an especially damaging signal – the pause or significant slowdown in firing at the oscillation’s trough gives time for the vesicle pool at the presynaptic terminal to be replenished, so when the oscillation enters an upstate, a sudden release of neurotransmitter excessively inhibits postsynaptic targets. Indeed, the induction of strong synaptic depression at pallidothalamic synapses is one of the hypotheses for DBS’s mechanism of symptom reduction (Erez et al. 2009; McIntyre et al. 2004). In the other direction, thalamic post-inhibitory rebound after an upstate in a GPi or SNr neuron’s delta oscillation can lead to undesired thalamic spiking, and DD has been shown to exaggerate post-inhibitory rebound in the mouse thalamus (Kim et al. 2017). More studies directly investigating the properties of BG-thalamic synapses and the thalamus’s response to various types of signals from GPi and SNr could determine if this mechanism is plausible.

While we are studying delta oscillations in the context of a motor disorder, delta oscillations are most famous for their role in a completely different akinetic state – unconsciousness. Multiple sleep disorders, including sudden onset of sleep without warning have been well established as nonmotor symptoms of PD (Comella 2007; Ito 2015); as such, we find the parallels between the delta oscillations observed in DD mice and those observed under anesthesia and non-rapid eye movement (NREM) sleep fascinating. Such states are characterized by strong delta oscillatory synchrony across the cortex, though notably this oscillation is not present in the sleeping or anesthetized basal ganglia in healthy conditions (Mallet et al. 2016; Walters et al. 2007). It is not clear how delta oscillations could be causal to the lack of motor activity in NREM sleep and under anesthesia, but if such a relationship exists, it is possible that the delta oscillations originating in the basal ganglia in PD which entrain M1 (and possibly thalamus) could essentially be mimicking a sleep-like state of low activity specifically in the motor system.

On the other hand, such oscillations could be unrelated. It is likely that there are many mechanisms by which slow oscillations can arise in the brain, and as we suggest through our phase lag analysis in Chapter 3, oscillations at these slow timescales may be particularly resistant to natural neural noise that can dampen faster oscillations, allowing relatively slow oscillations to arise more easily in the brain than those of higher frequencies. While delta oscillations in DD mice (0.5–4 Hz) match quite closely with the frequency of oscillations associated with sleep and anesthesia in both mice and humans, Parkinsonian delta oscillations in humans are slightly faster on average, with a range from 2–6 Hz, and thus overlap with the sleep delta band but do not match it perfectly. Depending on the frequency sensitivity of a hypothetical mechanism by which delta oscillations drive akinesia in both sleep and PD, this mismatch may pose problems with such a connection.

4.3 FUTURE DIRECTIONS FOR DELTA OSCILLATIONS AND SNR PHYSIOLOGY

Our thorough investigation of the oscillatory landscape of the mouse SNr in dopamine depletion demonstrates the importance of delta oscillations in DD and gives useful insights into SNr physiology and neural dynamics. But this research also sets the groundwork for further questions regarding delta oscillations and nigral physiology in the realms of clinical investigation, basic science, and computational modeling.

Perhaps the most obviously important question regards our findings' relationship to PD – that is, does the connection between motor symptoms and delta oscillations in mice translate to the analogous oscillations observed in PD? Many questions could be investigated in clinical research studies during the implantation of DBS electrodes which could mimic previous studies regarding beta oscillations – for instance, does delta power in BG nuclei or delta coherence to cortex change during a motor task? Do delta oscillations attenuate from treatment with levodopa or DBS, and does the time course of their modulation match the time course of motor symptom improvement? Are delta oscillations predictive of effective loci for DBS targeting? These questions may be difficult to answer from LFP recordings where there tends to be high levels of noise in low frequencies, but the notion of local stationarity which enabled our phase shift analysis to distinguish single unit oscillations from noise may have useful applications in LFP analysis as well. Such questions may even be able to be tackled outside of laboratory settings – as microelectrode technology improves, the popularity of DBS electrodes which can also serve as continuous recording devices has increased (Paff et al. 2020), and with large sets of data from many patients paired with behavioral or motor data from sources like wearable fitness trackers, it may be possible to relate neural signals such as delta oscillations to motor phenomena in more realistic situations.

In a more basic science direction, the question of where and how delta oscillations arise in DD is largely unclear. We have demonstrated that a loss of activation of D2 receptors is necessary and sufficient to generate delta oscillations in SNr, but it is not clear which effects of

a lack of action on D2Rs lead to delta oscillations or where these D2Rs reside. Targeted D2R antagonist injections or conditional knockouts or knockdowns of D2R's in specific BG nuclei could narrow down the locus of delta oscillation generation. However, we caution that the large dose of D2R antagonists needed for the development of delta oscillations may make such targeting difficult if an entire nucleus must be affected. Furthermore, it is possible that DD causes delta oscillations in multiple BG regions independently. In Chapter 2, we suggest some channels which are associated both with D2R-mediated signaling cascades and the generation of oscillations – namely, NMDARs and L-type Ca^{2+} channels – and targeted pharmacological manipulations of these or other targets could shed further light on the intracellular or network mechanisms underlying this oscillation generation.

In Chapter 2, we also discuss the parallels between the AP/IP dichotomy in SNr and the TA (arkypallidal) and TI (prototypic) populations in GPe. Such GPe populations were first defined by their relationship to M1 in DD under anesthesia (Mallet et al. 2008), much like we have done to define the AP and IP populations. Juxtacellular labeling of AP and IP neurons after electrophysiological identification may allow us to find distinct projection targets of AP and IP neurons which could demonstrate their distinct roles in BG neural circuits, and immunostaining for potential molecular differences in these populations driven by distinct genetic expression could lead to easier and more targeted experiments observing or manipulating these subpopulations (Mallet et al. 2012).

We proposed extensions to our biophysical model in the discussion of Chapter 3, but wide ranges of potential parameter choices make rigorously fitting such a model difficult to achieve manually, especially if additional complexity is added. An alternative could be to fit a computational model of the GPe-SNr (and perhaps STN) network using a statistical approach. New methods allow for the fitting of simpler models of neural populations (rather than individual spiking neurons) such as the Wilson-Cowan model (Wilson and Cowan 1972) directly from the spiking data like we recorded in Chapter 2 (René et al. 2020; Schwalger et al. 2017). This would

allow a more rigorous fit to our experimental data and could suggest how connections from GPe and/or STN differently innervate the AP and IP populations to achieve the dynamics we observe *in vivo*, producing useful and testable hypotheses regarding these novel populations' distinct roles in BG circuits.

4.4 FINAL REMARKS

Our results demonstrate that delta oscillations are a critical feature in dopamine depletion and its accompanying motor impairments. This suggests a reappraisal of delta oscillations in PD as a source of Parkinsonian symptoms beyond tremor. If such a connection can be made through further animal and human research, our results pose mice as a valuable animal model for further study into the generation, propagation, and pathological capabilities of delta oscillations and ways in which they could be targeted for PD treatments.

The oscillatory landscape of PD and animal models of PD is complex in many ways. Oscillations can be difficult to reliably detect amidst neural noise, especially at frequencies as low as delta oscillations. Multiple oscillating sources, within or between brain regions, can exhibit complex relationships with one another which can be computationally difficult to disentangle; these relationships can be further muddled when there are several concurrent oscillations at multiple frequencies, a phenomenon which occurs with beta and delta oscillations in many PD patients. Oscillation strength can vary dynamically, and because oscillations are processes evolving over time rather than distinct events, it can be especially difficult to rigorously relate them to behavioral states or events. Finally, the high variability of findings across different animal models further clouds a clear picture of oscillatory dynamics and their relevance to PD.

We are hopeful that the approaches taken in this work help to disentangle some of these difficulties through the use of new tools and lenses for the analysis of oscillations in PD and in general. Delta oscillations are not a new phenomenon in the PD literature, but in many ways

they have been neglected, and we are optimistic that a greater understanding of their physiology can improve our understanding and treatment of Parkinsonian dysfunction.

APPENDIX A

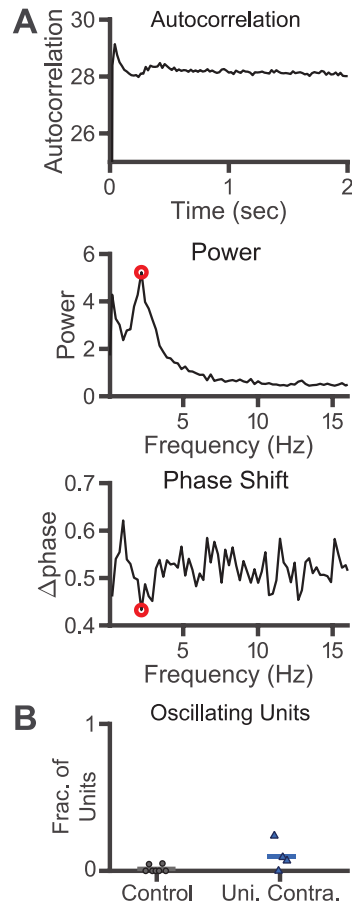


Figure A-1: Unilaterally depleted animals exhibit a small number of delta oscillating units in the SNr of their intact hemisphere.

A. Example autocorrelation (top), PSD (middle) and phase shift (bottom) for an example SNr unit exhibiting a delta oscillation in the intact hemisphere of a unilaterally depleted animal. **B.** Fraction of oscillating units in SNr for each animal in the control condition (black circle) and in the intact hemisphere of unilaterally depleted animals (dark blue triangle). The difference between these conditions is not significant at the $\alpha = 0.05$ level ($p = 0.0631$).

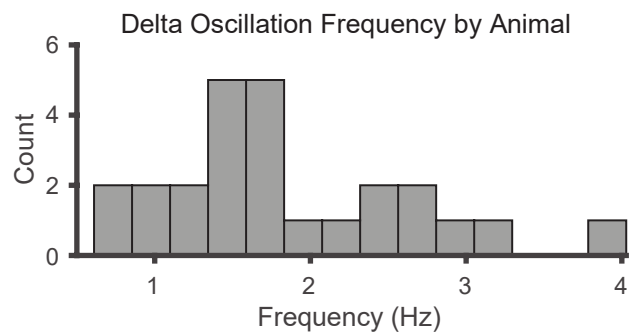


Figure A-2: Central delta oscillation frequency in SNr for each DD animal

Histogram showing median delta oscillation frequency in SNr, where each count is one animal. Data were pooled across bilaterally and unilaterally 6-OHDA-injected and reserpine-injected animals. Frequency bins were determined by the Rayleigh frequency of our windowing procedure (0.2441 Hz)

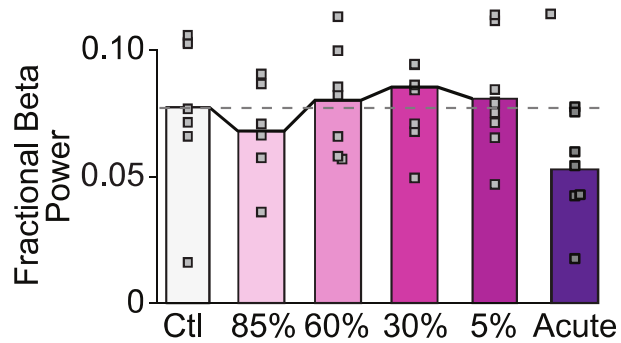


Figure A-3: Power of SNr LFP beta oscillations is not affected by DD.

Fractional beta power (compared to total 1–100 Hz power) in control animals (grey), animals gradually dopamine depleted to 85%, 60%, 30% or 5% striatal DA remaining (increasing shades of pink from left to right), and acutely dopamine depleted animals (purple). Grey squares illustrate individual animal means. No significant difference was found between conditions (ANOVA, $p = 0.7557$). A version of this figure was first published in Willard et al. 2019.

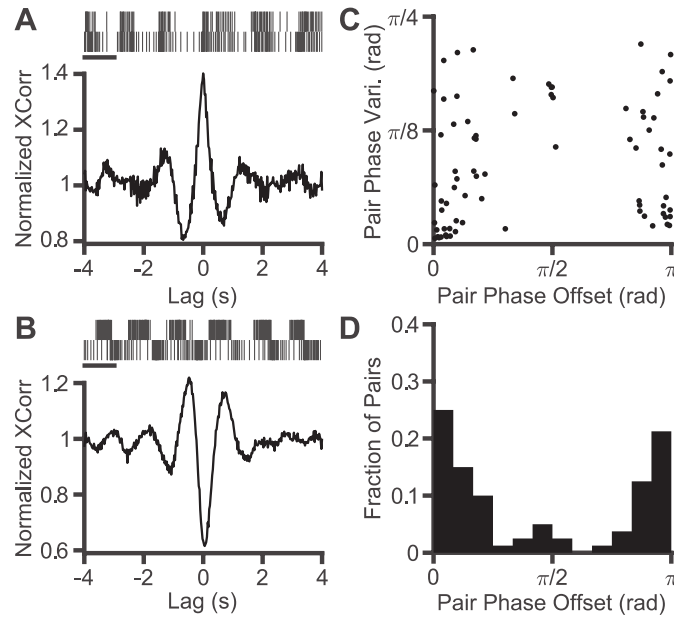


Figure A-4: Pairwise phase relationships corroborate the existence of two populations of oscillating units in dopamine depleted SNr.

A. Top: Spike rasters from a pair of simultaneously recorded SNr units, scale bar = 1 s. Bottom: Normalized cross correlations (see Neural Measures section of Methods) of the above pairs demonstrating an in-phase relationship. **B.** Same as a for a near anti-phase relationship. **C.** Scatterplot of all pairs of oscillating units. The horizontal axis measures their mean phase offset (0 indicating in phase, π indicating antiphase), and the vertical axis measures circular variance of phase offset computed across time windows. **D.** Histogram collapsing the above scatterplot to show counts of pairs based on their phase difference.

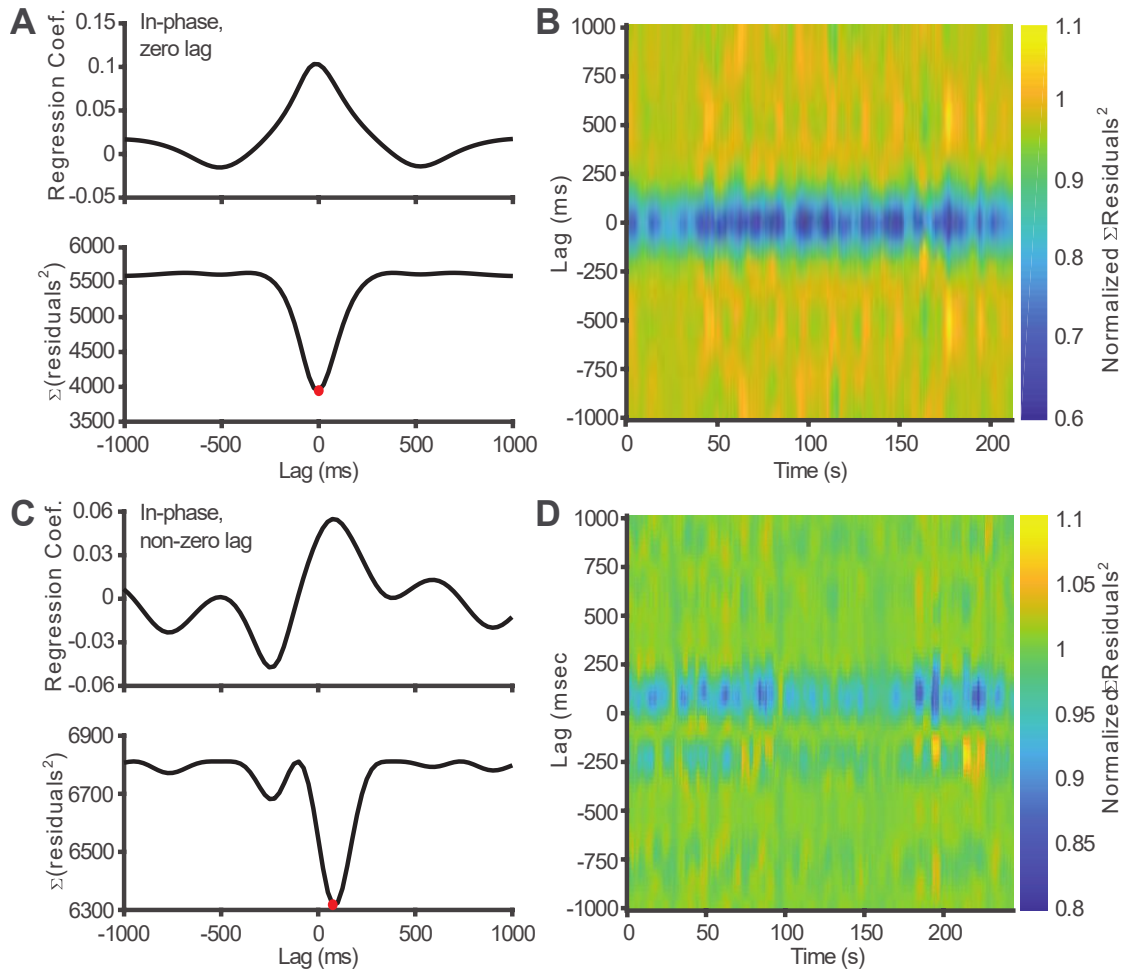


Figure A-5 Poisson regression on spike trains corroborates consistent non-zero lags within SNr populations.

A. Example regression results predicting single unit SNr firing with zero lag (i.e. perfect in-phase relationship). Top: regression coefficients for each individual lag. Bottom: sum of squared deviance residuals at each lag. Red circle indicates that the model using that lag significantly outperforms a purely autoregressive model of the spike train. This best model appears at a peak of the coefficients (top) indicating that the two neurons are from the same population. **B.** Heatmap indicating the fit of each model over time as measured by their sum of squared deviance residuals calculated over a moving 5-second window. Cooler (more blue) colors indicate lower residuals (i.e. better fit). **C-D.** Same as A-B with a pair who are from the same SNr population but whose phase relationship is consistently non-zero.

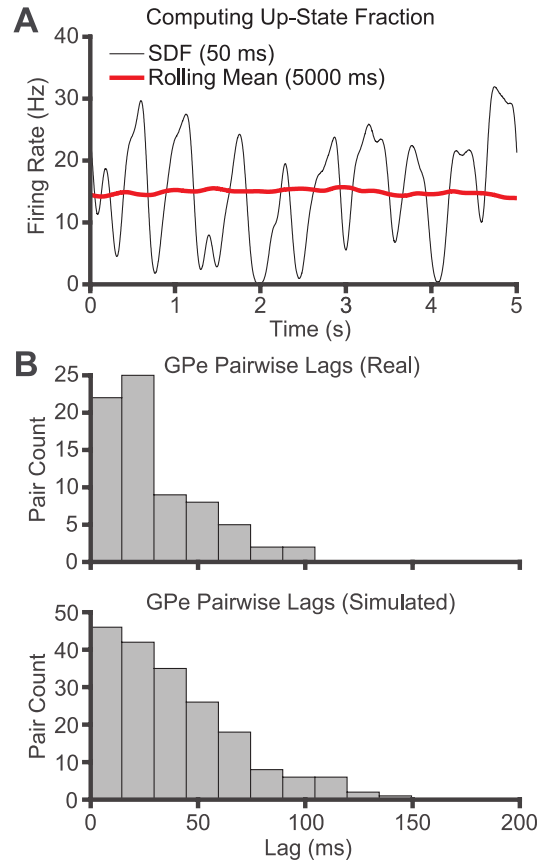


Figure A-6: Fitting simulated GPe spike trains.

A. Example visualization of the process for computing the mean fraction of time a GPe neuron spends in its upstate. The black line shows the SDF of the example neuron's spike train with visible delta oscillations. The red line shows a longer rolling mean of the neuron's firing rate. The fraction of time the SDF exceeds the rolling mean is the approximate time that neuron spent in its upstate. **B.** Computation of GPe pairwise lag distribution. Top: Histogram showing the pairwise delta phase lags of all simultaneously recorded pairs of prototypic GPe neurons which exhibited a significant delta oscillation *in vivo*. Bottom: One instantiation of the pairwise delta phase lag distribution computed from the GPe spike trains fed into the model after fitting the lag distribution to the top distribution.

Table A-1: Intrinsic current parameters for SNr biophysical model

Current	E	g_{\max}	Gate	$x_{1/2}$	k	τ^0	τ^1	$\tau^{1/2}$	σ^0	σ^1	x_{\min}
Na	50	35	m	-30.2	6.2	0.05	0.05	1	1	1	
			h	-63.3	8.1	0.59	35.1	-43.0	10.0	-5.0	
			s	-30.0	-0.4	10.0	50.0	-50.0	18.3	-10.0	0.15
NaP	50	0.175	m	-50.0	3.0	0.03	0.146	-42.6	14.4	-14.4	
			h	-57.0	-4.0	10.0	17.0	-34.0	26.0	-31.9	0.154
K	-90	50	m	-26.0	7.8	0.1	14.0	-26.0	13.0	-12.0	
			h	-20.0	-10.0	5.0	20.0	0	10.0	-10.0	0.6
Ca	13.27*	0.7	m	-27.5	3.0	0.5	0.5				
			h	-52.5	-5.2	18.0	18.0				
SK***	-90		m		0.4	0.1	0.1				
TRPC3	-37	0.2**									
Leak	-60	0.04									

Units for E , $x_{1/2}$, k , and σ are in mV, τ is in ms, g is in nS/pF.

* E_{Ca} is scaled by the log of the relative Ca^{2+} concentration, see Section 3.2.1.

** g_{TRPC} is only used in the control model, and is zero in DD.

*** Non-standard parameters for Ca^{2+} -activated SK current are in Table A-2.

Table A-2: Synaptic and miscellaneous parameters for SNr biophysical model

$C_S = 100 \text{ pF}$	$C_D = 40 \text{ pF}$
$[Ca_{out}] = 4.0 \text{ mM}$	$n_{SK} = 4$
$g_C = 26.5 \text{ nS}$	
$E_{GABA} = -70 \text{ mV}$	$\tau_{GABA}^S = 3 \text{ ms}$
$D_0 = 1.0$	$\tau_D = 1000 \text{ ms}$
$\alpha_D = 0.565$	$D_{min} = 0.67$
$W_{GABA}^{GPe} = 0.5 - 2.5 \text{ nS/pF}$	
$W_{GABA}^{SNr} = 0.5 - 2.5 \text{ nS/pF}$	
$g_{STN} = 0.15 - 0.25 \text{ nS/pF}^*$	

Values with ranges are sampled uniformly from that range for each neuron.

* The maximum and minimum for g_{STN} are each scaled by 1.5 in the control model, see Section 3.2.1.

BIBLIOGRAPHY

- Abbott LF, Varela JA, Sen K, Nelson SB.** Synaptic Depression and Cortical Gain Control. *Science* 275: 221–224, 1997.
- Abdi A, Mallet N, Mohamed FY, Sharott A, Dodson PD, Nakamura KC, Suri S, Avery SV, Larvin JT, Garas FN, Garas SN, Vinciati F, Morin S, Bezard E, Baufreton J, Magill PJ.** Prototypic and Arkypallidal Neurons in the Dopamine-Intact External Globus Pallidus. *J Neurosci* 35: 6667–6688, 2015.
- Abeles M.** *Local Cortical Circuits: An Electrophysiological Study*. Springer Science & Business Media, 1982.
- Ahn M, Lee S, Lauro PM, Schaeffer EL, Akbar U, Asaad WF.** Rapid motor fluctuations reveal short-timescale neurophysiological biomarkers of Parkinson's disease. *J Neural Eng* 17: 046042, 2020.
- Albin RL, Young AB, Penney JB.** The functional anatomy of basal ganglia disorders. *Trends in Neurosciences* 12: 366–375, 1989.
- Alonso-Frech F, Zamarbide I, Alegre M, Rodríguez-Oroz MC, Guridi J, Manrique M, Valencia M, Artieda J, Obeso JA.** Slow oscillatory activity and levodopa-induced dyskinesias in Parkinson's disease. *Brain* 129: 1748–1757, 2006.
- Anderson ME, Postupna N, Ruffo M.** Effects of High-Frequency Stimulation in the Internal Globus Pallidus on the Activity of Thalamic Neurons in the Awake Monkey. *Journal of Neurophysiology* 89: 1150–1160, 2003.
- Aristieta A, Ruiz-Ortega JA, Miguelez C, Morera-Herreras T, Ugedo L.** Chronic L-DOPA administration increases the firing rate but does not reverse enhanced slow frequency oscillatory activity and synchronization in substantia nigra pars reticulata neurons from 6-hydroxydopamine-lesioned rats. *Neurobiology of Disease* 89: 88–100, 2016.
- Aristieta A, Ruiz-Ortega JA, Morera-Herreras T, Miguelez C, Ugedo L.** Acute L-DOPA administration reverses changes in firing pattern and low frequency oscillatory activity in the entopeduncular nucleus from long term L-DOPA treated 6-OHDA-lesioned rats. *Experimental Neurology* 322: 113036, 2019.
- Baaske MK, Kramer ER, Meka DP, Engler G, Engel AK, Moll CKE.** Parkin deficiency perturbs striatal circuit dynamics. *Neurobiology of Disease* 137: 104737, 2020.
- Barter JW, Li S, Sukharnikova T, Rossi MA, Bartholomew RA, Yin HH.** Basal Ganglia Outputs Map Instantaneous Position Coordinates during Behavior. *J Neurosci* 35: 2703–2716, 2015.
- Belluscio MA, Kasanetz F, Riquelme LA, Murer MG.** Spreading of slow cortical rhythms to the basal ganglia output nuclei in rats with nigrostriatal lesions. *European Journal of Neuroscience* 17: 1046–1052, 2003.

- Belova EM, Semenova U, Gamaleya AA, Tomskiy AA, Sedov A.** Voluntary movements cause beta oscillations increase and broadband slope decrease in the subthalamic nucleus of parkinsonian patients. *Eur J Neurosci* , 2020. doi:10.1111/ejn.14715.
- Bergman H, Wichmann T, Karmon B, DeLong MR.** The primate subthalamic nucleus. II. Neuronal activity in the MPTP model of parkinsonism. *Journal of Neurophysiology* 72: 507–520, 1994a.
- Bergman H, Wichmann T, Karmon B, DeLong MR.** Parkinsonian Tremor is Associated with Low Frequency Neuronal Oscillations in Selective Loops of the Basal Ganglia. In: *The Basal Ganglia IV: New Ideas and Data on Structure and Function*, edited by Percheron G, McKenzie JS, Féger J. Springer US, p. 317–325.
- Beric A, Kelly PJ, Rezai A, Sterio D, Mogilner A, Zonenshayn M, Kopell B.** Complications of Deep Brain Stimulation Surgery. *SFN* 77: 73–78, 2001.
- Blandini F, Armentero M-T.** Animal models of Parkinson's disease. *The FEBS Journal* 279: 1156–1166, 2012.
- Blesa J, Phani S, Jackson-Lewis V, Przedborski S.** Classic and New Animal Models of Parkinson's Disease. *Journal of Biomedicine and Biotechnology* 2012Hindawi: e845618, 2012.
- Boëx C, Tyrand R, Horvath J, Fleury V, Sadri S, Corniola M, Burkhard PR, Momjian S.** What Is the Best Electrophysiologic Marker of the Outcome of Subthalamic Nucleus Stimulation in Parkinson Disease? *World Neurosurgery* 120: e1217–e1224, 2018.
- Boraud T, Bezard E, Guehl D, Bioulac B, Gross C.** Effects of L-DOPA on neuronal activity of the globus pallidus externalis (GPe) and globus pallidus internalis (GPi) in the MPTP-treated monkey. *Brain Research* 787: 157–160, 1998.
- Brown P.** Abnormal oscillatory synchronisation in the motor system leads to impaired movement. *Current Opinion in Neurobiology* 17: 656–664, 2007.
- Brown P, Oliviero A, Mazzone P, Insola A, Tonali P, Lazzaro VD.** Dopamine Dependency of Oscillations between Subthalamic Nucleus and Pallidum in Parkinson's Disease. *J Neurosci* 21: 1033–1038, 2001.
- Buzsáki G, Draguhn A.** Neuronal Oscillations in Cortical Networks. *Science* 304: 1926–1929, 2004.
- Cao C, Li D, Zhan S, Zhang C, Sun B, Litvak V.** L-dopa treatment increases oscillatory power in the motor cortex of Parkinson's disease patients. *NeuroImage: Clinical* 26: 102255, 2020.
- Capelli P, Pivetta C, Soledad Esposito M, Arber S.** Locomotor speed control circuits in the caudal brainstem. *Nature* 551: 373–377, 2017.
- Cassidy M, Mazzone P, Oliviero A, Insola A, Tonali P, Lazzaro VD, Brown P.** Movement-related changes in synchronization in the human basal ganglia. *Brain* 125: 1235–1246, 2002.
- Cazorla M, de Carvalho FD, Chohan MO, Shegda M, Chuhma N, Rayport S, Ahmari SE, Moore H, Kellendonk C.** Dopamine D2 Receptors Regulate the Anatomical and Functional Balance of Basal Ganglia Circuitry. *Neuron* 81: 153–164, 2014.
- Cenci M, Lindgren H.** Advances in understanding L-DOPA-induced dyskinesia. *Current Opinion in Neurobiology* 17: 665–671, 2007.
- Chan CS, Glajch KE, Gertler TS, Guzman JN, Mercer JN, Lewis AS, Goldberg AB, Tkatch T, Shigemoto R, Fleming SM, Chetkovich DM, Osten P, Kita H, Surmeier DJ.** HCN channelopathy in external globus pallidus neurons in models of Parkinson's disease. *Nature Neuroscience* 14: 85–92, 2011a.
- Chan V, Starr PA, Turner RS.** Bursts and Oscillations as Independent Properties of Neural Activity in the Parkinsonian Globus Pallidus internus. *Neurobiol Dis* 41: 2–10, 2011b.
- Chaudhuri KR, Healy DG, Schapira AH.** Non-motor symptoms of Parkinson's disease: diagnosis and management. *The Lancet Neurology* 5: 235–245, 2006.

- Chiken S, Nambu A.** Mechanism of Deep Brain Stimulation: Inhibition, Excitation, or Disruption? *Neuroscientist* 22: 313–322, 2016.
- Comella CL.** Sleep disorders in Parkinson's disease: An overview. *Movement Disorders* 22: S367–S373, 2007.
- Connelly WM, Schulz JM, Lees G, Reynolds JNJ.** Differential Short-Term Plasticity at Convergent Inhibitory Synapses to the Substantia Nigra Pars Reticulata. *J Neurosci* 30: 14854–14861, 2010.
- Connolly AT, Jensen AL, Bello EM, Netoff TI, Baker KB, Johnson MD, Vitek JL.** Modulations in Oscillatory Frequency and Coupling in Globus Pallidus with Increasing Parkinsonian Severity. *J Neurosci* 35: 6231–6240, 2015.
- Constantoyannis C, Berk C, Honey CR, Mendez I, Brownstone RM.** Reducing Hardware-Related Complications of Deep Brain Stimulation. *Canadian Journal of Neurological Sciences* 32: 194–200, 2005.
- Corbit VL, Whalen TC, Zitelli KT, Crilly SY, Rubin JE, Gittis AH.** Pallidostriatal Projections Promote β Oscillations in a Dopamine-Depleted Biophysical Network Model. *J Neurosci* 36: 5556–5571, 2016.
- Dawson TM, Ko HS, Dawson VL.** Genetic Animal Models of Parkinson's Disease. *Neuron* 66: 646–661, 2010.
- Deffains M, Iskhakova L, Katabi S, Israel Z, Bergman H.** Longer β oscillatory episodes reliably identify pathological subthalamic activity in Parkinsonism. *Movement Disorders* 33: 1609–1618, 2018.
- DeLong M, Wichmann T.** Changing Views of Basal Ganglia Circuits and Circuit Disorders. *Clin EEG Neurosci* 41: 61–67, 2010.
- DeLong MR.** Primate models of movement disorders of basal ganglia origin. *Trends in Neurosciences* 13: 281–285, 1990.
- Deng Y-P, Lei W-L, Reiner A.** Differential perikaryal localization in rats of D1 and D2 dopamine receptors on striatal projection neuron types identified by retrograde labeling. *Journal of Chemical Neuroanatomy* 32: 101–116, 2006.
- Devergnas A, Chen E, Ma Y, Hamada I, Pittard D, Kammermeier S, Mullin AP, Faundez V, Lindsley CW, Jones C, Smith Y, Wichmann T.** Anatomical localization of Cav3.1 calcium channels and electrophysiological effects of T-type calcium channel blockade in the motor thalamus of MPTP-treated monkeys. *Journal of Neurophysiology* 115: 470–485, 2015.
- Dogali M, Fazzini E, Kolodny E, Eidelberg D, Sterio D, Devinsky O, Beric A.** Stereotactic ventral pallidotomy for Parkinson's disease. *Neurology* 45: 753–761, 1995.
- Du G, Zhuang P, Hallett M, Zhang Y-Q, Li J-Y, Li Y-J.** Properties of oscillatory neuronal activity in the basal ganglia and thalamus in patients with Parkinson's disease. *Translational Neurodegeneration* 7: 17, 2018.
- Englot DJ, Hinkley LB, Kort NS, Imber BS, Mizuiri D, Honma SM, Findlay AM, Garrett C, Cheung PL, Mantle M, Tarapore PE, Knowlton RC, Chang EF, Kirsch HE, Nagarajan SS.** Global and regional functional connectivity maps of neural oscillations in focal epilepsy. *Brain* 138: 2249–2262, 2015.
- Erez Y, Czitron H, McCairn K, Bebelovsky K, Bar-Gad I.** Short-Term Depression of Synaptic Transmission during Stimulation in the Globus Pallidus of 1-Methyl-4-Phenyl-1,2,3,6-Tetrahydropyridine-Treated Primates. *J Neurosci* 29: 7797–7802, 2009.
- Filion M, Tremblay L.** Abnormal spontaneous activity of globus pallidus neurons in monkeys with MPTP-induced parkinsonism. *Brain Research* 547: 140–144, 1991.
- Fino E, Glowinski J, Venance L.** Bidirectional Activity-Dependent Plasticity at Corticostriatal Synapses. *J Neurosci* 25: 11279–11287, 2005.

- Foffani G, Ardolino G, Egidio M, Caputo E, Bossi B, Priori A.** Subthalamic oscillatory activities at beta or higher frequency do not change after high-frequency DBS in Parkinson's disease. *Brain Research Bulletin* 69: 123–130, 2006.
- Foster NN, Korobkova L, Garcia L, Gao L, Becerra M, Sherafat Y, Peng B, Li X, Choi J-H, Gou L, Zingg B, Azam S, Lo D, Khanjani N, Zhang B, Stanis J, Bowman I, Cotter K, Cao C, Yamashita S, Tugangui A, Li A, Jiang T, Jia X, Feng Z, Aquino S, Dan G, Fayzullina M, Mun H-S, Ustrell S, Boesen T, Santarelli A, Zhu M, Benavidez NL, Song M, Johnson DL, Xu H, Bienkowski MS, Yang XW, Gong H, Wickersham I, Luo Q, Lim BK, Zhang LI, Hintiryan H, Dong H.** The mouse cortico-basal ganglia-thalamic network. *bioRxiv* 2020.10.06.326876, 2020.
- Freeze BS, Kravitz AV, Hammack N, Berke JD, Kreitzer AC.** Control of Basal Ganglia Output by Direct and Indirect Pathway Projection Neurons. *J Neurosci* 33: 18531–18539, 2013.
- Fries P, Reynolds JH, Rorie AE, Desimone R.** Modulation of Oscillatory Neuronal Synchronization by Selective Visual Attention. *Science* 291: 1560–1563, 2001.
- Gage GJ, Stoetzner CR, Wiltschko AB, Berke JD.** Selective Activation of Striatal Fast-Spiking Interneurons during Choice Execution. *Neuron* 67: 466–479, 2010.
- Galati S, D'Angelo V, Olivola E, Marzetti F, Di Giovanni G, Stanzione P, Stefani A.** Acute inactivation of the medial forebrain bundle imposes oscillations in the SNr: A challenge for the 6-OHDA model? *Experimental Neurology* 225: 294–301, 2010.
- Gale JT, Shields DC, Jain FA, Amirnovin R, Eskandar EN.** Subthalamic nucleus discharge patterns during movement in the normal monkey and Parkinsonian patient. *Brain Research* 1260: 15–23, 2009.
- Galvan A, Wichmann T.** Pathophysiology of Parkinsonism. *Clinical Neurophysiology* 119: 1459–1474, 2008.
- Giannicola G, Marceglia S, Rossi L, Mrakic-Spota S, Rampini P, Tamma F, Cogiamanian F, Barbieri S, Priori A.** The effects of levodopa and ongoing deep brain stimulation on subthalamic beta oscillations in Parkinson's disease. *Experimental Neurology* 226: 120–127, 2010.
- Gibb WR, Lees AJ.** The relevance of the Lewy body to the pathogenesis of idiopathic Parkinson's disease. *Journal of Neurology, Neurosurgery & Psychiatry* 51: 745–752, 1988.
- Gilbertson T, Lalo E, Doyle L, Lazzaro VD, Cioni B, Brown P.** Existing Motor State Is Favored at the Expense of New Movement during 13-35 Hz Oscillatory Synchrony in the Human Corticospinal System. *J Neurosci* 25: 7771–7779, 2005.
- Guertin PA, Hounsgaard J.** NMDA-Induced Intrinsic Voltage Oscillations Depend on L-Type Calcium Channels in Spinal Motoneurons of Adult Turtles. *Journal of Neurophysiology* 80: 3380–3382, 1998.
- Halje P, Brys I, Mariman JJ, da Cunha C, Fuentes R, Petersson P.** Oscillations in cortico-basal ganglia circuits: implications for Parkinson's disease and other neurologic and psychiatric conditions. *Journal of Neurophysiology* 122: 203–231, 2019.
- Hammond C, Bergman H, Brown P.** Pathological synchronization in Parkinson's disease: networks, models and treatments. *Trends in Neurosciences* 30: 357–364, 2007.
- Hashimoto T, Elder CM, Okun MS, Patrick SK, Vitek JL.** Stimulation of the Subthalamic Nucleus Changes the Firing Pattern of Pallidal Neurons. *J Neurosci* 23: 1916–1923, 2003.
- Heimer G, Rivlin M, Israel Z, Bergman H.** Synchronizing activity of basal ganglia and pathophysiology of Parkinson's disease. In: *Parkinson's Disease and Related Disorders*, edited by Riederer P, Reichmann H, Youdim MBH, Gerlach M. Vienna: Springer, 2006, p. 17–20.

- Heiney SA, Wohl MP, Chettih SN, Ruffolo LI, Medina JF.** Cerebellar-Dependent Expression of Motor Learning during Eyeblink Conditioning in Head-Fixed Mice. *J Neurosci* 34: 14845–14853, 2014.
- Hernández-López S, Tkatch T, Perez-Garci E, Galarraga E, Bargas J, Hamm H, Surmeier DJ.** D2 Dopamine Receptors in Striatal Medium Spiny Neurons Reduce L-Type Ca²⁺ Currents and Excitability via a Novel PLCβ1–IP3–Calcineurin-Signaling Cascade. *J Neurosci* 20: 8987–8995, 2000.
- Higgs MH, Wilson CJ.** Unitary synaptic connections among substantia nigra pars reticulata neurons. *Journal of Neurophysiology* 115: 2814–2829, 2016.
- Higley MJ, Sabatini BL.** Competitive regulation of synaptic Ca²⁺ influx by D2 dopamine and A2A adenosine receptors. *Nature Neuroscience* 13: 958–966, 2010.
- Hirschmann J, Özkurt TE, Butz M, Homburger M, Elben S, Hartmann CJ, Vesper J, Wojtecki L, Schnitzler A.** Distinct oscillatory STN-cortical loops revealed by simultaneous MEG and local field potential recordings in patients with Parkinson's disease. *NeuroImage* 55: 1159–1168, 2011.
- Hirschmann J, Özkurt TE, Butz M, Homburger M, Elben S, Hartmann CJ, Vesper J, Wojtecki L, Schnitzler A.** Differential modulation of STN-cortical and cortico-muscular coherence by movement and levodopa in Parkinson's disease. *NeuroImage* 68: 203–213, 2013.
- Holt GR, Softky WR, Koch C, Douglas RJ.** Comparison of discharge variability in vitro and *in vivo* in cat visual cortex neurons. *Journal of Neurophysiology* 75: 1806–1814, 1996.
- Hornykiewicz O.** A brief history of levodopa. *J Neurol* 257: 249–252, 2010.
- Hurtado JM, Gray CM, Tamas LB, Sigvardt KA.** Dynamics of tremor-related oscillations in the human globus pallidus: A single case study. *PNAS* 96: 1674–1679, 1999.
- Hurtado JM, Rubchinsky LL, Sigvardt KA, Wheelock VL, Pappas CTE.** Temporal Evolution of Oscillations and Synchrony in GPi/Muscle Pairs in Parkinson's Disease. *Journal of Neurophysiology* 93: 1569–1584, 2005.
- Hutchison WD, Levy R, Dostrovsky JO, Lozano AM, Lang AE.** Effects of apomorphine on globus pallidus neurons in parkinsonian patients. *Annals of Neurology* 42: 767–775, 1997.
- Hutchison WD, Lozano AM, Davis KD, Saint-Cyr JA, Lang AE, Dostrovsky JO.** Differential neuronal activity in segments of globus pallidus in Parkinson's disease patients. *NeuroReport* 5: 1533–1537, 1994.
- Ito H.** Symptoms and Signs of Parkinson's Disease and Other Movement Disorders. In: *Deep Brain Stimulation for Neurological Disorders: Theoretical Background and Clinical Application*, edited by Itakura T. Springer International Publishing, p. 21–37.
- Ito J, Roy S, Liu Y, Cao Y, Fletcher M, Lu L, Boughter JD, Grün S, Heck DH.** Whisker barrel cortex delta oscillations and gamma power in the awake mouse are linked to respiration. *Nature Communications* 5: 1–10, 2014.
- Jackson-Lewis V, Blesa J, Przedborski S.** Animal models of Parkinson's disease. *Parkinsonism & Related Disorders* 18: S183–S185, 2012.
- Jenkinson N, Brown P.** New insights into the relationship between dopamine, beta oscillations and motor function. *Trends in Neurosciences* 34: 611–618, 2011.
- Jones BE.** From waking to sleeping: neuronal and chemical substrates. *Trends in Pharmacological Sciences* 26: 578–586, 2005.
- Kaminer J, Thakur P, Evinger C.** Frequency matters: beta-band subthalamic nucleus deep-brain stimulation induces Parkinsonian-like blink abnormalities in normal rats. *European Journal of Neuroscience* 40: 3237–3242, 2014.
- Kaneoke Y, Vitek JL.** Burst and oscillation as disparate neuronal properties. *Journal of Neuroscience Methods* 68: 211–223, 1996.

- Ketzef M, Silberberg G.** Differential Synaptic Input to External Globus Pallidus Neuronal Subpopulations *In vivo*. *Neuron* 109: 516-529.e4, 2021.
- Kim J, Kim Y, Nakajima R, Shin A, Jeong M, Park AH, Jeong Y, Jo S, Yang S, Park H, Cho S-H, Cho K-H, Shim I, Chung JH, Paik S-B, Augustine GJ, Kim D.** Inhibitory Basal Ganglia Inputs Induce Excitatory Motor Signals in the Thalamus. *Neuron* 95: 1181-1196.e8, 2017.
- Kita H, Kitai ST.** Efferent projections of the subthalamic nucleus in the rat: Light and electron microscopic analysis with the PHA-L method. *Journal of Comparative Neurology* 260: 435-452, 1987.
- Kühn AA, Kempf F, Brücke C, Doyle LG, Martinez-Torres I, Pogosyan A, Trottenberg T, Kupsch A, Schneider G-H, Hariz MI, Vandenberghe W, Nuttin B, Brown P.** High-Frequency Stimulation of the Subthalamic Nucleus Suppresses Oscillatory β Activity in Patients with Parkinson's Disease in Parallel with Improvement in Motor Performance. *J Neurosci* 28: 6165-6173, 2008.
- Kühn AA, Kupsch A, Schneider G-H, Brown P.** Reduction in subthalamic 8-35 Hz oscillatory activity correlates with clinical improvement in Parkinson's disease. *European Journal of Neuroscience* 23: 1956-1960, 2006.
- Lalo E, Thobois S, Sharott A, Polo G, Mertens P, Pogosyan A, Brown P.** Patterns of Bidirectional Communication between Cortex and Basal Ganglia during Movement in Patients with Parkinson Disease. *J Neurosci* 28: 3008-3016, 2008.
- Leão AHFF, Sarmiento-Silva AJ, Santos JR, Ribeiro AM, Silva RH.** Molecular, Neurochemical, and Behavioral Hallmarks of Reserpine as a Model for Parkinson's Disease: New Perspectives to a Long-Standing Model. *Brain Pathology* 25: 377-390, 2015.
- Leblois A, Meissner W, Bioulac B, Gross CE, Hansel D, Boraud T.** Late emergence of synchronized oscillatory activity in the pallidum during progressive parkinsonism. *European Journal of Neuroscience* 26: 1701-1713, 2007.
- Legendy CR, Salcman M.** Bursts and recurrences of bursts in the spike trains of spontaneously active striate cortex neurons. *Journal of Neurophysiology* 53: 926-939, 1985.
- Levy R, Ashby P, Hutchison WD, Lang AE, Lozano AM, Dostrovsky JO.** Dependence of subthalamic nucleus oscillations on movement and dopamine in Parkinson's disease. *Brain* 125: 1196-1209, 2002.
- Levy R, Dostrovsky JO, Lang AE, Sime E, Hutchison WD, Lozano AM.** Effects of Apomorphine on Subthalamic Nucleus and Globus Pallidus Internus Neurons in Patients With Parkinson's Disease. *Journal of Neurophysiology* 86: 249-260, 2001.
- Levy R, Hazrati L-N, Herrero M-T, Vila M, Hassani O-K, Mouroux M, Ruberg M, Asensi H, Agid Y, Féger J, Obeso JA, Parent A, Hirsch EC.** Re-evaluation of the functional anatomy of the basal ganglia in normal and Parkinsonian states. *Neuroscience* 76: 335-343, 1997.
- Lo YJ, Poo MM.** Activity-dependent synaptic competition in vitro: heterosynaptic suppression of developing synapses. *Science* 254: 1019-1022, 1991.
- Lobb CJ.** Abnormal bursting as a pathophysiological mechanism in Parkinson's disease. *Basal Ganglia* 3: 187-195, 2014.
- Lozano AM, Lang AE, Galvez-Jimenez N, Miyasaki J, Duff J, Hutchison WD, Dostrovsky JO.** Effect of GPi pallidotomy on motor function in Parkinson's disease. *The Lancet* 346: 1383-1387, 1995.
- Magill PJ, Bolam JP, Bevan MD.** Dopamine regulates the impact of the cerebral cortex on the subthalamic nucleus-globus pallidus network. *Neuroscience* 106: 313-330, 2001.
- Magnin M, Morel A, Jeanmonod D.** Single-unit analysis of the pallidum, thalamus and subthalamic nucleus in parkinsonian patients. *Neuroscience* 96: 549-564, 2000.

- Mallet N, Micklem BR, Henny P, Brown MT, Williams C, Bolam JP, Nakamura KC, Magill PJ.** Dichotomous Organization of the External Globus Pallidus. *Neuron* 74: 1075–1086, 2012.
- Mallet N, Pogosyan A, Márton LF, Bolam JP, Brown P, Magill PJ.** Parkinsonian Beta Oscillations in the External Globus Pallidus and Their Relationship with Subthalamic Nucleus Activity. *J Neurosci* 28: 14245–14258, 2008.
- Mallet N, Schmidt R, Leventhal D, Chen F, Amer N, Boraud T, Berke JD.** Arkypallidal Cells Send a Stop Signal to Striatum. *Neuron* 89: 308–316, 2016.
- Marras C, Beck JC, Bower JH, Roberts E, Ritz B, Ross GW, Abbott RD, Savica R, Van Den Eeden SK, Willis AW, Tanner CM.** Prevalence of Parkinson's disease across North America. *npj Parkinson's Disease* 4: 1–7, 2018.
- Mastro KJ, Bouchard RS, Holt HAK, Gittis AH.** Transgenic Mouse Lines Subdivide External Segment of the Globus Pallidus (GPe) Neurons and Reveal Distinct GPe Output Pathways. *J Neurosci* 34: 2087–2099, 2014.
- Mastro KJ, Zitelli KT, Willard AM, Leblanc KH, Kravitz AV, Gittis AH.** Cell-specific pallidal intervention induces long-lasting motor recovery in dopamine-depleted mice. *Nature Neuroscience* 20: 815–823, 2017.
- Maurice N, Mercer J, Chan CS, Hernandez-Lopez S, Held J, Tkatch T, Surmeier DJ.** D2 Dopamine Receptor-Mediated Modulation of Voltage-Dependent Na⁺ Channels Reduces Autonomous Activity in Striatal Cholinergic Interneurons. *J Neurosci* 24: 10289–10301, 2004.
- McCairn KW, Turner RS.** Deep Brain Stimulation of the Globus Pallidus Internus in the Parkinsonian Primate: Local Entrainment and Suppression of Low-Frequency Oscillations. *Journal of Neurophysiology* 101: 1941–1960, 2009.
- McCairn KW, Turner RS.** Pallidal stimulation suppresses pathological dysrhythmia in the parkinsonian motor cortex. *Journal of Neurophysiology* 113: 2537–2548, 2015.
- McCarthy MM, Moore-Kochlacs C, Gu X, Boyden ES, Han X, Kopell N.** Striatal origin of the pathologic beta oscillations in Parkinson's disease. *PNAS* 108: 11620–11625, 2011.
- McConnell GC, So RQ, Hilliard JD, Lopomo P, Grill WM.** Effective Deep Brain Stimulation Suppresses Low-Frequency Network Oscillations in the Basal Ganglia by Regularizing Neural Firing Patterns. *J Neurosci* 32: 15657–15668, 2012.
- McGeer PL, McGeer EG.** Inflammation and neurodegeneration in Parkinson's disease. *Parkinsonism & Related Disorders* 10: S3–S7, 2004.
- McGregor MM, Nelson AB.** Circuit Mechanisms of Parkinson's Disease. *Neuron* 101: 1042–1056, 2019.
- McIntyre CC, Savasta M, Kerkerian-Le Goff L, Vitek JL.** Uncovering the mechanism(s) of action of deep brain stimulation: activation, inhibition, or both. *Clinical Neurophysiology* 115: 1239–1248, 2004.
- Melgari J-M, Curcio G, Mastrolilli F, Salomone G, Trotta L, Tombini M, di Biase L, Scarscia F, Fini R, Fabrizio E, Rossini PM, Vernieri F.** Alpha and beta EEG power reflects L-dopa acute administration in parkinsonian patients. *Front Aging Neurosci* 6, 2014.
- Miller WC, DeLong MR.** Altered Tonic Activity of Neurons in the Globus Pallidus and Subthalamic Nucleus in the Primate MPTP Model of Parkinsonism. In: *The Basal Ganglia II*, edited by Carpenter MB, Jayaraman A. Boston, MA: Springer US, 1987, p. 415–427.
- Modolo J, Henry J, Beuter A.** Dynamics of the Subthalamo-pallidal Complex in Parkinson's Disease During Deep Brain Stimulation. *J Biol Phys* 34: 251–266, 2008.
- Muralidharan A, Jensen AL, Connolly A, Hendrix CM, Johnson MD, Baker KB, Vitek JL.** Physiological changes in the pallidum in a progressive model of Parkinson's disease: Are oscillations enough? *Experimental Neurology* 279: 187–196, 2016.

- Nakano K.** Neural circuits and topographic organization of the basal ganglia and related regions. *Brain and Development* 22: 5–16, 2000.
- Naoi M, Maruyama W.** Cell death of dopamine neurons in aging and Parkinson's disease. *Mechanisms of Ageing and Development* 111: 175–188, 1999.
- Nevado-Holgado AJ, Mallet N, Magill PJ, Bogacz R.** Effective connectivity of the subthalamic nucleus–globus pallidus network during Parkinsonian oscillations. *The Journal of Physiology* 1429–1455, 2014.
- Obeso JA, Jahanshahi M, Alvarez L, Macias R, Pedroso I, Wilkinson L, Pavon N, Day B, Pinto S, Rodríguez-Oroz MC, Tejeiro J, Artieda J, Tallelli P, Swayne O, Rodríguez R, Bhatia K, Rodríguez-Díaz M, Lopez G, Guridi J, Rothwell JC.** What can man do without basal ganglia motor output? The effect of combined unilateral subthalamotomy and pallidotomy in a patient with Parkinson's disease. *Experimental Neurology* 220: 283–292, 2009.
- Paff M, Loh A, Sarica C, Lozano AM, Fasano A.** Update on Current Technologies for Deep Brain Stimulation in Parkinson's Disease. *J Mov Disord* 13: 185–198, 2020.
- Pan HS, Walters JR.** Unilateral lesion of the nigrostriatal pathway decreases the firing rate and alters the firing pattern of globus pallidus neurons in the rat. *Synapse* 2: 650–656, 1988.
- Parr-Brownlie LC, Poloskey SL, Bergstrom DA, Walters JR.** Parafascicular thalamic nucleus activity in a rat model of Parkinson's disease. *Experimental Neurology* 217: 269–281, 2009.
- Pavlidis A, Hogan SJ, Bogacz R.** Improved conditions for the generation of beta oscillations in the subthalamic nucleus–globus pallidus network. *European Journal of Neuroscience* 36: 2229–2239, 2012.
- Phillips RS, Rosner I, Gittis AH, Rubin JE.** The effects of chloride dynamics on substantia nigra pars reticulata responses to pallidal and striatal inputs. *eLife* 9: e55592, 2020.
- Plenz D, Kital ST.** A basal ganglia pacemaker formed by the subthalamic nucleus and external globus pallidus. *Nature* 400: 677–682, 1999.
- Poewe W.** Non-motor symptoms in Parkinson's disease. *European Journal of Neurology* 15: 14–20, 2008.
- Priori A, Foffani G, Pesenti A, Tamma F, Bianchi AM, Pellegrini M, Locatelli M, Moxon KA, Villani RM.** Rhythm-specific pharmacological modulation of subthalamic activity in Parkinson's disease. *Experimental Neurology* 189: 369–379, 2004.
- Ray NJ, Jenkinson N, Wang S, Holland P, Brittain JS, Joint C, Stein JF, Aziz T.** Local field potential beta activity in the subthalamic nucleus of patients with Parkinson's disease is associated with improvements in bradykinesia after dopamine and deep brain stimulation. *Experimental Neurology* 213: 108–113, 2008.
- Raz A, Vaadia E, Bergman H.** Firing Patterns and Correlations of Spontaneous Discharge of Pallidal Neurons in the Normal and the Tremulous 1-Methyl-4-Phenyl-1,2,3,6-Tetrahydropyridine Vervet Model of Parkinsonism. *J Neurosci* 20: 8559–8571, 2000.
- René A, Longtin A, Macke JH.** Inference of a Mesoscopic Population Model from Population Spike Trains. *Neural Computation* 32: 1448–1498, 2020.
- Rivlin-Etzion M, Ritov Y, Heimer G, Bergman H, Bar-Gad I.** Local Shuffling of Spike Trains Boosts the Accuracy of Spike Train Spectral Analysis. *Journal of Neurophysiology* 95: 3245–3256, 2006.
- Roseberry TK, Lee AM, Lalive AL, Wilbrecht L, Bonci A, Kreitzer AC.** Cell-Type-Specific Control of Brainstem Locomotor Circuits by Basal Ganglia. *Cell* 164: 526–537, 2016.
- Rossi L, Marceglia S, Foffani G, Cogiamanian F, Tamma F, Rampini P, Barbieri S, Bracchi F, Priori A.** Subthalamic local field potential oscillations during ongoing deep brain stimulation in Parkinson's disease. *Brain Research Bulletin* 76: 512–521, 2008.

- Rubin JE, Terman D.** High Frequency Stimulation of the Subthalamic Nucleus Eliminates Pathological Thalamic Rhythmicity in a Computational Model. *J Comput Neurosci* 16: 211–235, 2004.
- Ruskin DN, Bergstrom DA, Walters JR.** Nigrostriatal Lesion and Dopamine Agonists Affect Firing Patterns of Rodent Entopeduncular Nucleus Neurons. *Journal of Neurophysiology* 88: 487–496, 2002.
- Salenius S, Avikainen S, Kaakkola S, Hari R, Brown P.** Defective cortical drive to muscle in Parkinson's disease and its improvement with levodopa. *Brain* 125: 491–500, 2002.
- Schober A.** Classic toxin-induced animal models of Parkinson's disease: 6-OHDA and MPTP. *Cell Tissue Res* 318: 215–224, 2004.
- Schwalger T, Deger M, Gerstner W.** Towards a theory of cortical columns: From spiking neurons to interacting neural populations of finite size. *PLOS Computational Biology* 13: e1005507, 2017.
- Seeger-Armbruster S, von Ameln-Mayerhofer A.** Short- and long-term unilateral 6-hydroxydopamine lesions in rats show different changes in characteristics of spontaneous firing of substantia nigra pars reticulata neurons. *Exp Brain Res* 224: 15–24, 2013.
- Shreve LA, Velisar A, Malekmohammadi M, Koop MM, Trager M, Quinn EJ, Hill BC, Blumenfeld Z, Kilbane C, Mantovani A, Henderson JM, Brontë-Stewart H.** Subthalamic oscillations and phase amplitude coupling are greater in the more affected hemisphere in Parkinson's disease. *Clinical Neurophysiology* 128: 128–137, 2017.
- Simmons DV, Higgs MH, Lebby S, Wilson CJ.** Indirect pathway control of firing rate and pattern in the substantia nigra pars reticulata. *Journal of Neurophysiology* 123: 800–814, 2020.
- Smith Y, Bolam JP.** Neurons of the substantia nigra reticulata receive a dense GABA-containing input from the globus pallidus in the rat. *Brain Research* 493: 160–167, 1989.
- Soares J, Kliem MA, Betarbet R, Greenamyre JT, Yamamoto B, Wichmann T.** Role of External Pallidal Segment in Primate Parkinsonism: Comparison of the Effects of 1-Methyl-4-Phenyl-1,2,3,6-Tetrahydropyridine-Induced Parkinsonism and Lesions of the External Pallidal Segment. *J Neurosci* 24: 6417–6426, 2004.
- Starr PA, Rau GM, Davis V, Marks WJ, Ostrem JL, Simmons D, Lindsey N, Turner RS.** Spontaneous Pallidal Neuronal Activity in Human Dystonia: Comparison With Parkinson's Disease and Normal Macaque. *Journal of Neurophysiology* 93: 3165–3176, 2005.
- Steigerwald F, Pötter M, Herzog J, Pinsker M, Kopper F, Mehdorn H, Deuschl G, Volkmann J.** Neuronal Activity of the Human Subthalamic Nucleus in the Parkinsonian and Nonparkinsonian State. *Journal of Neurophysiology* 100: 2515–2524, 2008.
- Steriade M, McCormick DA, Sejnowski TJ.** Thalamocortical oscillations in the sleeping and aroused brain. *Science* 262: 679–685, 1993.
- Surmeier DJ, Mercer JN, Chan CS.** Autonomous pacemakers in the basal ganglia: who needs excitatory synapses anyway? *Current Opinion in Neurobiology* 15: 312–318, 2005.
- Surmeier DJ, Song W-J, Yan Z.** Coordinated Expression of Dopamine Receptors in Neostriatal Medium Spiny Neurons. *J Neurosci* 16: 6579–6591, 1996.
- Sveinbjornsdottir S.** The clinical symptoms of Parkinson's disease. *Journal of Neurochemistry* 139: 318–324, 2016.
- Swan CB, Schulte DJ, Brocker DT, Grill WM.** Beta frequency oscillations in the subthalamic nucleus are not sufficient for the development of symptoms of parkinsonian bradykinesia/akinesia in rats. *eNeuro* ENEURO.0089-19.2019, 2019.
- Tang JKH, Moro E, Mahant N, Hutchison WD, Lang AE, Lozano AM, Dostrovsky JO.** Neuronal Firing Rates and Patterns in the Globus Pallidus Internus of Patients With

- Cervical Dystonia Differ From Those With Parkinson's Disease. *Journal of Neurophysiology* 98: 720–729, 2007.
- Terman D, Rubin JE, Yew AC, Wilson CJ.** Activity Patterns in a Model for the Subthalamopallidal Network of the Basal Ganglia. *J Neurosci* 22: 2963–2976, 2002.
- Thoenen H.** Neurotrophins and activity-dependent plasticity. In: *Progress in Brain Research*. Elsevier, p. 183–191.
- Tort ABL, Ponsel S, Jessberger J, Yanovsky Y, Brankač J, Draguhn A.** Parallel detection of theta and respiration-coupled oscillations throughout the mouse brain. *Scientific Reports* 8: 1–14, 2018.
- Tseng KY, Kasanetz F, Kargieman L, Pazo JH, Murer MG, Riquelme LA.** Subthalamic nucleus lesions reduce low frequency oscillatory firing of substantia nigra pars reticulata neurons in a rat model of Parkinson's disease. *Brain Research* 904: 93–103, 2001a.
- Tseng KY, Kasanetz F, Kargieman L, Riquelme LA, Murer MG.** Cortical Slow Oscillatory Activity Is Reflected in the Membrane Potential and Spike Trains of Striatal Neurons in Rats with Chronic Nigrostriatal Lesions. *J Neurosci* 21: 6430–6439, 2001b.
- Turner RS, Desmurget M.** Basal ganglia contributions to motor control: a vigorous tutor. *Current Opinion in Neurobiology* 20: 704–716, 2010.
- Turrigiano GG.** The Self-Tuning Neuron: Synaptic Scaling of Excitatory Synapses. *Cell* 135: 422–435, 2008.
- Uhlhaas PJ, Singer W.** Abnormal neural oscillations and synchrony in schizophrenia. *Nature Reviews Neuroscience* 11: 100–113, 2010.
- Uno M, Ozawa N, Yoshida M.** The mode of pallido-thalamic transmission investigated with intracellular recording from cat thalamus. *Exp Brain Res* 33: 493–507, 1978.
- Valsky D, Heiman Grosberg S, Israel Z, Boraud T, Bergman H, Deffains M.** What is the true discharge rate and pattern of the striatal projection neurons in Parkinson's disease and Dystonia? *eLife* 9: e57445, 2020.
- Vitek JL, Bakay RAE, Freeman A, Evatt M, Green J, McDonald W, Haber M, Barnhart H, Wahlay N, Triche S, Mewes K, Chockkan V, Zhang J-Y, DeLong MR.** Randomized trial of pallidotomy versus medical therapy for Parkinson's disease. *Annals of Neurology* 53: 558–569, 2003.
- Vitek JL, Zhang J, Hashimoto T, Russo GS, Baker KB.** External pallidal stimulation improves parkinsonian motor signs and modulates neuronal activity throughout the basal ganglia thalamic network. *Experimental Neurology* 233: 581–586, 2012.
- Volkman J.** Deep Brain Stimulation for the Treatment of Parkinson's Disease. *Journal of Clinical Neurophysiology* 21: 6–17, 2004.
- Walters JR, Hu D, Itoga CA, Parr-Brownlie LC, Bergstrom DA.** Phase relationships support a role for coordinated activity in the indirect pathway in organizing slow oscillations in basal ganglia output after loss of dopamine. *Neuroscience* 144: 762–776, 2007.
- Wang M, Wong AH, Liu F.** Interactions between NMDA and dopamine receptors: A potential therapeutic target. *Brain Research* 1476: 154–163, 2012.
- Wang Y, Zhang QJ, Liu J, Ali U, Gui ZH, Hui YP, Chen L, Wang T.** Changes in firing rate and pattern of GABAergic neurons in subregions of the substantia nigra pars reticulata in rat models of Parkinson's disease. *Brain Research* 1324: 54–63, 2010.
- Ward LM.** Synchronous neural oscillations and cognitive processes. *Trends in Cognitive Sciences* 7: 553–559, 2003.
- Wei W, Rubin JE, Wang X-J.** Role of the Indirect Pathway of the Basal Ganglia in Perceptual Decision Making. *J Neurosci* 35: 4052–4064, 2015.
- Weinberger M, Mahant N, Hutchison WD, Lozano AM, Moro E, Hodaie M, Lang AE, Dostrovsky JO.** Beta Oscillatory Activity in the Subthalamic Nucleus and Its Relation to Dopaminergic Response in Parkinson's Disease. *Journal of Neurophysiology* 96: 3248–3256, 2006.

- Whalen TC, Willard AM, Rubin JE, Gittis AH.** Delta oscillations are a robust biomarker of dopamine depletion severity and motor dysfunction in awake mice. *Journal of Neurophysiology* 124: 312–329, 2020.
- Whitton PS.** Inflammation as a causative factor in the aetiology of Parkinson's disease. *British Journal of Pharmacology* 150: 963–976, 2007.
- Wichmann T, Bergman H, Starr PA, Subramanian T, Watts RL, DeLong MR.** Comparison of MPTP-induced changes in spontaneous neuronal discharge in the internal pallidal segment and in the substantia nigra pars reticulata in primates. *Exp Brain Res* 125: 397–409, 1999.
- Wichmann T, Soares J.** Neuronal Firing Before and After Burst Discharges in the Monkey Basal Ganglia Is Predictably Patterned in the Normal State and Altered in Parkinsonism. *Journal of Neurophysiology* 95: 2120–2133, 2006.
- Willard AM, Isett BR, Whalen TC, Mastro KJ, Ki CS, Mao X, Gittis AH.** State transitions in the substantia nigra reticulata predict the onset of motor deficits in models of progressive dopamine depletion in mice. *eLife* 8: e42746, 2019.
- Williams D, Tijssen M, van Bruggen G, Bosch A, Insola A, Lazzaro VD, Mazzone P, Oliviero A, Quartarone A, Speelman H, Brown P.** Dopamine-dependent changes in the functional connectivity between basal ganglia and cerebral cortex in humans. *Brain* 125: 1558–1569, 2002.
- Wilson HR, Cowan JD.** Excitatory and Inhibitory Interactions in Localized Populations of Model Neurons. *Biophysical Journal* 12: 1–24, 1972.
- Xia X-M, Fakler B, Rivard A, Wayman G, Johnson-Pais T, Keen JE, Ishii T, Hirschberg B, Bond CT, Lutsenko S, Maylie J, Adelman JP.** Mechanism of calcium gating in small-conductance calcium-activated potassium channels. *Nature* 395: 503–507, 1998.
- Yelnik J.** Functional anatomy of the basal ganglia. *Movement Disorders* 17: S15–S21, 2002.
- Zhou F-W, Jin Y, Matta SG, Xu M, Zhou F-M.** An Ultra-Short Dopamine Pathway Regulates Basal Ganglia Output. *J Neurosci* 29: 10424–10435, 2009.
- Zhou F-W, Matta SG, Zhou F-M.** Constitutively Active TRPC3 Channels Regulate Basal Ganglia Output Neurons. *J Neurosci* 28: 473–482, 2008.
- Zhuang P, Hallett M, Meng D, Zhang Y, Li Y.** Characteristics of oscillatory activity in the globus pallidus internus in patients with Parkinson's disease (P1.8-028). *Neurology* 92: P1.8-028, 2019.